Reservoir characterization and sedimentological interpretations at the Aurora CO_2 storage site: seismic facies analysis and clinoform decompaction

Maren Bruflodt Løge

Master Thesis in Geoscience
Sedimentology, Paleontology, and Stratigraphy
60 Credits

Department of Geoscience

Faculty of mathematics and natural science

UNIVERSITY OF OSLO

May 2022

Main heading: Reservoir characterization and sedimentological interpretations at the Aurora CO_2 storage site: seismic facies analysis and clinoform decompaction

Supervisors: Anja Sundal, Ingrid Anell

This work is published digitally through DUO – Digitale Utgivelser ved UiO

http://www.duo.uio.no/

Printed: Reprosentralen, Universitetet i Oslo

Acknowledgments

I would like to express my gratitude to my main supervisor Anja Sundal and co-supervisor Ingrid Anell, for their guidance and encouragement at every stage of this process. Their feedback and fruitful discussions have been greatly appreciated. In addition, I would like Postdoctoral Fellow Muhammed Hassaan (UiO) for being helpful and patient in terms of the challenges faced in Petrel and the IT department at the Department of Geoscience.

Also, I would like to thank my fellow student and friends at the Geoscience M.Sc. program at UiO for their support, enjoyable conversations, and countless coffee breaks. This process would not have been as enjoyable without their encouragement. And to Emma McLarney, for taking her time improving my writing.

Finally, a particular thank you goes to my husband, Leon Løge, and my family for being so supportive and encouraging, showing such patience throughout this process, and for trying their best to match my enthusiasm for the field of geology.

Maren Bruflodt Løge

Oslo, Norway. May 16th, 2022

Preface

This master's thesis (ECTS 60) was submitted to the Department of Geoscience, University of Oslo (UiO), in the candidacy of the Master of Science in Geoscience (ETCS 120) under the program of Sedimentology, Paleontology, and Stratigraphy. The main supervisor of this thesis is Associate professor Anja Sundal (UiO), together with co-supervisors Associate professor Ingrid Anell (UiO).

The thesis is a part of the collaboration with UiO and the Norwegian CCS Research Center (NCCS). Seismic data is in courtesy of Gassnova SF, well data is in courtesy of NPD diskos repository and the Northern Lights project (Equinor ASA, Total E&P Norge AS, and A/S Norske Shell). Software is in courtesy of Schlumberger (Petrel E&P Software Platform).

Abstract

Assessment of depositional environments and variations in reservoir properties play an important role within CO_2 storage sites, as even small-scale heterogeneities have a significant impact on the subsurface behavior of CO_2. The proposed Aurora CO_2 storage site is located on the Horda Platform, in the northern North Sea. The Lower Jurassic Dunlin Group forms the storage complex, and the primary and secondary storage units comprise the saline aquifers of the Johansen Formation and the Cook Formation, respectively. Analysis supports the Lower Drake Formation as an extensive relatively homogeneous primary sealing unit. Injection of CO_2 is planned into the Johansen Formation sandstones. The formation developed as a westward prograding delta with delta-scale subaqueous sand-prone clinoforms building into shallow-marine waters, which could potentially baffle CO_2 migration.

Seismic facies analysis and clinoform decompaction were tested as methods for reservoir characterization. To determine the possible influence of lateral variations of the sedimentary environments and sediment partitioning within the primary and secondary storage reservoir, seismic facies analysis was performed utilizing the GN10M1 3D seismic survey and well data. Thereafter, clinoform geometries were analyzed and decompacted to enhance the prediction of lithological distributions, seismic facies, and reservoir properties of the prograding clinoforms. Clinoform geometries and heterogeneities observed within the Aurora storage site create baffles and contribute to plume dispersion, that may result in increased secondary trapping mechanisms which has a positive impact on CO_2 storage. This study shows that seismic data resolution is a limiting factor for seismic facies- and clinoform decompaction analysis. Considering the poor well-control in the south, it is advised that precautions should be taken to avoid rapid pressure buildup caused by extensive baffles.

Preformed seismic facies analysis in this study show laterally changing depositional environments within the Johansen Formation, where the injection area comprises a heterogeneous sediment composition influenced by a fluctuating tidal energy environment, sediment redistribution and washover processes in relation to an observed NW-SE prograding spit bar. In contrast, the northern area comprises a coarse-grained sand-rich homogeneous sediment composition, inferring a change in depositional processes to a high-energy, shallow-marine environment. The steepest dipping clinoform systems are observed in the northern study area, from which this study infers that the area is affected by lower sedimentation rates.

Table of contents

1 Introduction

This study provides an assessment of the seismic facies distributions, the depositional environments, and the stratigraphical evolution within the Aurora Storage site. In addition to an analysis of plausible clinoform geometries with implications for CO_2 storage. This chapter establishes the background for this thesis and introduces the Aurora Exploitation License, previous research, and this study's main research objectives.

1.1 Background

Carbone Capture and Storage (CCS) is considered as one of the essential technologies in limiting global warming to 2°C, preferably 1.5°C, within the year 2100, as stated by the Paris agreement in means of reducing the irreversible impacts and risks of climate change significantly (IPCC, 2021; United Nations, 2015). Additionally, it is a key aspect in reaching the goal of net-zero emission from the energy sector by 2050 (IEA, 2021). The atmospheric CO_2 concentration is rapidly rising as a result of elevated utilization of fossil fuel, due to the world's increasing energy demand this largest contributor to greenhouse gas emissions will likely continue as the world's main energy source (Bachu & Adams, 2003; Halland et al., 2011). CO_2 sequestration can theoretically account for half of this century's emissions, however, technical challenges need solving and increased levels of experience before this level of CO_2 storage is realistic.

The Norwegian government emphasizes Carbone Capture and Storage as a measure for reducing CO_2 emissions (Norwegian Ministry of Petroleum and Energy, 2020), and the NPD's CO_2 storage atlas of the northern North Sea confirms a theoretical storage of 70 Gt in saline aquifers, abandoned hydrocarbon fields and producing fields, corresponding Norway's annual CO_2 emissions for a millennia (Halland et al., 2011). Norway has been a forerunner of CO_2 sequestration technology, as the North Sea Sleipner field in 1996 was the world's first case of industrial-scale CCS (Arts et al., 2004), followed by the Snøhvit field in the Barents sea in 2008 (Shi et al., 2013). Equinor Energy AS is the operator for both gas fields and has 25 years of experience with CO_2 storage from industrial emissions going into Norway's planned full-scale CCS operation by 2024. The Norwegian government named the project Longship, a full-scale CCS project which will contribute to carbon capture, transport, and

storage technologies (Regjeringen, 2020). In the first phase the of Longship project, CO_2 will be captured from large point sources at Norcem cement factory in Breivik, and Oslo Fortum Varme waste-to-energy plant in Oslo. Liquid CO_2 will be shipped to the onshore terminal (Natrugassparken) in Øygarden (Figure 1.1), then injected by pipelines into the saline sandstone aquifers approximately 2.6 km below the seabed (Northern Lights, 2022). The transport and storage of Longship are operated by the Northern Lights project, a collaboration between Equinor ASA, A/S Norske Shell, and Total E&P Norge AS. The Norwegian CCS research center (NCCS) works alongside the Northern lights with the ambition to fast-track CCS deployment (NCCS, 2019).

The first phase of the Northern Lights project will inject 1.5 Mt CO_2 annually into the proposed Aurora storage site for 25 years (Equinor, 2019). Storage site simulations estimate the total injected volume to 81 Mt CO_2 by only utilizing one well, and the possibility of ramping up to six injection wells is existent and would increase the storage to 322 Mt (Lothe et al., 2019). The presented storage scenario of 2050 is 5.5 million tonnes CO_2 annually, promising futuristic storage possibilities.

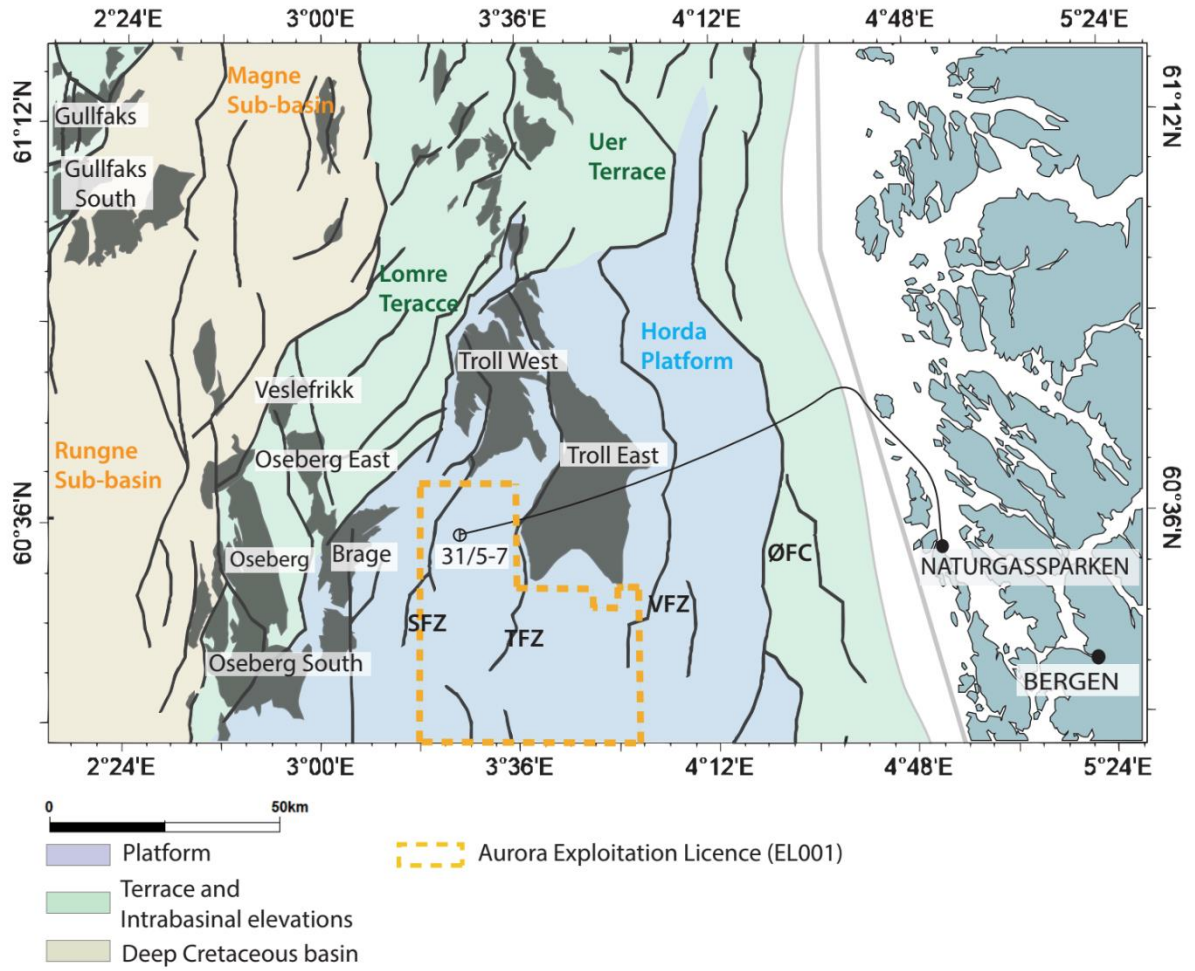

Figure 1.1 Map displaying the location of the Aurora Exploitation License (EL001) and hydrocarbon discoveries (grey). Outline of hydrocarbon discoveries, structural elements, Aurora license and pipelines are compiled from NPD fact maps and NPD fact pages. Only the injection well, 31/5-7, have been included in the map. Abbreviations: ØFC = Øygarden Fault Zone, VFZ= Vette Fault Zone, TFZ = Tusse Fault Zone, SFZ = Svartalv Fault Zone.

1.2 The Aurora Exploitation License (EL001)

In January 2019, the Aurora Exploitation License (EL001) was awarded to the Northern Lights by the Norwegian authorities as the very first exploitation license for CO_2 sequestration (Furre et al., 2020; NPD, 2020). The storage site is located on the western part of the established oil and gas producing Horda Platform, situated west of the Tusse Fault complex that divides the gas-producing Troll East from Troll West in the northern North Sea (Figure 1.1). It is located approximately 60 km West of Natrugassparken in Øygarden, 15 km east of Veslefrikk, Oseberg East, and Brage hydrocarbon fields.

The Lower Jurassic Dunlin Group has by the Norwegian authorities been proposed as the primary storage complex (i.e., storage and seal units) within the Aurora storage site (Halland et al., 2011). The primary and secondary storage units comprise the saline sandstone aquifers of the Johansen and Cook formations. The marine mud-rich Drake Formation can be subdivided into a Lower homogeneous and Upper heterolithic unit, where the Lower unit is considered the primary seal of the storage complex (Furre et al., 2020; Gassnova, 2012)(outlined 2.1.3).

The Aurora storage complex is gently southwards dipping, and it is therefore estimated by the Northern lights project that injected CO_2, over time, will migrate northwards into the Troll license (Equinor, 2019). However, injected CO_2 will accumulate in the proposed storage unit within the Aurora Exploration license located below the Troll reservoir, approximately 500m below the producing Troll Field (Furre et al., 2020). The planned migration route of the injected CO_2 will likely enhance secondary CO_2 trapping mechanisms and expectedly enhance storage capacity (de Silva et al., 2015; Zhang & Song, 2014) (outlined 2.2.4). Pressure data indicates a hydraulic seal between the Aurora storage complex of the Dunlin Group and the Troll Field located in the Viking Group, as no pressure communication is observed between the two reservoirs, confirming the sealing capabilities of the Lower Drake Formation. Leakage risk assessment results indicate that there are low risks of fault reactivation and fault flow of CO_2 out of the Dunlin Group (Equinor, 2019).

On the 2nd of December 2019, the Northern Lights Project began the drilling of the conformation well 31/5-7 (EOS) to confirm the presence of suitable storage and seal units within the Aurora exploration license. The well is located approximately 10 km south of the border between the Aurora exploitation license and the Troll license (Equinor, 2019). It was completed in February 2020, confirming a water-bearing sandstone reservoir with properties well suited for CO_2 storage. There has been no previous production of oil and gas from these formations in this area. The well 31/5-7 will later be re-entered, side-traced, and used as a CO_2 injector into a deep saline aquifer 80 km offshore Western coast of Norway at 2700 meters depth (Furre et al., 2020).

1.3 Previous research

In the process of advancing relevant research objectives, previous studies in regards to the evaluation and effect of reservoir qualities and variations in relation to CO_2 storage, or in the proximity of the Aurora storage complex in the northern Horda Platform are reviewed.

The storage complex and the northern North Sea structural interior are dominated by numerous faults formed by multiple rift phases, and the structural characterization and evolution of the area have been thoroughly studied (Figure 2.1) (Færseth, 1996; Gabrielsen et al., 2010; Ziegler, 1975). The structural evolution of the northern Horda Platform will have implications for the depositional evolution, as the tectonic activity in the area greatly affects accommodation and rate of sedimentation, which thus affect the internal structures of the different stratigraphical units and their development. Examples of recent studies within or in proximity to the Aurora Storage complex are Sundal et al. (2015, 2016), assessing sedimentary architecture, reservoir qualities, and characteristics of the primary storage unit, and Lothe et al. (2019), focusing on reservoir potential within the Aurora storage complex. The troll West and East fields are documented by relatively new studies (e.g., Deng et al., 2017; Duffy et al., 2015; Patruno, Hampson, Jackson, & Whipp, 2015; Wu et al., 2021) in relation to the structural development of the northern Horda Platform influencing the stratigraphy and fault seal analysis of the study area.

In a CO_2 storage site, reservoir characteristics have great importance for injectivity rate, storage, and migration (Flett et al., 2007). In a classic oil and gas reservoir, a homogeneous reservoir is desirable. However, regarding CO_2 storage heterogeneities in addition to high porosity and permeability, can enhance storage capacities by secondary trapping mechanisms (Shukla et al., 2010; Zhang & Song, 2014). Hence, a thorough understanding of reservoir qualities is of great importance for CO_2 storage. Extensive rapports by Gassnova (2012) have been generated to assess variations within the storage complex, in addition to the performed regional assessment of CO_2 storage sites within the Norwegian North Sea by Halland et al. (2011), including the Dunlin Group of the Aurora storage complex.

Several studies have covered the depositional evolution and stratigraphic analysis of the Johansen Formation, from the earliest by Vollset & Doré et al. (1984) and Marjanac & Steel (1997), to newer interpretations by Charnock et al. (2001) and Husmo et al. (2003), and the most frequent revision by Sundal et al. (2016). All established the Lower Jurassic Dunlin group

as shallow to marginal marine, deposited in periods of transgression and regression, with shallow-marine wave-dominated prograding delta deposits defining the primary and secondary reservoirs (e.g., Johansen Formation and Cook Formation, respectively). As the overlying Sognefjord Formation forms the reservoir of the producing Troll field, extensive studies are present on the formation (e.g, Dreyer et al., 2005; Patruno, Hampson, Jackson, & Dreyer, 2015; Patruno, Hampson, Jackson, & Whipp, 2015). They are of great interest in comparison to Johansen as the formations are fed by the same source but dominated by different tectonic settings, and to further investigate how this influences the internal geometries and reservoir properties of the Johansen Formation. As clinoform development is existent in the Sognefjord Formation, comparison to the clinoforms present in the Johansen Formation is of interest as they may act as potential baffles to CO_2 migration.

Furthermore, extensive seismic facies analysis within the Aurora storage complex has not been published, and the implications it may have for storage potential, injectivity and migration. As studies on facies analysis from well-logs and core descriptions display variations in reservoir characteristics (e.g, Gassnova, 2012; Sundal et al., 2016), a seismic facies analysis between wells would bring valuable information to the Aurora storage complex.

1.4 Research objectives

This study seeks to contribute to a better understanding of the storage complex heterogeneities, pore-space reductions, and the lateral and regional variations within the Aurora storage complex, contributing to de-risking of CO_2 storage within the storage complex. Aiming to enhance the value and importance of seismic facies analysis, clinoform analysis, and decompaction analysis during the characterization of reservoir properties and depositional environments within the Aurora storage complex. The main objectives of this study are to:

i) Assess the presence and distribution of seismic facies and clinoform geometries.

ii) Establish sedimentary environments and sediment partitioning within the succession.

iii) Discuss the plausible influence of reservoir heterogeneities for CO_2 injection, migration, and storage.

The objectives are achieved through generating detailed seismic interpretations of the Lower Jurassic Dunlin Group, undertaking analysis of seismic stratigraphy and terminations through seismic facies analysis, in addition to seismic attributes to assess the sedimentary environments and sediment distributions within the succession. Mainly focusing on the Johansen Formation (i.e., primary reservoir), the Cook Formation (i.e., secondary reservoir), and the Lower Drake Formation (i.e., primary seal). Interpretations of facies variability from 3D seismic data and correlated well logs along and across depositional strike were performed, in addition to interpretations of facies variability in relation to fault strike. The sedimentary understanding and model will provide a framework for evaluating variations within the reservoir units along and across the Tusse fault. Through these described tasks, this thesis will contribute in de-risking of CO_2 storage within the Aurora storage complex.

1.5 Study outline

This thesis is outlined as follows. Chapter 2 introduces the background of the stratigraphic and structural evolution of the northern North Sea, focusing on the northern Horda Platform. In addition to introducing the main theoretical aspects regarding seismic facies analysis, clinoform decompaction and CO_2 reservoir properties and trapping mechanisms. Chapter 3 presents the data utilized for the study and its limitation, in addition to methods used to generate detailed seismic surface interpretations, seismic facies analysis, and clinoform decompaction analysis. Chapter 4 introduces the produced results of the study, i) results in relation to seismic facies analysis, ii) stratigraphic characterization, and iii) clinoform decompaction analysis. In chapter 5, the importance of the attained results is discussed, focusing on i) implications of seismic facies analysis, ii) evolution of depositional environments and reservoir predictions, iii) clinoform decompaction analysis for reservoir properties, iv) controlling factors, and v) implications for CO_2 storage. Chapter 6, the final chapter, concludes the thesis by providing a summary of the main findings.

2 Background

This section places the study area and Aurora storage complex in a geological context (2.1), focusing on the structural and stratigraphical framework and the geological evolution of the northern North Sea, in particular the Horda Platform. In addition to introducing the necessary theoretical background (2.2) for performing seismic facies analysis and clinform decompaction analysis.

2.1 Geological background

2.1.1 Regional setting

The Norwegian Continental Shelf (NCS), offshore western Norway, comprises the three main provinces: the North Sea, the Mid-Norwegian continental margin, and the Western Barents Sea (Faleide, Bjørlykke, et al., 2015). Bordering the Norwegian Sea in the north (62°N) and the Norwegian-Danish Basin in the south and southeast (56°N). Multiple rift events during the Mesozoic resulted in the dominant structural feature of the North Sea trilete rift system, comprising the three rift arms; Viking Graben, The Central Graben, and the Moray Firth Basin (Figure 2.1A) (Bartholomew et al., 1993; Davies et al., 2001; Whipp et al., 2014)

The northern North Sea is a province located within the North Sea as an approximately 200 km wide and primarily N-S trending intracratonic basin, a basin located upon the continental crust (Faleide, Bjørlykke, et al., 2015). Characteristics of the northern North Sea is mainly N-S, NE-SW, and NW-SE striking normal faults (Figure 2.1B). The main structural features of the northern North Sea developed during Jurassic to Cretaceous times includes the Viking Graben continuing into Sognegraben in the north, the East Shetland basin and Tampen Spur in the west, and the Horda Platform in the east (Figure 2.1A) (Faleide, Bjørlykke, et al., 2015).

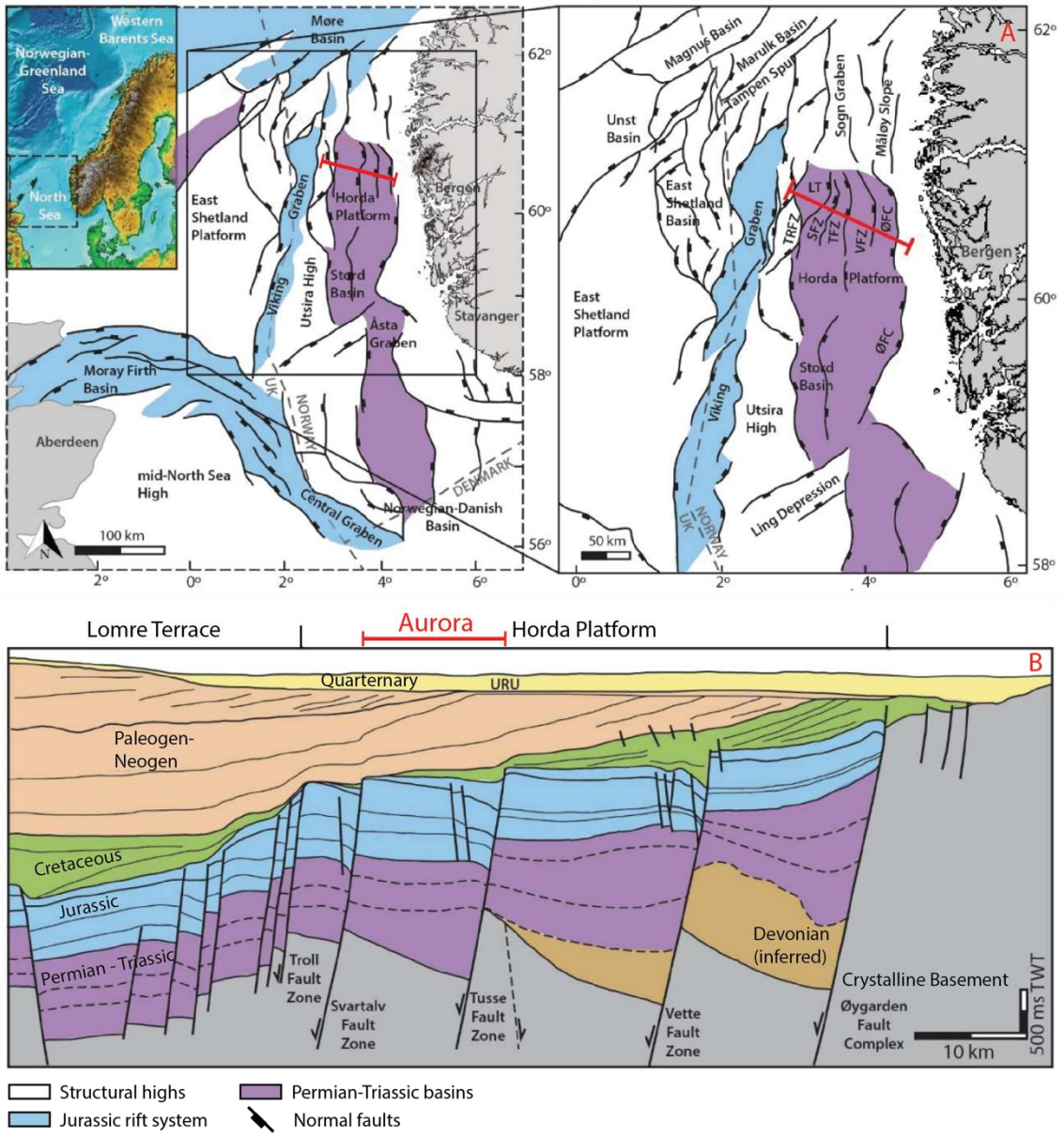

Figure 2.1 A) Structural elements of the North Sea and the northern North Sea (black outline). Figure Modified from Holden (2021) and Faleide et al. (2015), structural element maps are compiled from Færseth et al. (1996) and Whipp et al. (2014). B) Interpreted crossline displayed in red in A), of the Horda Platform. Modified from Holden (2021) and Whipp et al. (2014): Abbreviations: LT = Lomre Terrace, TRFZ = Troll Fault Zone, SFZ = Svartalv Fault Zone, TFZ = Tusse Fault Zone, VFZ = Vette Fault Zone, ØFC = Øygarden Fault Complex, URU = Upper Regional Unconformity

The Horda Platform is located offshore Bergen, on the eastern margin of the northern North Sea. The N-S trending structural high within the northern North Sea reaches 300 km in length and 50 km in width, bordered by the northern part of the Viking graben to its west and by the Øygarden Fault Complex to its east (Figure 2.1A) (Duffy et al., 2015; Færseth, 1996). A fault network comprising N-S striking faults active in Rift Phase 1 and 2, and a broadly NW-SE striking set active in Rift Phase 2, dissects the northern part of the Horda Platform (Duffy et al., 2015; Whipp et al., 2014). The N-S striking basement involved faults includes from the west;

Svartalv, Tusse, Vette, and Øygarden fault systems (Figure 2.1B). The westward dipping faults have an average spacing of 6-15 km and a 5 km throw, and they define the east-tilted half grabens filled with (3km) Permian-Triassic sediments (Bell et al., 2014; Duffy et al., 2015; Færseth, 1996; Whipp et al., 2014)(Figure 2.1B).

The Aurora CO_2 storage complex is located in a tilted fault block on the western part of the Horda Platform, south-west of the producing Troll Field, bound by the Tusse fault system to the east and Svartalv fault system to the west (Figure 2.1B) (Lothe et al., 2019; Wu et al., 2021). The storage complex is located in the Lower Jurassic Dunlin Group, overlying the Statfjord Group (Figure 2.2) (Deegan & Scull, 1977; Halland et al., 2014). The Dunlin Group is subdivided into five formations, and four of them are present at the Aurora storage site. The formations represent a sandstone-mudstone succession comprising the Johansen Formation primary reservoir, the Amundsen Formation secondary seal, the Cook Formation secondary reservoir, and the Drake Formation primary seal (Halland et al., 2014; Lothe et al., 2019; Thompson et al., 2022). The Johansen and Cook formations represent mainly marginal marine sandstones, separated by the marine mudstones of the Amundsen Formation (Marjanac & Steel, 1997). The Lower Drake Formation marine mudstones represent the primary seal, overlain by the deltaic Brent Group.

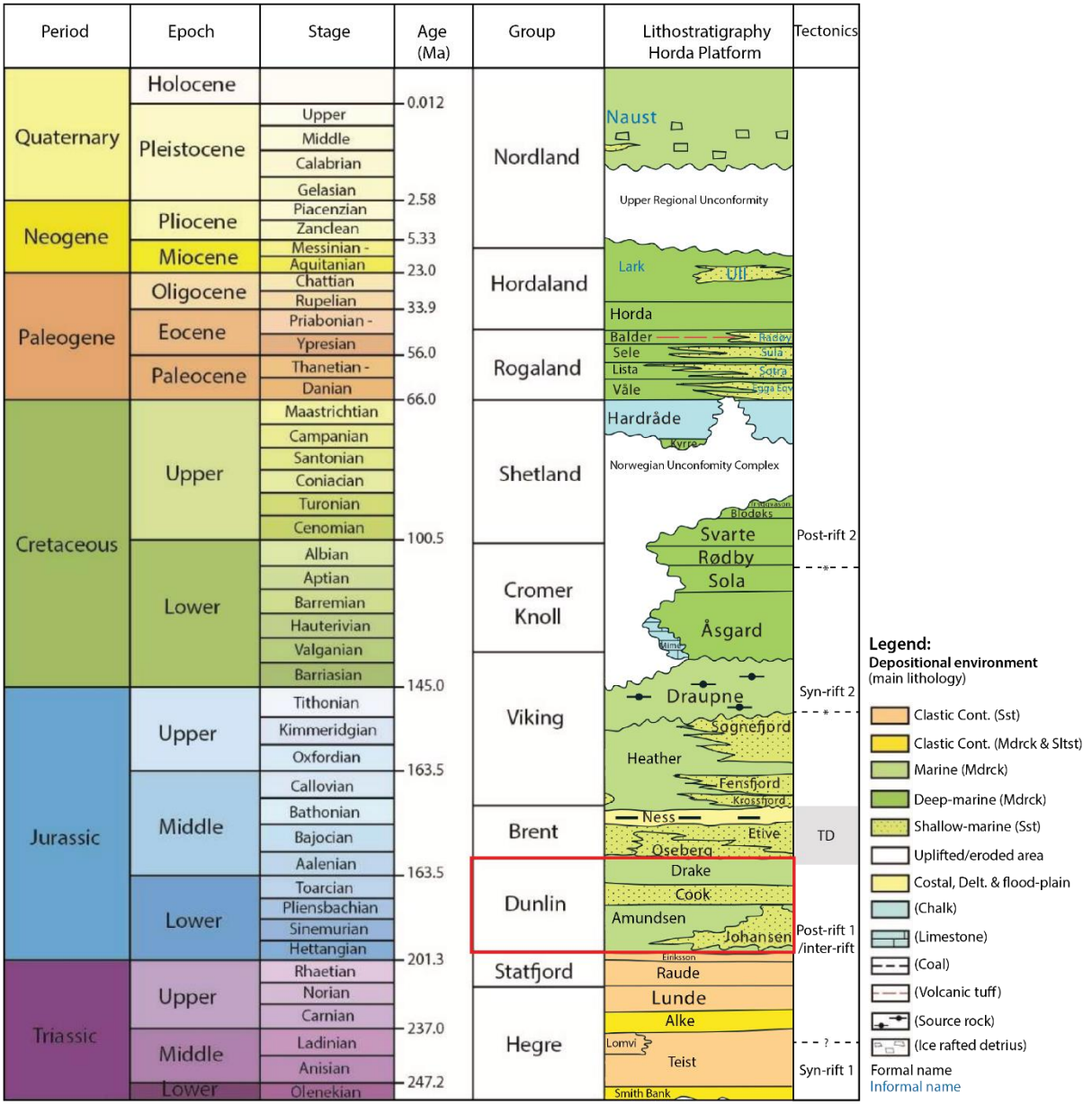

Figure 2.2 Stratigraphic chart displaying the Triassic to Quaternary deposits of the Horda Platform. Red outline marks the formations of the Aurora storage unit. Modified from Holden (2021), NPD (2014), tectonic events based in Tusse Fault Zone activity described by Whipp et al. (2014). Abbreviations: TD = Growth and collapse of the Central North Sea Dome, Sst = Sandstone, Mdrck = Mudstone, Sltst = Siltstone. * Timing of the onset and cessation of Syn-rift 2 is interpreted to be diachronous across the Horda Platform (Bell et al., 2014).

2.1.2 Tectonic setting

The intracratonic sedimentary basin of the northern North Sea was developed through multiple failed rift events and simultaneous thermal cooling and subsidence after the collapse of the Caledonian orogeny (Færseth, 1996). Contractional tectonics during Ordovician to Devonian times led to the formation of the Caledonian Orogeny (Gee et al., 2008; Ziegler, 1975). During Mid to Late Silurian, the final phase of the Caledonian Orogeny, the western margin of Baltica subsided under the Laurentian lithospheric plate (Gabrielsen et al., 2010; Gee et al., 2008; Ziegler, 1975), leading to the closure of the Iapetus Ocean and the Scandian continent collision (ca 430-390 Ma), resulting in the formation of the Caledonian Orogeny. In the southern part of the orogeny, the tectonic regime changed from contractional to extensional shortly before 400 Ma (Gee et al., 2008), leading to the rapid gravitational collapse of the Caledonian Orogeny during the Early Devonian (Gabrielsen et al., 2010). In response to the collapse, the deposition of red arid continental sandstones known as the thick Devonian Old Red Sandstone sourced from the east emerged (Faleide, Bjørlykke, et al., 2015; Vollset & Doré, 1984). The sandstones of western Norway underwent high-grade metamorphism making them unsuitable reservoirs. Post-orogenic crustal relaxation in the Devonian led to the development of major extensional shear zones, that influenced the northern North Sea basin through geometric constraints on the Mesozoic rift system and influenced thermal subsidence in the Cenozoic (Bartholomew et al., 1993; Duffy et al., 2015; Whipp et al., 2014).

The first major rift event in the Late Permian to Early Triassic was initiated as a result of the break-up of Pangea, with an E-W extension (Figure 2.2) (Færseth, 1996; Wu et al., 2021). It affected the width of the northern North Sea basin with extensional influence reaching the West Shetland basin and rift axis located underneath the Horda Platform (Bell et al., 2014; Færseth, 1996; Wu et al., 2021). Throughout the Triassic continental deposits accumulated in the rapidly subsiding rift system, coarse-grained fluvial deposits accumulated closer to the basin margins, while finer-grained alluvial and floodplain deposits accumulated in the basin center (Vollset & Doré, 1984). The climate gradually changed from arid to humid simultaneously with the northward drift of Pangea during the Middle Triassic to Late Jurassic (Nystuen et al., 2014). The rifting event developed easterly tilted pre-Jurassic half grabens bounded by several N-S striking, large displacement basement involved normal fault systems (Færseth, 1996; Thompson et al., 2022; Wu et al., 2021).

The Late Triassic to Late Jurassic marks a period of tectonic quiescence and post-rift thermal subsidence on the Horda Platform (Gabrielsen et al., 2010; Whipp et al., 2014), resulting in the deposition of an almost tabular inter-rift sedimentary package consisting of fluvio-deltaic to shallow marine deposits (Thompson et al., 2022; Whipp et al., 2014; Wu et al., 2021). This comprises the Statfjord Group, the Dunlin Group, the Brent Group, and the Viking Group (Figure 2.2).

Renewed rifting occurred in the Late Jurassic to Early Cretaceous (Bell et al., 2014; Færseth, 1996; Underhill & Partington, 1993; Whipp et al., 2014). The initiation and cessation of the secondary rift event throughout the northern North Sea are interpreted as diachronous, rift initiation on the Horda Platform is set to Bajocian (167-170 Ma) (Bell et al., 2014). Rift initiation was likely driven by the Middle to Late Jurassic collapse of the Central North Sea thermal dome and far-field tensional stages related to the opening of the Arctic North Atlantic rift system (Bartholomew et al., 1993; Bell et al., 2014; Whipp et al., 2014). Resulting in marine conditions in the area, with shale accumulations in basin centers and marine sands on the basin flanks and highs (Vollset & Doré, 1984). The secondary rift event is characterized by large-scale reactivation of the N-S striking Permian-Triassic faults, but also the formation of new smaller NW-SE striking faults that cross-cut or abut the larger faults (Bell et al., 2014; Duffy et al., 2015; Færseth, 1996; Whipp et al., 2014). Late Jurassic to Early Cretaceous rifting resulted in the formation of the trilete North Sea rift system, which includes the Viking Graben, Moray Firth, and Central Graben (Bell et al., 2014; Davies et al., 2001)

2.1.3 Lithological description

An in-depth description of the nearly tabular fluvio-deltaic to shallow marine inter-rift sedimentary package observed on the Horda Platform, comprising the successions from the Statfjord Group to the Viking Group sandstones, deposited in the first intra-rift phase (Thompson et al., 2022; Whipp et al., 2014; Wu et al., 2021).

2.1.3.1 The Statfjord Group

The Upper Triassic to Lower Jurassic Statfjord Group conformably overlies the Triassic Hegre Group on the Horda Platform. Its base is characterized by the turning point between an upwards

fining to an upwards coarsening mega-sequence (Deegan & Scull, 1977; Halland et al., 2011; Lervik, 2006). The Statfjord Group consists of the Raude, Eiriksson, and Nansen formations (Figure 2.2), revealing the transition from a semi-arid alluvial plane to dominantly fluvial sandstones with marine influence in the uppermost part (Halland et al., 2011). The group is well developed in the Viking Graben, thinning both NW towards Tampen Spur and SE towards the Horda Platform (Halland et al., 2011). The large thickness variations are due to regional differential subsidence.

The red-colored Raude Formation consists of silty claystone with sandstone and dolomitic limestone, a variable but low sand/shale ratio with a kaolinitic rich matrix (Deegan & Scull, 1977; Røe & Steel, 1985). Large scale cross-bedding, scour and fill dominate the sedimentary structures in the upper part of the formation and are interpreted as braided stream deposits in a semi-arid alluvial plane (Halland et al., 2011). The transition into the overlying fluvial dominated sandstones of the Eiriksson Formation is sharp or gradational, likely caused by the progressively more humid climate conditions during the Rhaetian- Sinemurian (Deegan & Scull, 1977; Røe & Steel, 1985; Ryseth, 2001). The Eiriksson Formation is characterized by massive sandstones interbedded with hard micaceous and carbonaceous rich shales. The sandstones contain thin horizons of very coarse granules, pebbles, and lignite fragments. It is interpreted to be deposited in a proximal braided stream as part of a coastal to shallow marine fan-delta system (Røe & Steel, 1985). Deegan and Scull (1977) interpreted the formation as a marginal marine environment, varying from coastal backswamp to coastal barriers, due to marine fossils and glauconite documented in the upper part of the formation. The Nansen Formation is composed of homogeneous, medium-to-coarse, calcite-cemented sandstones and a subordinate kaolinite matrix (Deegan & Scull, 1977). Glauconitic material is common for the formation and the upper part contains shaly beds with presence of marine fossils, reflecting a more open marine depositional environment likely caused by a transgressional phase prior to the deposition of the marine mudstones of the Dunlin Group (Deegan & Scull, 1977; Røe & Steel, 1985; Ryseth, 2001).

2.1.3.2 The Dunlin Group

The Dunlin Group was deposited during the Early Jurassic (Hettangian to Bajocian) (Partington et al., 1993), in a thermally subsiding basin during the tectonic quiescence following the first rift phase (Gabrielsen et al., 2010). The Lower Jurassic Dunlin Group, a major marine

transgressive sequence, overlies the Statfjord Group on the Horda Platform (Halland et al., 2011). It comprises the Amundsen, Johansen, Burton, Cook, and Drake formations (Figure 2.2) (Deegan & Scull, 1977; Thompson et al., 2022; Vollset & Doré, 1984). The Dunlin Group occurs on the western (United Kingdom) and eastern (Norway) side of the Viking Graben, except for the Johansen Formation, which is confined to the Horda Platform (Marjanac & Steel, 1997).

The group mainly consists of dark argillaceous marine sediments, with presence of well-developed light, fine to medium-grained, well-sorted marine sandstones at several stratigraphic levels in the marginal areas of the basin (Vollset & Doré, 1984). The Amundsen Formation mainly comprises light to dark gray siltstones and shales (Vollset & Doré, 1984). The exclusively marine formation was deposited in an outer shelf environment (Marjanac & Steel, 1997) during a period of regionally extensive transgression, draping the underlying Statfjord Group (Ryseth, 2001; Sundal et al., 2016). The Amundsen Formation is subdivided into a lower and upper unit as it interfingers with the Johansen Formation at the Horda Platform (Marjanac & Steel, 1997).

The Johansen Formation is typically subdivided into three units; lower, main and uppermost unit (Vollset & Doré, 1984). The lower unit is dominated by upwards coarsening, medium to fine-grained well-sorted sandstones, the main unit is composed of poorly cemented medium-grained sandstones, and the uppermost unit is composed of upwards fining medium to fine-grained micaceous sandstones (Vollset & Doré, 1984). The Johansen Formation was deposited on a high-energy shallow marine shelf, with sediments sources from the east (Halland et al., 2011; Vollset & Doré, 1984). It was deposited as a westward prograding delta system with internal geometries characterized by basinward-dipping clinoforms (Marjanac & Steel, 1997; Sundal et al., 2016). During an aggradational phase, NNW-SSE oriented sandy spit bar deposits developed. Rapid transgression and retrogradation dominated the latest stage of deposition and resulted in prevented significant erosion resulting in the preservation of the spit deposits (Sundal et al., 2016). The Johansen Formation is present on the Horda Platform with a maximal thickness of 160 m (Thompson et al., 2022).

The Burton Formation consists of marine mudstones deposited in an open marine basin (Halland et al., 2011; Vollset & Doré, 1984). Towards the margins in the east, the basinal facies of the Burton Formation encounter and grade into the Amundsen Formation. It is absent on the Horda Platform but located over wide areas of the northern North Sea.

The Cook Formation is dominated by sandstones on the Horda Platform and western margins, conformably overlying the Amundsen Formation, or unconformably the Johansen Formation (Sundal et al., 2016). Based on the depositional environment and basin geometry, the sandstones of the Cook Formation can be divided into three units (Vollset & Doré, 1984). The first is a unit comprising centimeter-to-decimeter thick tidally influenced heterolithic facies, progradational basinward-dipping deposits deposited in a lower to middle marine shoreface environment after the initiation of sea-level fall (Marjanac & Steel, 1997). The second is characterized by millimeter-to-centimeter thick wave-generated sand beds with form-discordant ripple-lamination. The final unit comprises units of fine-to-coarse grained massive or cross-stratified sandstones, referred to as the Cook sandstones, characterized by blocky to abrupt upwards coarsening patterns. Alternating presence of cross-stratification, great basinward extent, and coarseness indicate the presence of both tidal and fluvial influenced deposits (Halland et al., 2011; Marjanac & Steel, 1997). The depositional environment represents a tidal-dominated deltaic to outer estuarine setting.

The uppermost part of the Dunlin Group is the mudstones of the Drake Formation, deposited during sea-level rise in a pro-delta and delta-front environment (Halland et al., 2011; Vollset & Doré, 1984). The Drake Formation either interfingers or overlies the Cook Formation on an abrupt ravinement surface (Marjanac & Steel, 1997). It can be divided into a lower part of homogeneous upward-fining shallow-marine mudstones and an upper part of coarse-grained deposits of mixed shales, siltstones, and sandstone lenses (Thompson et al., 2022).

2.1.3.3 The Brent Group

The uppermost Lower Jurassic to Middle Jurassic Brent Group overlies the Dunlin Group conformably (Figure 2.2). On the Horda Platform, the Brent Group consists of the Oseberg, Rannoch, Etive, Ness, and Tarbert formations (Deegan & Scull, 1977; Halland et al., 2011). The Brent Group records a massive outbuilding of a major deltaic sequence from the western and northern side of the Horda Platform (Halland et al., 2011; Helland-Hansen et al., 1992). It is commonly subdivided into three units; lateral sediment infill of the Oseberg Formation, progradation of the Brent delta represented by Rannoch, Etive and lower part of Ness formations, and the retrogradation of the delta and drowning the Brent Group represented by the upper part of Ness and Tarbert formations (Helland-Hansen et al., 1992). The North Sea thermal dome reached its maximum in the Aalenian, and the tectonic uplift led to a basinward

shift in the sediment transport direction during the deposition of the early lateral infill of the Oseberg Formation (Underhill & Partington, 1993).

The deposition of the Oseberg Formation is a response to relative sea-level fall, and the homogeneous, medium to coarse-grained, shallow marine sandstones are sourced from the east (Halland et al., 2011; Helland-Hansen et al., 1992). Wave-reworked sand units in the upper part of the formation represent a transgressive unit during relative sea-level rise. The overlying Rannoch Formation is dominated by well-sorted, upwards-coarsening mica-rich sandstones (Deegan & Scull, 1977; Vollset & Doré, 1984). Deposited as a part of a major regressive wedge, during the progradation of the Brent Delta, in a lower to middle shoreface environment (Helland-Hansen et al., 1992). A gradual transition into the less micaceous sandstones of the Etive Formation marks a change into an upper shoreface depositional environment (Deegan & Scull, 1977). The grey-brown to clean, fine to massive coarse-grained sandstones of Etive show presence of calcite carbonate stringers on the Horda Platform (Deegan & Scull, 1977; Vollset & Doré, 1984).

Recording of predominantly simple transition from marine delta-front to continental delta-plain of the Ness Formation, implies a straight shoreline progradation of the Rannoch-Etive deposits (Helland-Hansen et al., 1992). Heterolithic delta-plain deposits containing coals, mudstones, siltstones, and fine to medium sandstones characterizes the Ness Formation (Deegan & Scull, 1977). The formation is highly carbonaceous with rootlet horizons and grey fissile shales (Vollset & Doré, 1984). It can be divided into a lower progradational unit dominated by upward-fining fluvial sand bodies and an upper retrogradational unit (Helland-Hansen et al., 1992). The marginal marine Tarbert Formation overlies the continental deposits of the Ness Formation. The retrogradational succession comprises fine to medium massive sandstones with occasionally thin silt, shale and coal bands (Deegan & Scull, 1977). On the Horda Platform, the formation displays a coarsening-upward sequence with increasingly argillaceous deposits downwards (Vollset & Doré, 1984). In some areas, the deposition of the uppermost Ness and Tarbert formations occurred simultaneously with the Middle Jurassic to Early Cretaceous rifting (i.e, Second rift event) (Helland-Hansen et al., 1992). The thermal dome of the northern North Sea collapsed in Callovian times in addition to rising sea levels, bringing back marine conditions to the area (Vollset & Doré, 1984)

2.1.3.4 The Viking Group

The fully marine Viking Group conformably overlies the Brent Group, and on the Horda platform it comprises the Heather, Krossfjord, Fensfjord, Sognefjord, and Draupne formation (Vollset & Doré, 1984). The proximal sandstones of the Krossfjord, Fensfjord, and Sognefjord formations are restricted to the Horda Platform and deposited as a part of the observed nearly tabular inter-rift sedimentary package with little thickness variations (Thompson et al., 2022; Whipp et al., 2014; Wu et al., 2021). During the depositional period of the costal shallow marine formations Krossfjord, Fensfjord, and Sognefjord, the Horda Platform was a passively subsiding block in a period of relative tectonic quiescence, with the Øygarden Fault complex controlling along the eastern margins (Whipp et al., 2014). The Krossfjord Formation overlies the shelfal deposits of the Heather Formation, the unit is medium to coarse-grained, well sorted with a slightly argillaceous and carbonaceous lower portion (Vollset & Doré, 1984). The overlying Fensfjord Formation displays similar characteristics but a higher grade of consolidation, often carbonaceous and occasionally mica rich (Vollset & Doré, 1984). The sandstones of the Sognefjord Formation are friable to unconsolidated, clean, and weakly micaceous and argillaceous. The upper boundary of the Formation is marked by a distinct change in lithology to the mudstones of the Draupne Formation (Vollset & Doré, 1984). Within the lower part of the Sognefjord Formation two 10- to 60-meter-thick coarsening upwards regressive-transgressive units are distinguished, each with internal architecture corresponding to westerly dipping subaqueous delta-scale clinoform sets (Patruno, Hampson, Jackson, & Dreyer, 2015). The clinoforms were sourced from a river outlet in the northeast, prograding westward over the Horda Platform displaying a sub-parallel orientation to the edge of the platform. Late Jurassic to Early Cretaceous marine flooding formed a marine depositional environment with anaerobic conditions and restricted bottom circulation, resulting in the highly radioactive and organic-rich deposits of the deep marine Draupne Formation (Vollset & Doré, 1984). Sognefjord Formation was deposited in the early phase of the second rift event, displaying thickness changes and minor rotated onlaps towards the N-S striking westward dipping Tusse Fault (Whipp et al., 2014; Wu et al., 2021)

The large thickness variations occurring within the Viking Group are caused by pre and syndepositional tectonic activities leading to deposition on tilted fault blocks (Vollset & Doré, 1984).

2.2 Theoretical background

2.2.1 Seismic signal processing

Seismic signals are typically transient waveforms generated from a localized man-made seismic source emitting a pulse. When emitted, seismic reflections are generated from interfaces where acoustic properties of the rocks change and form the basis of understanding seismic data (Brown, 2011). The acoustic impedance (AI) of a rock is the product of its compressional wave velocity (v) and bulk rock density (ρ) and affects the strength of the reflected seismic signal. Velocity and density vary as a function of depth and petrophysical properties, and impedance contrasts normally concur with lithological interfaces and determine the polarity of the seismic reflection. Hydrocarbon exploration and reservoir characterization in the subsurface greatly depends on the utilization of seismic reflection data.

Seismic imaging of the subsurface is done by measuring the time (ms) seismic reflection waves take to propagate down to the interface and reflect up to the receiver (two-way-time; TWT). The seismic vertical resolution generally ranges from 1/8 λ to 1/4 λ and defines the ability to distinguish two closely spaced individual reflectors (Brown, 2011; Sheriff, 1977). It has two limitations, the limit of separability, ¼ of a wavelength (λ) defining the minimum bed thickness corresponding to the closest separation of two wavelets. The limit of visibility, defining the minimum bed thickness before the reflected signal is masked by background noise, a variable fraction of a wavelength-dependent on the acoustic impedance (Brown, 2011).

The wavelength is the quotient of the formation velocity and predominant frequency (Eq 1), which increases and decreases with depth because of compaction and quicker attenuation, respectively. Consequently, wavelength increases with depth resulting in poorer resolution (Brown, 2011).

$$\lambda_d = \frac{v}{f_d} \tag{1}$$

A seismic reflection is described as a reflection point. From wave theory, this reflection point is the center of the area of reflection integration, known as the Fresnel zone, defined as the reflecting interface zone where seismic energy is reflected back at the receiver within half of a wavelength, constructively interfering to increased reflected signals (Denham & Sheriff, 1981;

Lindsey, 1989). The horizontal resolution can be described by the Fresnel zone, and reflectivity changes in distances less than the Fresnel zone will be masked by the seismic expression (Brown, 2011; Lindsey, 1989). Hydrocarbon exploration and reservoir characterization in the subsurface greatly depends on the utilization of seismic reflection data. In three-dimensional (3D) seismic data, the dimensions of the data are matched with the dimension of the earth, providing a data volume for easier visualization. Exploration can be acquired systematically over an area, with cross-sections derived in any orientation within the seismic survey.

Seismic polarity defines if the seismic wiggle drawn on the seismic section represents a negative or positive reflection amplitude number (a trough or a peak) (Veeken, 2007). According to the Society of Exploration Geophysicists (SEG) polarity convention, seismic polarity can be divided into normal and reverse polarity conventions. Normal polarity convention defines an increase in acoustic impedance with depth, registered on the field tapes as a negative number, as a trough. A peak represents an increase in acoustic impedance with depth registered on the field tapes as a positive number. The opposite is true for the reverse polarity convention. The seismic polarity convention for a survey can be defined by analyzing a seismic reflector with a known or predictable acoustic impedance (Brown, 2011). For example, the seabed reflector represents an increase in acoustic impedance when transitioning from water to sediments. An oil-water contact also represents a downwards increase in acoustic impedance when transitioning from a hydrocarbon-saturated unit into a water-saturated unit. The GN10M1 survey is consistent with the normal polarity convention, as the seabed reflection and the Troll flatspot event is identified by a peak, that represents a downward increase in acoustic impedance.

2.2.2 Clinoforms

A clinoform is a sigmoidal sedimentary body recognized on numerous scales, formed by aggradational and progradational processes on shelf margins, continental margins, deltas, and shorelines in both siliciclastic and carbonatic systems (Johannessen & Steel, 2005; Patruno & Helland-Hansen, 2018). The clinoform term was previously used to describe the dipping depositional surface observed at shelf margins, the sloping sigmoidal part (Rich, 1951). Now it is used to describe the seaward-dipping foreset, the topset and bottomset are located up-dip and downdip, respectively (Gilbert, 1885; R. Steel & Olsen, 2002). Clinoforms are building out

from shallow basin margins into deep waters, displaying basinward-fining sedimentary deposits and accretionary units like clastic wedges and prisms, representing basic regressive-to-transgressive blocks bounded by major transgressive flooding surfaces in the stratigraphic succession (R. Steel & Olsen, 2002). The term clinothem refers to the rock body and its lithological details. The clinothem sedimentary prisms create platforms when deposited at the basin margin, while the clinoform refers to the dipping depositional surface within the prograding sedimentary prisms (Anell & Midtkandal, 2017; Rich, 1951; R. Steel & Olsen, 2002).

2.2.2.1 Clinoform morphology

A clinoform normally comprises a topset-, foreset-, and bottomset fragment (Figure 2.3) (Helland-Hansen & Hampson, 2009). The most proximal shallowest segment of the clinoform is represented by the topset, a gently sloping platform area normally with a basinward slope of >0.3° (Anell & Midtkandal, 2017; R. Steel & Olsen, 2002). The foreset marks the transition into the deeper water as the steepest sloping part of the clinoform, with an angle < 3°rearly exceeding 6°, and the length of the segment is dictated by water depth (Anell & Midtkandal, 2017; Johannessen & Steel, 2005). The bottomset represents the most distal part of the clinoform, displaying a reduction of slope angle that grades into the basin floor (Anell & Midtkandal, 2017; Johannessen & Steel, 2005).

The point of maximum curvature also referred to as the rollover point, can be observed at two places (Figure 2.3) when studying a clinoform profile. Their stacking patterns form the trajectory of the shoreline and shelf edge (Patruno, Hampson, Jackson, & Whipp, 2015). The proximal topset-to-foreset rollover point predicts the shoreline trajectory, and the foreset-to-bottomset rollover point the shelf edge trajectory. Flat to low angle downwards dipping trajectories indicates a stable to slightly falling relative sea-level dominated by erosion and sediment bypass into the deep water, associated with oblique clinoform types (Anell & Midtkandal, 2017; Johannessen & Steel, 2005; R. Steel & Olsen, 2002). High angle trajectories indicate an overall sea-level rise with greater sediment accumulations on the shelf, associated with sigmoidal clinoform types. The cycle of shelf progradation, aggradation, and retrogradation will be reflected in ascending, descending, and flat shoreline trajectories (Anell & Midtkandal, 2017).

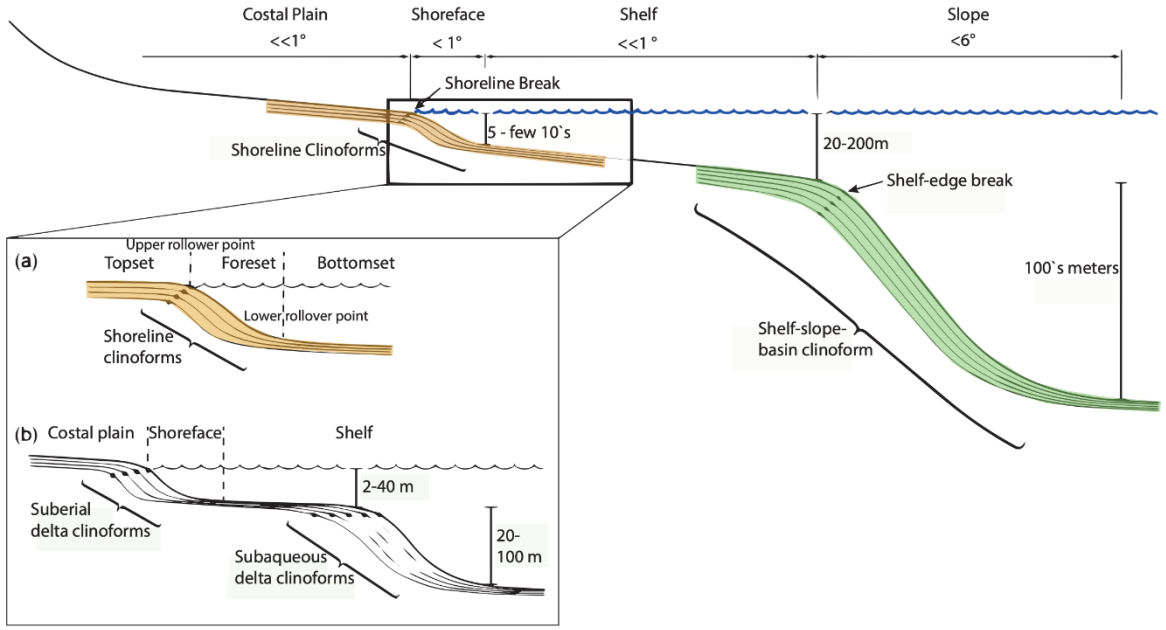

Figure 2.3 A simplified depositional-dip topographic profile, highlighting clinoform slopes, dimensions, and physiographic provinces. Clinoform development is related to water depth. Black outline emphasizes how development from coastal plain to shelf may consist of either a single (a) or a compound (b) clinoform set. Modified from (Helland-Hansen & Hampson, 2009)

2.2.2.2 Clinoform scales

Clinoform development is dominantly controlled by accommodation. Limited accommodation contributes to shelf-edge advance and low trajectory angles, while increasing accommodation contributes to increased shelf deposition and higher trajectory angles (Anell & Midtkandal, 2017). Clinoforms occur in various spatial scales based on clinoform morphology, outbuilding, and depositional settings, clinoforms can be divided into four basic types; 1-2) delta scale clinoforms, subdivided into shoreline and subaqueous clinoforms delta-scale, 3) shelf-edge clinoforms, 4) Continental-margin clinoforms (Figure 2.3) (Patruno & Helland-Hansen, 2018). The development of the different clinoform systems is associated as shoreline clinoforms transport sediments into the deeper basin where shelf-edge clinoforms are developing (Figure 2.3) (R. Steel & Olsen, 2002). To be seismically imaged clinoforms need a higher relief than the vertical seismic resolution, wider spacing than the tuning effect, and either lined with cemented carbonate layers or associated with boundaries of different acoustic properties (Patruno & Helland-Hansen, 2018).

Delta-scale clinoforms (tens of meters high) develop in a relatively short time and is related to shoreline progradation (Figure 2.3). They are characterized by low progradation/aggradation rates and relatively flat trajectory trends due to laterally extensive accommodation and sediment

supply proximity (Patruno & Helland-Hansen, 2018). A delta-scale clinoform may develop on the verge of seismic resolution (Helland-Hansen & Hampson, 2009). Shoreline delta-scale clinoform accrete where river systems meet still bodies of water. The fluvial-dominated sediments may be normally oriented to the river mouth or reworked by wave and tide-dominated processes resulting in alongshore and across-shelf deposits (Patruno & Helland-Hansen, 2018). Subaqueous delta-scale clinoforms develop where high energy water on the shelf transitions into low energy systems, they accrete basinward parallel to the shoreline and display greater preservation potential and maximum accumulation rates on foreset where wave and current influence decreases due to more proximal placement (Figure 2.3) (Patruno, Hampson, Jackson, & Dreyer, 2015).

Shelf-edge scale clinoforms (hundreds of meters high) develop at marine or lacustrine margins, in water depths of minimum few hundred meters separating shallow fluvial deposits from deepwater deposits (Figure 2.3). High angle trajectories, basial processes, and fine-grained sediments result in the development of clear sigmoidal shapes. (Patruno & Helland-Hansen, 2018). Continental margin scale clinoforms (thousands of meters high) develop at the outer edge of the shelf, usually mud-prone and dominated by low progradation/aggradation rates (Figure 2.3). In cases of high sedimentation rate and/or relative sea-level fall, sand deposition can occur beyond the shelf edge, resulting in reservoir-forming sandstone deposits in continental margin clinoform systems (Carvajal et al., 2009).

2.2.2.3 Clinoform geometries

The geometry and stacking patterns of a clinothem can provide information about tectonostratigraphic evolution of the depositional system, progradation and aggradation rates and sediment influx and related facies (Figure 2.4) (Patruno, Hampson, Jackson, & Dreyer, 2015; Patruno, Hampson, Jackson, & Whipp, 2015). Quiquerez and Dromat (2006) defined the three clinoform endmembers as oblique, tangential, and sigmoidal (Figure 2.4). Oblique clinoforms display a straight morphology and linear slope, described by a linear curvature deposited in periods of limited accommodation and sediment bypass dominating the topset resulting in sediment supply and deposition on the foreset and bottomset (Adams & Schlager, 2000; Anell & Midtkandal, 2017; Quiquerez & Dromart, 2006). Sigmoidal clinoforms with the clinoform characteristic s-shape described by a gaussian curvature, are associated with increasing accommodation and high depositional rate on the shelf (Adams & Schlager, 2000;

Anell & Midtkandal, 2017). Tangential clinoforms displaying a concave upwards morphology described by an exponential curvature are associated with a decrease in sediment transport exponentially from the sediment source (Adams & Schlager, 2000; Quiquerez & Dromart, 2006).

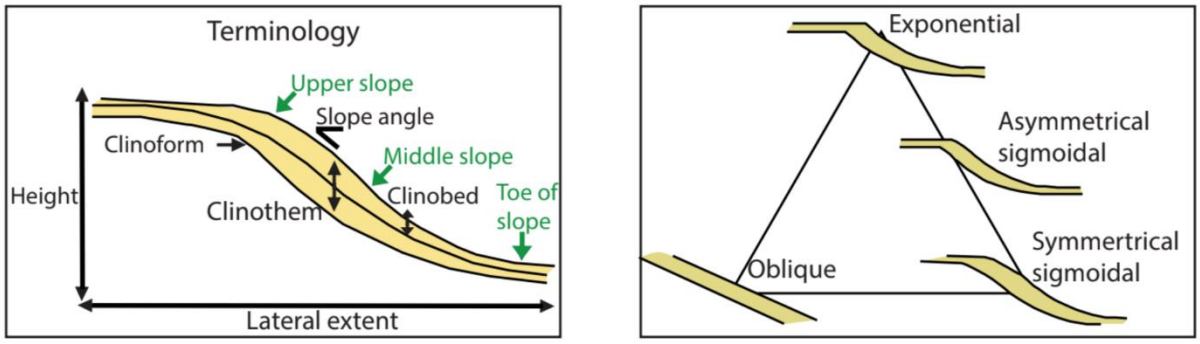

Figure 2.4 Simple model of terminology and definitions used in this study for clinoform description and analysis. Modified from(Quiquerez & Dromart, 2006).

2.2.3 Clinoform decompaction

The original depositional geometric shape of an ancient clinoform usually differs from its present-day shape (Deibert et al., 2003). Post depositional processes such as differential compaction, faulting, and erosion complicate the geometries of ancient clinoforms. They are usually semi-quantitatively described, and when compared with modern clinoform geometry analogs there will range an uncertainty to the value of the comparison (Klausen & Helland-Hansen, 2018).

Sediment porosity decreases as a function of burial depth, and mechanical compaction controlled by effective stress dominates the first part of sediment burial (0-2km depth). The main processes during compaction are grain crushing, fracturing, deformation, and re-orientating of grains as a function of composition, porosity, grain size, mineralogy, and sorting (Bjørlykke & Jahren, 2015). Coarse-grained minerals are more compressible than fine-grained minerals due to fewer grain-to-grain contacts, leading to higher stress per grain contact and more compaction (Fawad et al., 2011). A normal geothermal sedimentary basin is dominated by mechanical compaction until around 70-80 °C and 2 km depth, then precipitation of quartz cement occurs and stabilizes the mineral framework preventing further mechanical compaction (Bjørlykke & Jahren, 2015).

The mechanical compaction trend for sand and mudstones is very different, the critical porosity of mudstones (0.8-0.6) is much higher than for sandstones (0.38-0.5) caused by different grain shapes (Bjørlykke & Høeg, 1997). At shallower depths, there is a significant porosity reduction in the mudstones compared to a more even compaction trend in the sandstones. At larger depths, the low permeability of mudstone results in slower compaction as the compaction rate is a function of permeability (Bjørlykke & Høeg, 1997).

Chemical compaction occurs in sedimentary basins with high temperatures >70°C to drive dissolution and precipitation reactions that strengthen the rock and reduce its volume, which is considered the main driver for porosity reduction in sandstones (Bjørlykke & Jahren, 2015; Fawad et al., 2011). A kick in compaction of sandstones when entering the chemical compaction domain is the effect of quartz cementation dissolution and precipitation. For a progressively subsiding basin, chemical compaction transforms sandstones to quartzite with porosity close to zero (Bjørlykke & Jahren, 2015).

The effect of lateral changes in lithology within a clinoform may result in differential decompaction, as mud and sand deposits display different compaction trends. Potentially leading to tilting and altering of the clinoform geometry, dimensions, and depositional angles (Deibert et al., 2003). Clinoform decompaction is performed to restore the depositional geometric shape of clinoforms, providing a framework for discussing the clinoform development considering their restored geometric expressions. Hence, providing information regarding their depositional environment and distribution that potentially impact the lithological distributions within the Aurora storage complex.

2.2.4 CO_2 reservoir properties and storage mechanisms

In the North Sea, deep saline aquifers or depleted oil and gas fields display the greatest potential for suitable CO_2 reservoirs, as they provide sufficient porosity and permeability for injection of supercritical CO_2 at a feasible rate (Halland et al., 2011). The geothermal regime of the sedimentary basin, controlled by surface temperature and geothermal gradient, is one of the crucial factors regarding CO_2 sequestration (Bachu, 2003). CO_2 needs to be injected at its critical state to increase safety and efficiency within the geological storage unit, as it will act as a gas by entering all available volumes but in a dense liquid form. The supercritical state is reached at 31.1°C and 7.38 megapascals (MPa). In the North Sea, this state is reached at 800

meters or deeper below surface level (Halland et al., 2012). Cold reservoirs are more desirable than warm, as CO_2 density is directly dependent on temperature and CO_2 buoyancy increases in warmer reservoirs. The Johansen Formation within the Aurora storage site displays optimal storage at depths lower than 2000 meters in terms of porosity, as observations of increased quartz cementation with depth is existent (Fawad & Mondol, 2018).

The presence of heterogeneities within a storage reservoir that still provides efficient injectivity and maintains reservoir qualities could enhance secondary tapping mechanisms and increase storage potential (Hovorka, Doughty, Benson, et al., 2004). As heterogeneities contribute to dispersing the injected plume, better reservoir contact is attained, enhancing the CO_2 dissolution within the formation water (de Silva et al., 2015; Doughty & Pruess, 2004; Shukla et al., 2010; Zhang & Song, 2014). Resulting in enhanced secondary trapping mechanisms, providing better migration control, reducing early reliance on the primary seal, and is desirable to fully exploit the storage capacity within the Johansen Formation (Baklid et al., 1996; Doughty & Pruess, 2004; Flett et al., 2007; Hovorka, Doughty, & Holtz, 2004). Sequestration of CO_2 within a saline aquifer comprises four different trapping mechanisms, both physical and geomechanical (Shukla et al., 2010); i) Hydrodynamic trapping, ii) Residual trapping, iii) Solubility trapping, and iv) Mineral trapping (Zhang & Song, 2014).

Hydrodynamic trapping is the process of injecting supercritical CO_2 into a structural trap, sealed by low-permeable cap rock, to avoid migration of CO_2 to the surface (Gunter et al., 2004; Zhang & Song, 2014). Preferably CO_2 is injected downdip from the structural closure to facilitate residual trapping along the migration path to the final structural closure. Residual trapping, also referred to as capillary trapping, occurs when CO_2 within the pores is displaced by brine. The added pressure of brine traps and immobilizes significant saturation of CO_2 as small clusters within the pore brine (Halland et al., 2011; Zhang & Song, 2014).

Injected CO_2 initially acts as a separate phase from brine, through molecular diffusion, CO_2 dissolves and increases the brine density by approximately 1% (Zhang & Song, 2014). As denser brine sinks to the bottom of the reservoir, it enhances the mixing processes and the now denser brine will reduce upward migration of CO_2, increasing the storage capacity (Halland et al., 2011; Zhang & Song, 2014). When CO_2 dissolves as a part of the brine, it forms the beginning of geochemical processes. CO_2 may react with formation rock minerals to form stable minerals. This process is called mineral trapping and is the safest and most permanent sequestration method (de Silva et al., 2015).

3 Data and Methods

This chapter covers the data supporting this study, including a discussion of the limitations of the applied data. In addition, a description of methods and the workflow utilized in this study to achieve the main objectives.

3.1 Data

This section describes the data utilized in this thesis and the methods used to process, visualize, and interpret the data. The dataset includes 3D seismic data, well data, and imported interpretations. Surface interpretations performed by Holden (2021) and Sundal et al. (2016) (Gassnova, 2012) within the Dunlin Group and overlying Brent Group were imported into the dataset. This dataset has been used to create detailed seismic interpretations of the study area, and perform a detailed seismic facies analysis and clinoform analysis.

3.1.1 3D seismic data

The data utilized for this thesis is the 3D seismic survey GN10M1, which is a merge of several seismic surveys (Table 3.1). The GN10M1 survey has an aerial coverage of 1370 km^2 in the Norwegian blocks 31/2, 31/5, and the northernmost part of 31/8 within the Horda Platform (Figure 3.1) (Gassnova, 2012). The Aurora exploitation license, EL001, is located in the southern part of the seismic survey, while the Troll West Field is located in the northern part of the survey. The GN10M1 seismic survey domain is TWT and recorded down to 4000 ms TWT (Gassnova, 2012).

Seismic 3D	Acqusition year	Acerage km²	Inline direction	Company	Quality	Comments about quality
GN1001	2010	503	E-W	Gassnova SF	Excellent	Especially from to Draupne Fm down to Statfjord Fm
NPD-TW-08-4D-TROLLCO2	2008	293	E-W	Norwegian Petroleum Directorate	Good	Large number of faults in northern part
NH0301	2003	718	NE-SW	Norsk Hydro Produksjon AS	Good/very good	Excellent above top Brent GP, large number of faults
GN10M1	2010	1370	E-W	Gassnova SF	Good/very good	Fault interpretation better in NH0301 in the Troll West area

Table 3.1 Summary of the 3D seismic surveys used to merge the GN10M1 utilized in this thesis. Information about the seismic quality from Gassnova (2012) and surveys from the NPD Diskos repository.

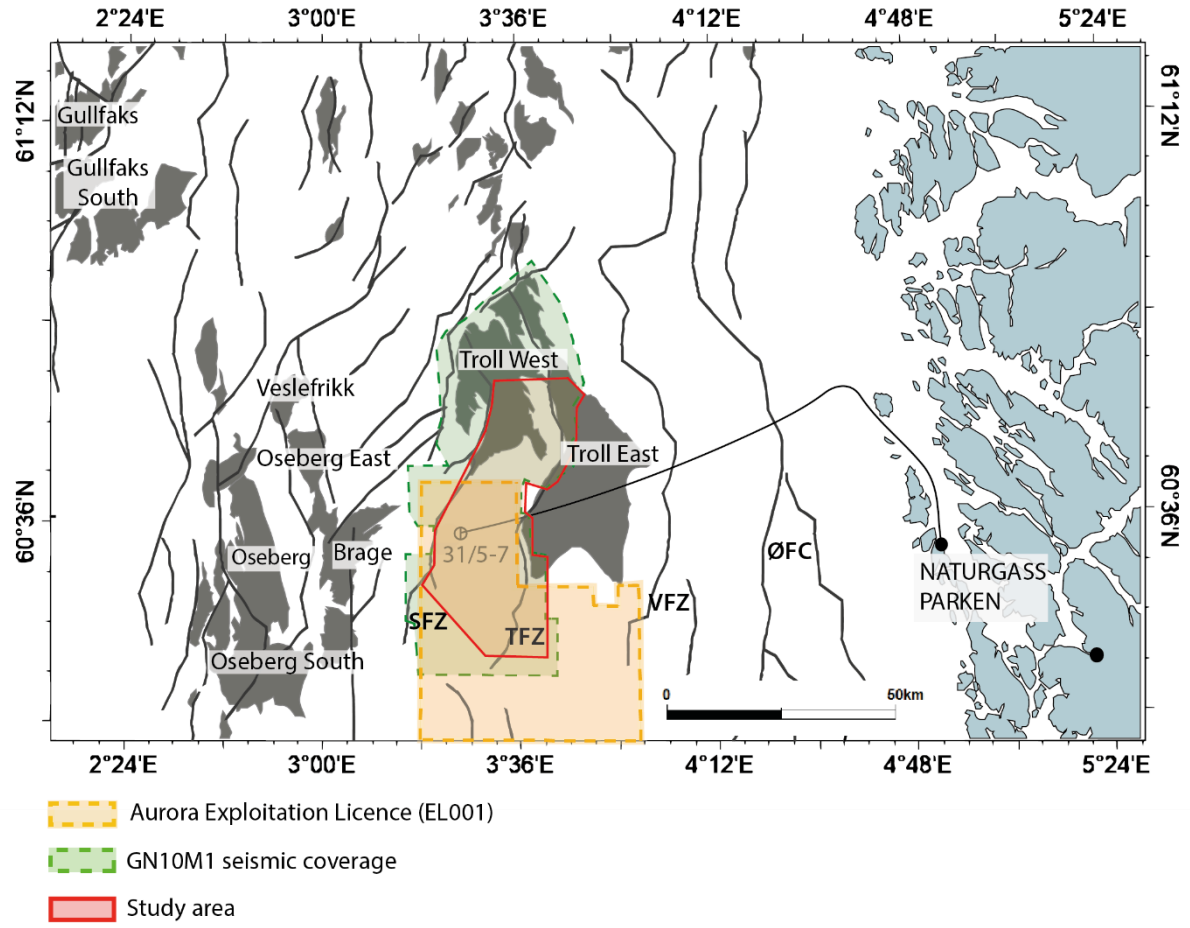

Figur 3.1 Map outlining the GN10M1 seismic survey coverage utilized in this thesis (green), outline of the Aurora Exploitation License (EL001) (yellow), outline of the defined study area (red). Location of the injectionwell 31/5-7 within the EL001, note that not all wells have been included in the map. Abbreviations: ØFC = Øygarden Fault Zone, VFZ= Vette Fault Zone, TFZ = Tusse Fault Zone, SFZ = Svartalv Fault Zone.

The 3D seismic survey GN10M1 is a pre-stack merge of the three 3D seismic surveys: GN1001, NPD-TW-08-4D-TROLLCO2, and NH0301 (Table 3.1)(Gassnova, 2012). The merge was performed through processing field data into the new seismic volume, with quality considered to be good to very good for the target depth of the Lower Jurassic storage complex. Inline traces trending W-E with a bin size of 25 m and the crossline traces trending N-S with a bin size of 12.5 m.

The GN10M1 survey is consistent with the normal polarity convention (outlined 2.2.1) (Veeken, 2007), as the seabed reflection and the Troll Flat spot identified within the survey display a downward increase in acoustic impedance as a peak. In this study, a peak (increase in acoustic impedance) is displayed using red, and a through (decrease in acoustic impedance) is displayed using blue. The Troll flatspot can also be analyzed to determine the phase of the seismic survey, as it is a high amplitude reflection known to represent a single sharp interface (Brown, 2011). The flatspot is characterized by a single high-amplitude reflection event with low and symmetrical side lobes, matching the zero-phase wavelet signatures. Hence, the GN10M1 seismic cube is interpreted as a zero-phase survey.

3.1.2 Well data

There were 46 wells available for analysis in this study. Only 26 of them are covered by the GN10M1 seismic survey, located in the Norwegian quadrant 31, in blocks: 31/8, 31/5, 31/2, and the western part of 31/6 and 31/3. Wellbore information was collected from the NPD Discos repository. 9 of the 26 wells penetrate the Lower Jurassic Johansen Formation storage complex and have been used to correlate well and seismic data and provide detailed lithological information (Figure 3.2). Six of the nine wells are located within the study area, the other three are within the GN10M1 coverage: 31/2-4, 31/2-3, 31/2-5. The majority of the wells used in this thesis are located north and northeast in the study area, close to the Troll West and Troll East fields (Figure 3.2, Table 3.2). 31/5-7 and 31/8-1 are the two wells located within the Aurora exploitation license EL001, only 31/5-7 is present within the study area. The Northern Lights project drilled the 31/5-7 confirmation well, as previously mentioned, it will be re-entered and used as the injector well within the Aurora storage site. It established a 116-meter-thick primary storage unit in the Johansen Formation, a secondary storage unit of 57 meters in the Cook Formation, and a 128-meter-thick seal in the Drake Formation at 2.6 km TVD RKB (Table 3.2).

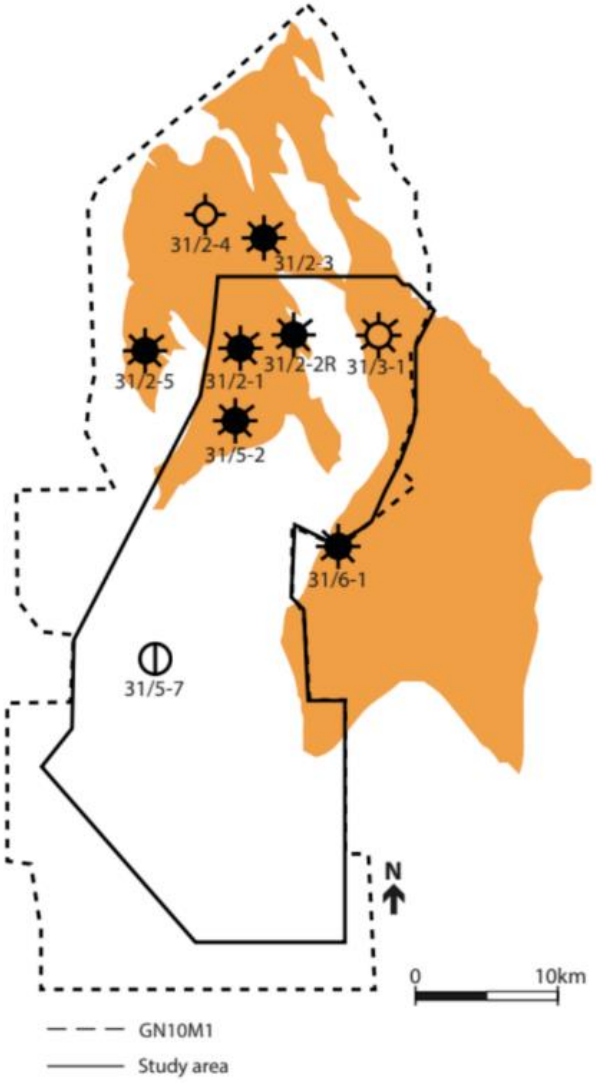

Figure 3.2 Map displaying the locations of the wells utilized in this thesis. Great well coverage in the north due to the Troll Field, only 31/5-7 present in the south. Dashed outlines mark the GN10M1 seismic coverage, and the solid outline marks the study area.

Figure 3.3 displays the nine utilized wells together with gamma-ray log to demonstrate and compare the variations in the main interpreted horizons. This includes the wells 31/5-7, 31/5-2, 31/2-1, 31/2-2R, 31/3-1, 31/6-1, 31/2-4, 31/2-3, and 31/2-5 (Figure 3.2, Table 3.2). Gamma-ray logs have been used to describe the lithological variations within the formations and different seismic facies expressions. Gamma-ray, neutron-density, sonic-logs, and resistivity log curve signatures have been used when creating well-ties (sub-section 3.2.1).

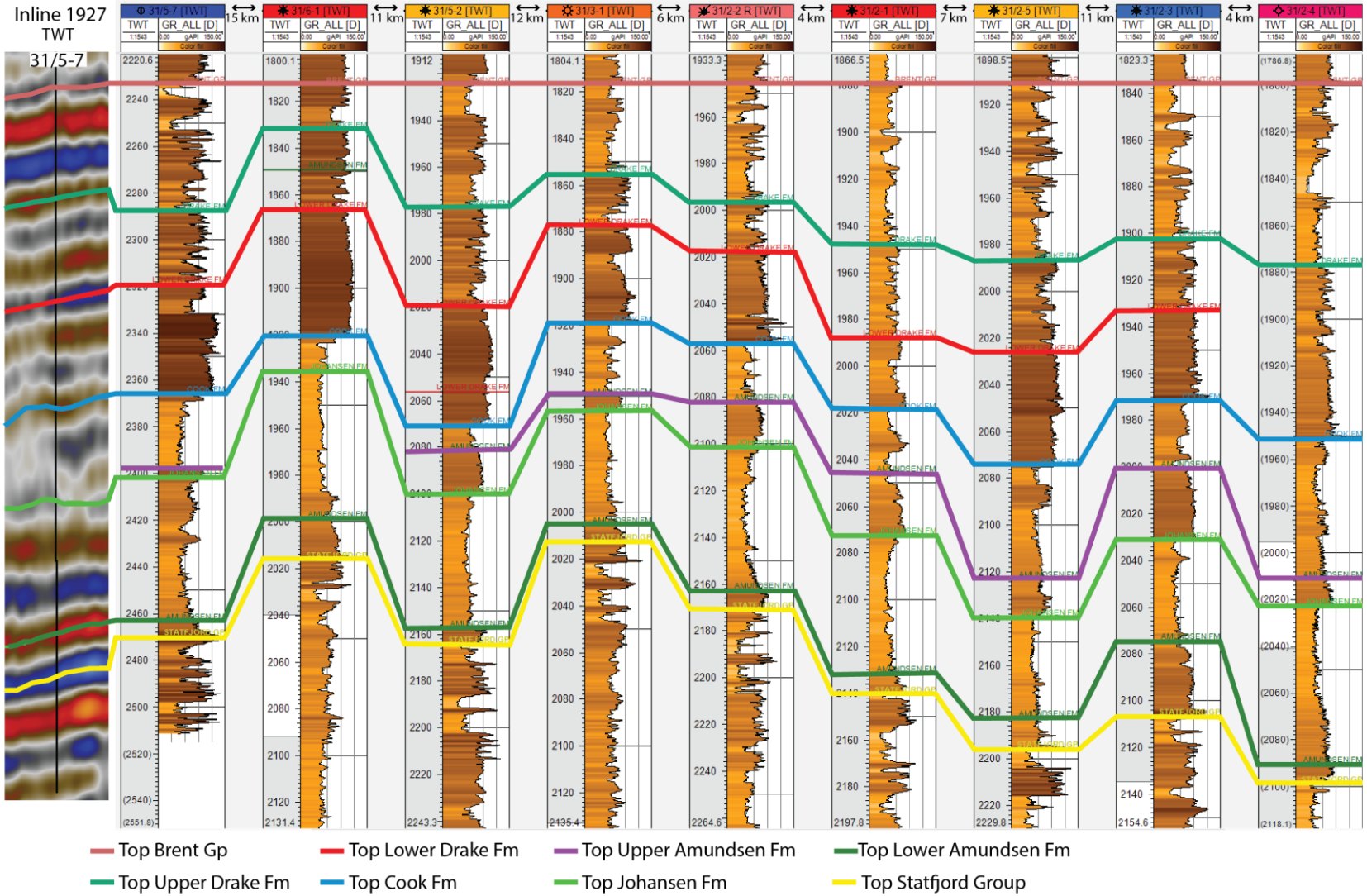

Figur 3.3 Well correlations flattened on Top Brent to display thickness variations within the Dunlin Group, gamma-ray logs and NPD formation tops. Seismic trace form 31/5-7 is displayed to view the seismic expression in the well. Formation tops in 31/5-7 are by Equinor ASA. Abbrevatitions: Fm = Formation, Gp = Group, GR= gamma-ray, TWT= Two-way-time.

Drilling opperator / Completed Date (year)	Equinor Energy AS	Saga Petroleum ASA	A/S Norske Shell	A/S Norske Shell	Den norske stats Oljeselskap a.s	Norsk Hydro Produksjon AS	A/S Norske Shell	A/S Norske Shell	A/S Norske Shell
	2020	1983	1979	1980	1983	1983	1980	1980	1980
Well name / Well top and depth (m MD RKB)	**31/5-7**	**31/5-2**	**31/2-1**	**31/2-2R**	**31/3-1**	**31/6-1**	**31/2-4**	**31/2-3**	**31/2-5**
Completed Date (year)	2020	1983	1979	1980	1983	1983	1980	1980	1980
Top Brent Gp.	2424	1956	1881	1985	1796	1805	1784	1811	1957
Top Upper Drake Fm.	2510	2036	1985	2070	1843	1835	1902	1902	2070
Top Lower Drake Fm.	2585	2102*	2044	2105	1881	-	-	1952	2135
Top Cook Fm.	2638	2175	2093	2162	1945	1962	2008	2010	2200
Top Upper Amundsen Fm.	2695	2194	2135	2202	1992	-	2106	2055	2277
Top Johansen Fm.	2702	2224	2175	2233	2001	1980	2126	2096	2308
Top Lower Amundsen Fm.	2818	2323	2272	2344	2088	2083	2241	2176	2380
Top Statfjord Gp.	2832	2336	2293	2360	2105	2110	2256	2236	2404

Table 3.2 Table displaying the drilling operator and date of completion of the wells utilized in this study. The depth of well tops and wells penetrating the storage complex within the study area. * Depth of the Lower drake Formation in 31/5-2 is inferred for this study, as for 51/5-7 the depth of Lower Drake Formation is acquired from Equinor ASA. Well locations are displayed in Figure 3.2.

3.1.3 Velocity Model

A northern Horda Platform velocity model was created by Emma Michie as a part of the NCCS team at UiO in 2021. The velocity model is applied to this study to convert data interpreted in time-domain (ms TWT) to depth domain (m), for performing clinoform decompaction analysis (Figure 3.4). The velocity model was created using quality-controlled average velocity from wells in the northern part of the Horda Platform: 35/12-3 S, 35/11-1D, 31/2-8, 31/2-19 S, 31/2-4 R, 31/1-1, 31/3-3, 31/2-2 R, 31/2-2, 31/5-6 31/5-2, 32/2-1, 32/4-1, 31/6-6, 30/6-5, 31/6-1, 31/4-3, 31/5-7, 31/6-2 R, 32/4-3 S, 31/8-1. The two-way time logs have been quality controlled to ensure that there are no serious mis-ties between well picks and adjacent seismic data.

The velocity model is purely dependent on the velocity of the lithologies the wells penetrate and does not account for gas accumulations of pore fills. This needs to be considered when analyzing the results generated from the velocity model, as the northern areas of the Aurora storage complex are located under large gas accumulations in the Troll field in the younger overlying strata and could potentially effect the seismic resolution.

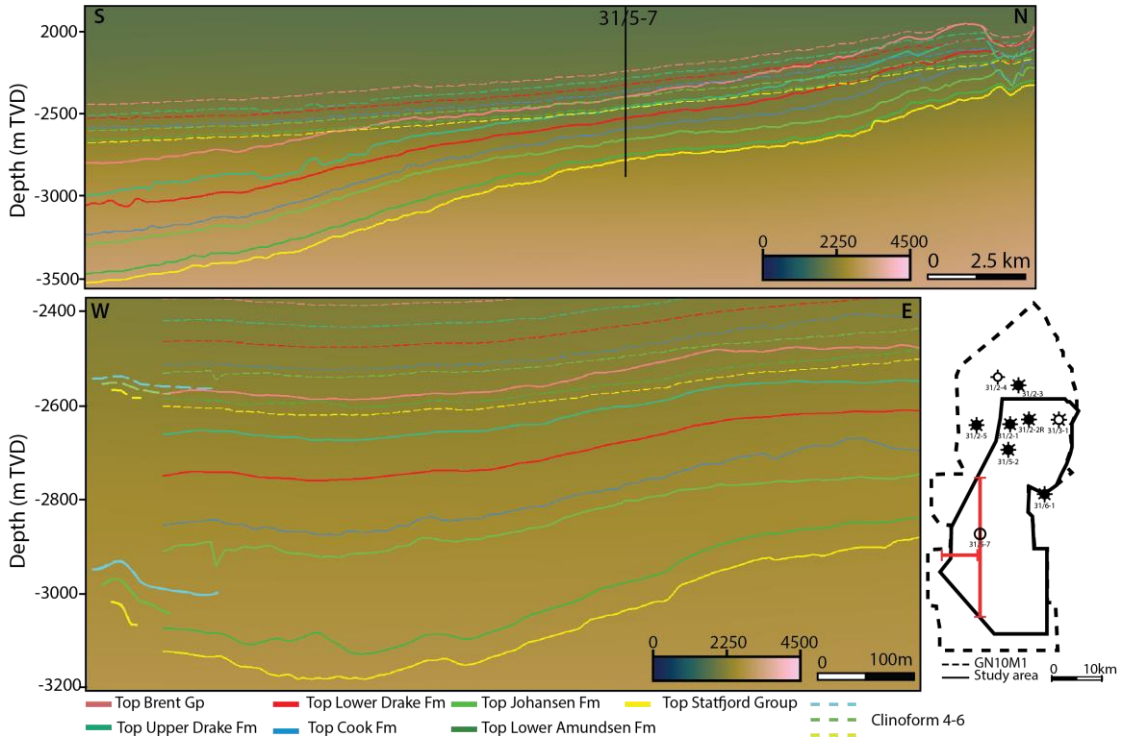

Figure 3.4 Seismic cross-sections displaying interpreted surfaces and clinoforms before (dashed lines) and after (solid lines) depth conversion utilizing the Northen Horda Platform Velocity model created by Emma Michie as a part of the NCCS UiO team in 2021. Preformed depth conversion with the aim of restoring clinoform geometry. Vertical exaggeration = 5.

3.1.4 Data limitations

As previously described in section 2.2.1, the vertical seismic resolution ranges from 1/8 to 1/4 of the dominant wavelength (λ_d) of the pulse (Sheriff, 1977). The dominant wavelength can be found by measuring the distance between peaks or by dividing seismic velocity (v) by the dominant frequency (f_d) of the seismic data (Sheriff, 1977). A simple estimation of the dominant frequency can be performed by measuring the time difference over a given set of peaks. In the GN10M1 seismic survey, ten peaks were measured at the depth interval from 2500 to 2700, and the time difference between all ten peaks was 0.293 seconds. Giving an average value of 0.0293 seconds between peaks, which results in a dominant frequency of 34 Hz (Eq 2). By using the previously described Northern Horda platform velocity model, the average velocity at 2500 m depth is approximately 2250 ms^{-1}.

$$f_d = \frac{1}{0.0293\ s} = 34\ Hz \quad \rightarrow \quad \lambda_d = \frac{v}{f_d} = \frac{2250\ ms^{-1}}{34\ Hz} = 66.18 \approx 66 \qquad (2)$$

The dominant wavelength of the GN10M1 survey is calculated to be 66 meters, and the vertical resolution ranges from 8.25 meters to 16.5 meters (λ/8 - λ/4), respectively. Features below the vertical resolution won't be visible in the seismic.

3.2 Methods

3.2.1 Well ties

In this study, 3D seismic data and wellbore data (outlined in 3.1.2) are utilized to identify and interpret stratigraphic surfaces, perform seismic well ties, and study the sedimentological and seimic facies development at the Aurora Storage site. Compared to the seismic data, the wellbore data provides higher vertical resolution but little lateral information. In areas with wellbore penetrations, the wellbore can be tied to the seismic data and provide points of higher data accuracy (Figure 3.5).

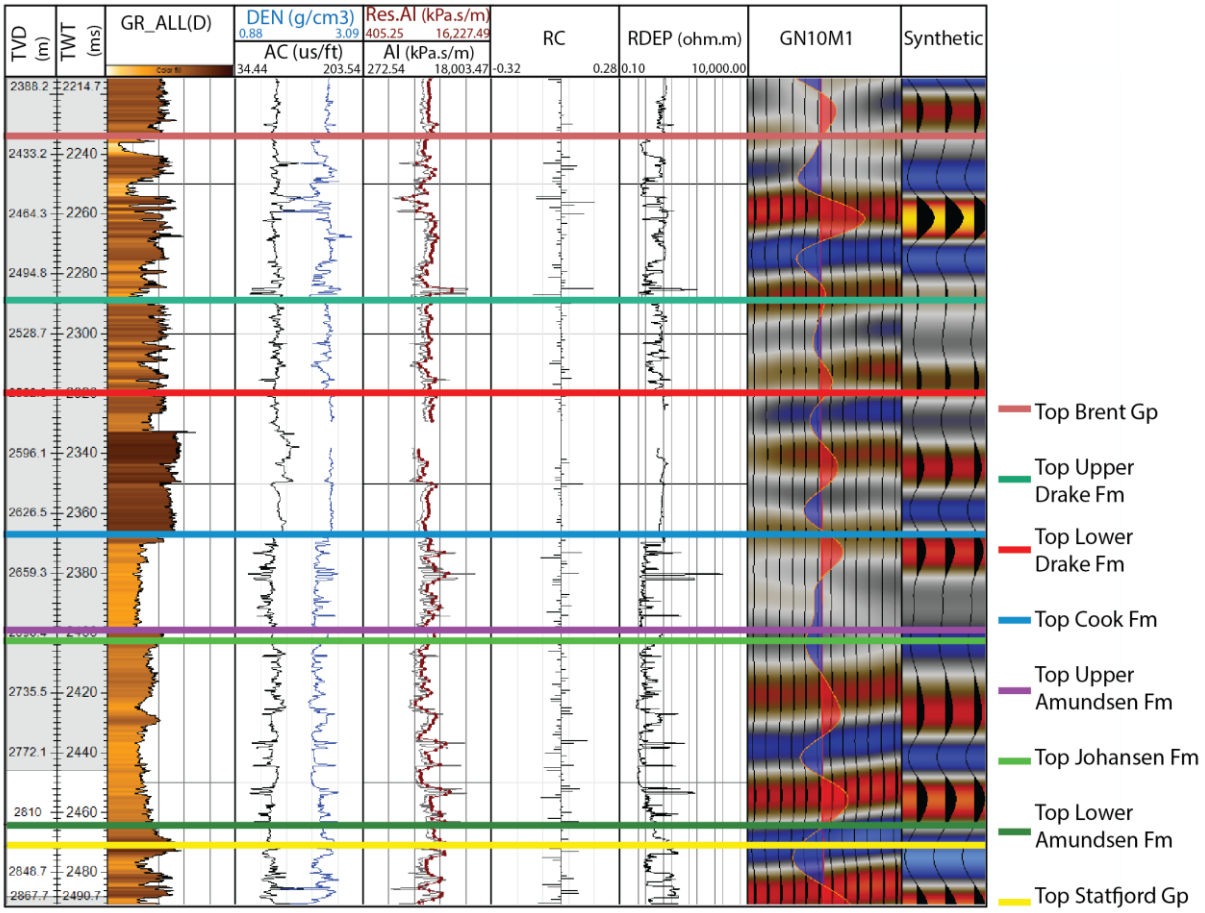

Figure 3.5 Well-tie for the injection well 31/5-7. Displaying the interpreted Formations, well log data and synthethic seismograms. Vertical scale in both TVD (M) and TWT (ms). Abbreviations : GR = Gamma-ray, DEN = Density, AC = Sonic, RES.AI = Resampled. AI, RDEP = Deep Resisitivity

3.2.2 Horizon interpretation

Detailed interpretation of the storage complex is essential to provide a detailed sedimentary analysis of depositional environments, sediment partitioning, seismic facies distributions and clinoform analysis. The main target unit for CO_2 storage within the Aurora storage complex is the Lower Jurassic Dunlin Group, including the Amundsen, Cook, Johansen, and Drake formations (outlined 2.1.3.2). The Amundsen Formation is subdivided into a lower and upper unit; the Lower Amundsen Formation overlying the Statfjord Group, and the Upper Amundsen Formation overlying the Johansen Formation. The Upper Amundsen is absent in the southern part and pinches out in the northern part, is considered too thin (7 m in 31/5-7), and lacks lateral continuity to provide the primary seal (Gassnova, 2012; Sundal et al., 2015). The Lower

Amundsen has been interpreted as the overlying reflector to Top Statfjord Group, which underlies the Dunlin Group.

The primary sealing unit, the Drake Formation, can be divided into a lower clay-rich unit with low permeability and high capillary entry pressure, and an upper unit comprising a higher degree of coarse-grained deposits (Gassnova, 2012). In similarity to Gassnova (2012), the Drake Formation is interpreted on two reflectors; the Upper Drake Formation and the Lower Drake Formation. Surface interpretations from Holden (2021) (Table 3.3) were imported into the project, covering the mid-part of the study area. The imported surfaces Top Cook Formation and Top Johansen Formation, were analyzed in detail before they were merged with interpretations generated in this study to produce one continuous surface. Imported surface interpretations by Sundal et al. (2016) were utilized for comparison.

Imported surfaces	Reflector pick	Reflector pick in Holden (2021)	Reflector pick in Sundal et al. (2016)
Top Brent Gp.	Peak	-	Trough (s-crossing)
Top Upper Drake	Peak	-	Trough
Top Lower Drake	Trough	-	s-crossing
Top Cook Fm.	Peak	Peak	-
Top Johansen Fm.	Trough	Trough	-
Top Lower Amundsen Fm.	Peak	-	-
Top Statfjord Fm.	Trough	Trough	-

Table 3.3 List of interpreted horizons within the GN10M1 3D seismic volume in this study. Reflectors picked in Holden (2021) and Sundal et al. (2016) are listed. Abrevatitions: Gp = Group, Fm = Formation.

Based on this information, the following seven horizons have been interpreted: Top Statfjord Group, Top Lower Amundsen Formation, Top Johansen Formation, Top Cook Formation, Top Lower Drake Formation, Top Upper Drake Formation, Top Brent Group. These seven interpretations bound five successions, referred to as the primary storage unit (e.g., the Johansen Formation), the secondary storage unit (e.g., the Cook Formation), and the primary seal unit (e.g., the Lower Drake Formation), the Upper Drake Formation and the Brent Group. Reflection picks have been performed based on well-ties to generate synthetic seismic (Figure 3.6).

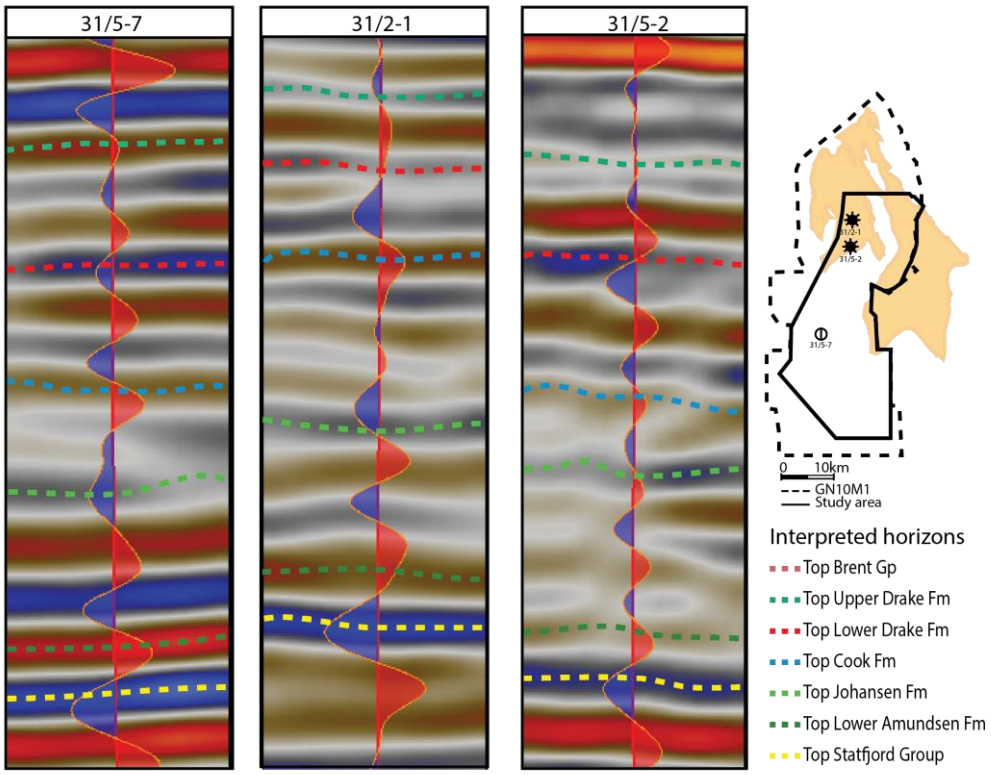

Figur 3.6 Seismic sections with generated synthetic wiggle traces and interpreted horizons (stippled) for three wells. Inserted map displays the location of the wells.

The first stage is the interpretation of the target horizons from survey inlines and crosslines (Figure 3.7). Firstly, horizon interpretations were performed on every 64th inline and crossline, generating a coarse grid with an 800x1600 meter resolution covering the whole study, then filling in the grid with closer inline and crossline spacing, systematically reducing the spacing increment by eight. The horizons of importance or high complexity were generated by interpretation on every 8th and 16th inline and crossline, respectively (Figure 3.7B). In areas of high structural complexity or faults of interest, an even denser spacing was applied. If the interpreted reflector is below the vertical resolution, the reflector above or belove has been selected for simplicity. Flattening on horizons is a useful technique when interpreting complex horizons, as this vertically shifts the seismic image to a horizontal datum representing basin geometry at the time of deposition. The seismic resolution in the area footwall of the Tusse Fault Zone is of poor resolution in the eastern part of the GN10M1, correlation with well 31/6-1 was applied to select accurate reflectors.

The created grid from interpreted inlines and crosslines creates a framework of the interpreted surfaces. By applying 3D-auto tracking to the interpretations, the un-interpreted areas are infilled (Figure 3.7C). The autotracking was performed with a confidence of 0.40.

Interpretations errors as a result of the auto-tracking were fixed by reducing the line spacing to improve and correct the interpretation. When the auto-tracked horizons reached a high-quality level and geologically validity, they were converted to surfaces displayed as time-structure maps (Figure 3.7D). All surfaces were generated with a 50 x 50 meter grid increment spacing, and fields within the study area with missing data were infilled by the surface generation (i.e., gaps in autotracking). As previously mentioned, interpretations by Holden (2021) covering the central part of the study area were merged with own finalized surfaces of Top Cook and Top Johansen formations as a measure to reduce the time spent on detailed interpretations.

Irregularities in the surface can be the effect of poor seismic resolution or complex reflectors, by applying a smoothing operation these irregularities are reduced (Figure 3.7E). This operation can lead to uncertainties or remove important geological features, therefore smoothing was applied no more than two times with an iteration and a filter width of one. The smoothed surfaces were then analyzed in seismic-cross section to validate that the surface still represented the geology of the subsurface. Variance seismic attribute map can better visualize structural features within the surface,

Seismic amplitude attribute maps provide stratigraphic and reservoir information (Brown, 2011). Displaying a derivative of basic seismic measurements such as time, amplitude, frequency, and attenuation. The post-stack Root Mean Square (RMS), minimum, and maximum amplitude seismic surface attribute maps were applied to the finalized surfaces. RMS computes the root mean square of single-trace samples, used to detect amplitude variations for channels with density changes to the surroundings (Figure 3.7F). A minimum amplitude attribute map is applied for surfaces picked on a through, and maximum amplitude is applied for surfaces picked on a peak. The final step in the horizon interpretation workflow was to create thickness maps by measuring the vertical thickness between two depth-structure surfaces (i.e., isochron map)(Figure 3.7G).

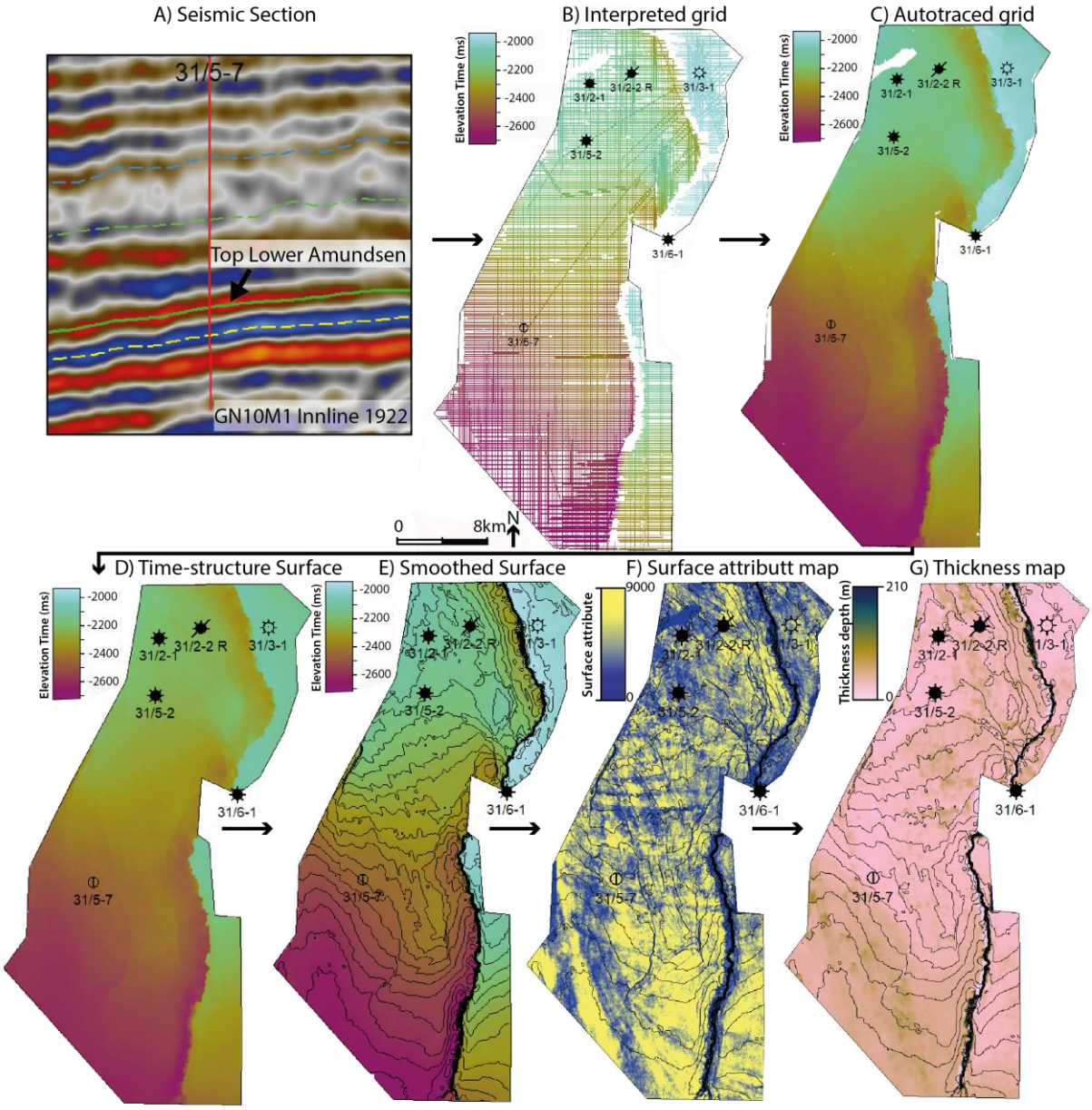

Figur 3.7 Figure illustrating the 7 step workflow of horizon interpretation. A) Pick horizon on seismic reflector. B) Generating a detailed interpreted grid, horizons of importance or high complexity were picked on every 8th and 16th inline and crossline respectively. C) 3D- autotracing applied for the interpreted grid. D) Time-structure map generated. E) Smoothed time-structure map with contour lines (increment spacing of 40). F) Surface attribute map. G) Thickness map of the Formation. Figre B-E utilizing "Hawaii" colour scale, Figure G is utilizing the "batlow" color scale from Crameri et al. (2020).

3.2.3 Seismic facies interpretations

Seismic facies interpretation and analysis are based on variations in seismic reflection records, characteristics and linking observed features to geological factors generating the reflections (Boggs, 2014). According to Rocksandic (1978), a seismic facies is a sedimentary unit

displaying different seismic characteristics than the adjacent sedimentary units. A thorough understanding of factors generating seismic reflections and the limits of the seismic resolution is critical for seismic facies and stratigraphy interpretations. Seismic amplitude is an indicator of bed thickness and spacing, and is affected by the fluid content of the sedimentary beds. No hydrocarbons have been encountered within the Johansen Formation (Sundal et al., 2016), and fluid content is confirmed as saline pore water (NPD Factpages, 2022)

Thick gas accumulations in the overlying Sognefjord Formation, the reservoir of the Troll Field are present in the northern part of the study area. The thick gas accumulation will have a strong effect on compressional waves, as the bulk modulus is severely distorted (White, 1975). Reflection amplitude and traveltime are highly affected by the presence of gas, and seismic processing can only marginally compensate for this effect. Therefore gas accumulations will influence the seismic signal and hence change the seismic signature of an area (Roksandic, 1978). This effect is especially important to take into consideration when interpreting seismic facies in the northern part of the study area.

3.2.4 Clinoform decompaction

Performed clinoform decompaction used herein follows the principles outlined in Klausen and Helland-Hansen (2018). Clinoform geometry and dimensions are potentially affected by sediment loading and compacting. Hence, decompaction from maximum burial is necessary for calculations of the original clinoform height and dip. Through decompaction, the aim is to restore the original depositional geometries of clinoforms, providing a systematic description and classification of the clinoforms to help the prediction of lithological distributions and facies (Klausen & Helland-Hansen, 2018; Patruno & Helland-Hansen, 2018).

An ideally paleohorizontal regional datum is defined above the clinoform to provide an important reference point for estimating relief, post-depositional compaction, or subsidence. This is performed to create a reliable framework for comparing clinoform geometries. Decompaction is performed on the succession between the investigated clinoform and a regional datum, according to the weight of the removed overburden (y1´n and y2´n), following the equation from Allen and Allen (2005), later modified by Patruno et al. (Patruno, Hampson, Jackson, & Whipp, 2015).

$$y2' - y1' = y2 - y1 - \left(\frac{\phi_0}{C}\right)\{e^{-Cy1} - e^{-Cy2}\} + \left(\frac{\phi_0}{C}\right)\{e^{-Cy1'} - e^{-Cy2'}\} \quad (3)$$

As described in Klausen and Helland-Hansen (2018), the equation input parameter y2 represents a point along the clinoform surface of interest, y1 represents the corresponding point on the reference datum above (Figure 3.8). y1´ is defined as the reference point at zero burial, assuming that y1´= 0 for simplicity, while y2´ is the corresponding point on the clinoform surface now shifted vertically relative to the new decompacted thickness of the strata. y2´-y1´ is the decompacted thickness, ϕ_0 represents the surface porosity utilizing a porosity constant given for the area. C is the compaction coefficient for the specified lithologies between the clinoform surface and its reference point (Klausen & Helland-Hansen, 2018). Decompaction was performed for a 50% sandstone/mudstone composition (ϕ_0 = 0.56, C = 0.39), sandstone end-member (ϕ_0 = 0.49, C = 0.27) and mudstone end-member (ϕ_0 = 0.62, C = 0.50), values adapted from (Midtkandal et al., 2020) which was inferred from Sclater & Christie (1980). Interpretations and clinoform measurements were carried out in seismic profiles parallel to the dip direction.

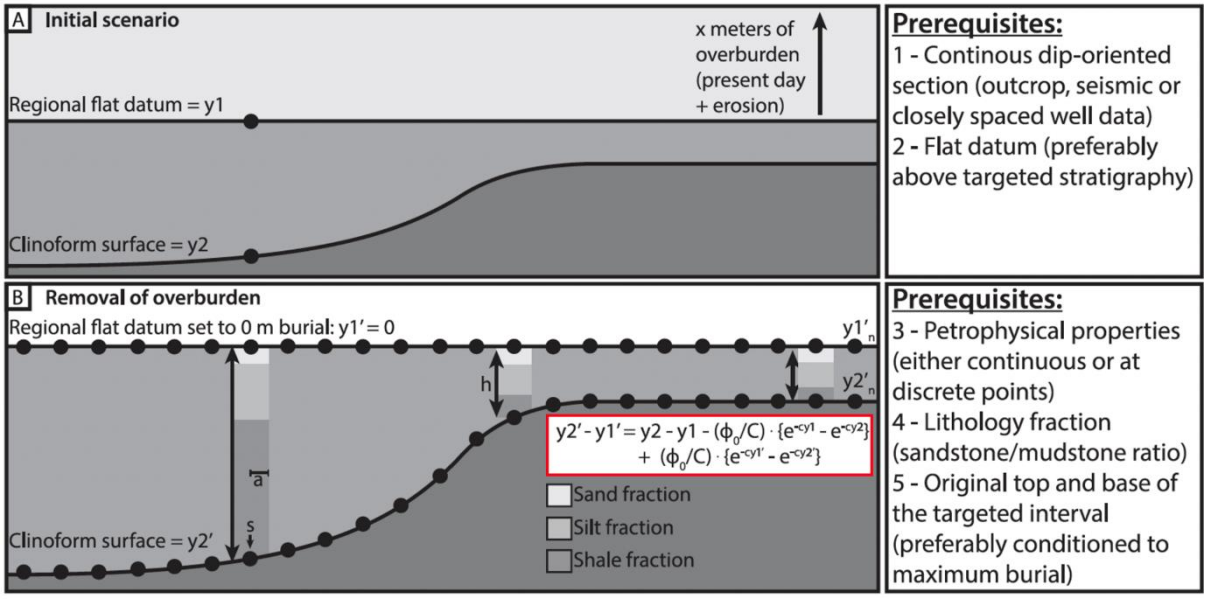

Figure 3.8 Conceptual model displaying the different steps to the performed clinoform decompaction. A) Clinform surface prior to decompaction. B) Decompaction of the strata between points in the reference datum (y1) and corresponding points on the clinoform surface (y2). Modified from (Klausen & Helland-Hansen, 2018).

Clinoforms were interpreted in the time domain as single horizons in the 3D seismic GN10M1 cube. Interpretations were depth converted, using the in-house Northern Horda Platform velocity model by Emma Michie (outlined in 3.1.4), to perform clinoform measurements in meters. The individual clinoforms length, height, foreset length, and foreset height were

measured (Figure 3.9). The length was defined as a horizontal measurement between the upper and lower inflection point of the clinoform, while the height was measured as the vertical distance between the two inflection points. The foreset length and height were measured at the steepest part of the foreset, to be able to calculate the foreset angle using the inverse tangent (Eq 4).

$$x = \mathrm{Tan}^{-1}\left(\frac{\mathrm{Height}}{\mathrm{Length}}\right) \tag{4}$$

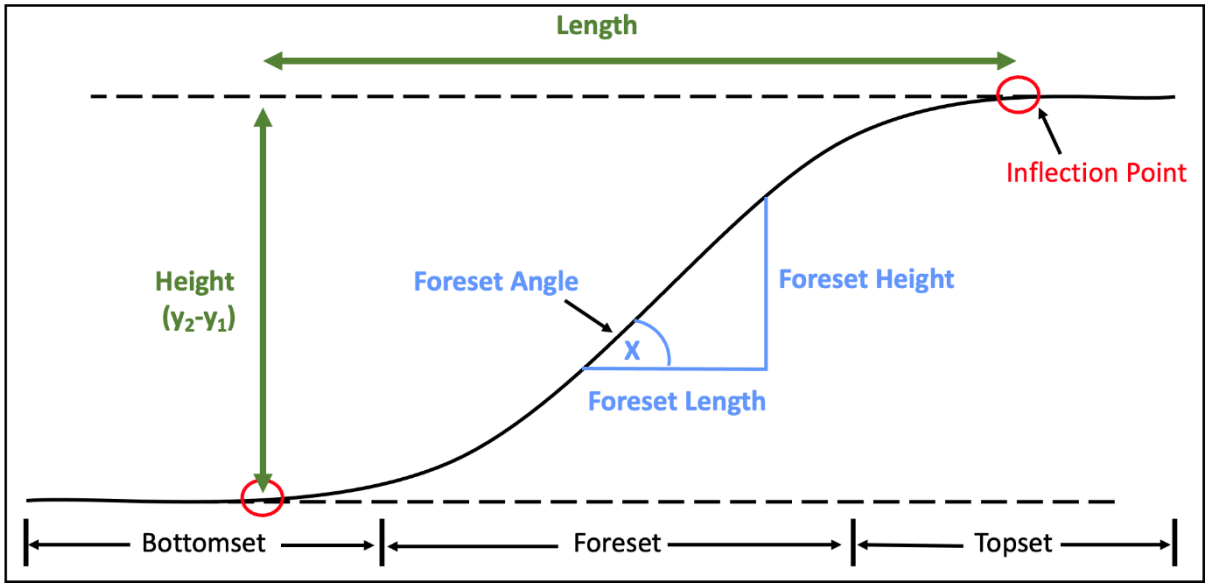

Figure 3.9 Illustrating the clinoform measurements that were measured in the depth converted GN10M1.

4 Results

The main objective of this study is to determine sedimentary environments and sediment partitioning within the Dunlin Group at the Aurora storage site, contributing to the understanding of the storage complex heterogeneity and pore-space reduction with high impact on storability and injection rates. The results presented in this chapter describe the seismic facies distributions (4.1), sedimentary distributions and stratigraphic architecture (4.2), and clinoform decompaction analysis (4.3). Figures are displayed in time-domain (elevation depth is given in TWT), with the exception of thickness maps and measurements for performed clinoform decompaction (elevation is given in meters).

4.1 Seismic facies analysis

In total six main seismic facies expressions are recognized and defined in the high-resolution data of the GN10M1. Great variations in seismic amplitudes are observed, frequency is less variable as a result of formation thickness in relation to seismic resolution and variations in reflection characteristics. The overlying gas accumulations of the Troll Field in the Sognefjord Formation may to some degree influence and weaken the seismic signal. Seismic facies characteristics in the gamma-ray are based on log signature and related lithological interpretation from well-logs.

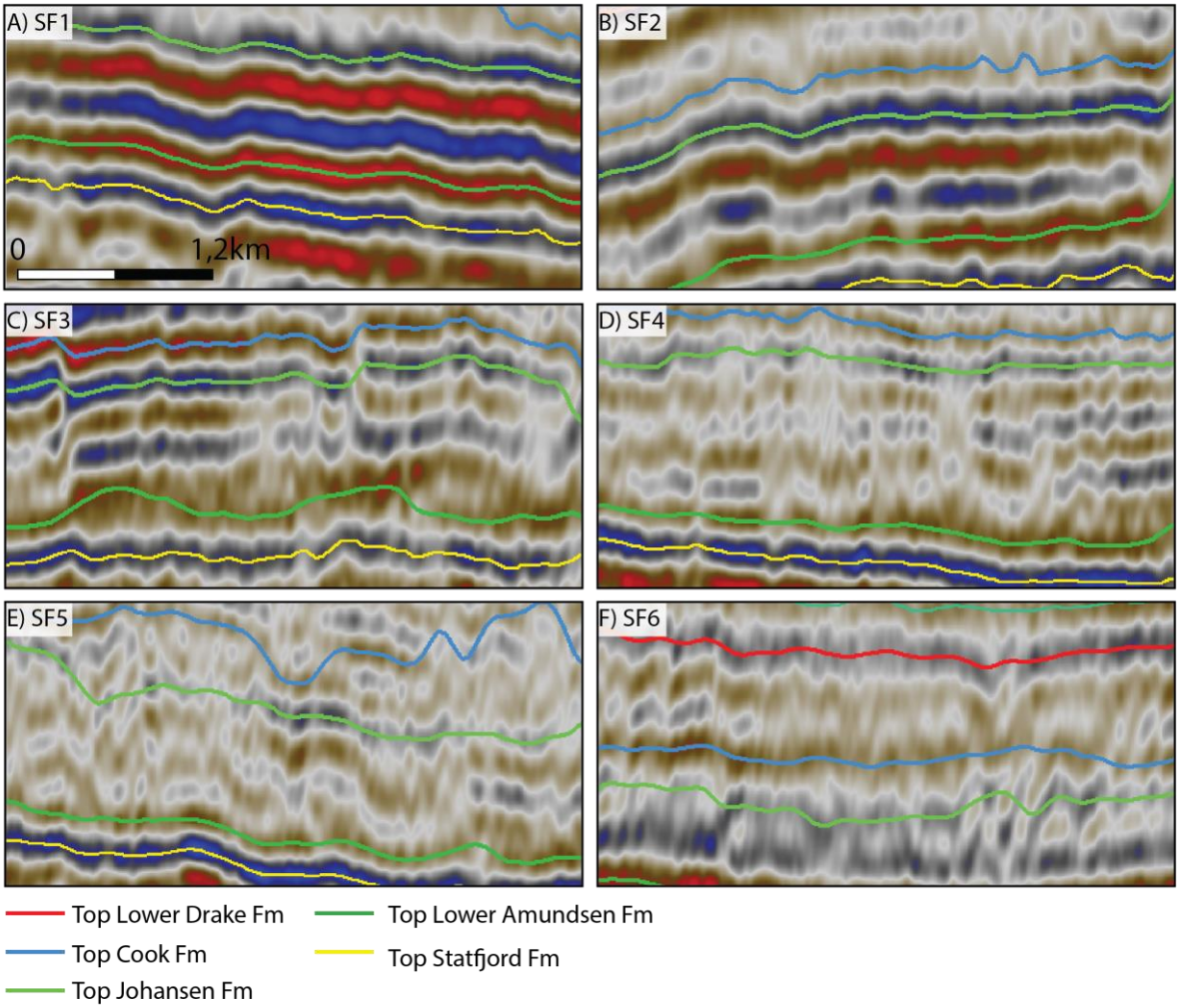

Figur 4.1 Seismic facies with examples from inlines in seismic 3D volume GN10M1. A) SF1. High amplitude parallel reflectors. B) SF2. Lower amplitude parallel reflectors. C) SF3 Sub-parallel reflectors (medium-low amplitude). D) SF4 Sub parallel to chaotic reflectors, internally terminating. E) SF5 Chaotic reflectors. F) SF6 tilted angular reflectors. Note that seismic inlines is displayed in time-domain

4.1.1 SF1- High amplitude Parallel Reflectors

4.1.1.1 Description:

SF1 is characterized by high amplitude (>6000-7000) parallel laterally continuous reflectors, and troughs generally display higher amplitudes than peaks (Figure 4.1A). It is mainly present in the southwestern part of the study area but also found further north in the Lower Drake Formation (Figure 4.2A). An NW-SE trending elongated body with high amplitude parallel reflectors are present southwest, measuring over 20 km in length, 2-3 km wide, and a maximum thickness of 170 meters. Well 31/5-7 penetrates the SF1 directly in the transition zone between the SF1 and SF3 (sub-parallel reflectors) within the Johansen Formation (Figure 4.2A).

4.1.1.2 Interpretation:

The high amplitude parallel reflectors and serrated gamma-ray log indicate heterolithic facies. Parallel reflectors imply that sediments were deposited at a uniform rate, on a uniform subsiding or stable basin. (Boggs, 2014). The high seismic amplitudes of SF1 could be a fluid effect or large property differences of the deposits. Well logs indicate sand-rich lithologies, yielding large impedance contrast due to over and underlying mud-rich lithologies (Figure 3.3).

Reflection continuity, dependent on density-velocity contrast continuity, indicates stratified continuous deposits. Bell-shaped gamma-ray signature in 31/5-7 (Figure 3.3) illustrates a coarsening and cleaning upward sand rich sub-sequence, with a sudden spike in gamma-ray values indicating presence of fine-grained mud deposits. The faint funnel-shaped gamma-ray signature of the upper part of Top Johansen Formation indicates upward fining deposits and a more mud rich sub-sequence.

4.1.2 SF2- Lower Amplitude Parallel reflectors

4.1.2.1 Description

SF2 is characterized by parallel reflectors that decrease in amplitude from the high amplitudes of SF1 (Figure 4.1A, B). Seismic amplitude values are relatively consistent below 4000-5000, but internal increases and decreases in amplitude are observed. The seismic facies is usually present in the transition from the high amplitude parallel reflectors of SF1. Towards the southern part of the study area, the peak displays a more disrupted seismic reflector than the continuous overlying trough. SF2 is most prominent on the western part extending from south to north in Top Lower drake, but also present southwest in Top Cook (Figure 4.2A,B). Well 31/5-7 penetrates the SF2 in Top lower Drake directly in the transition zone to SF4 (Figure 3.3).

4.1.2.2 Interpretation

Parallel seismic reflectors indicate deposition at a uniform rate, on a uniform or stable shelf/basin. Overall high gamma-readings reflect the presence of fine-grained mud-rich deposits in the Lower Drake Formation, the blocky cylindrical gamma-ray signature indicates little influence of sand-rich deposits. High amplitudes reflect significant property contrasts to over-and-underlying units, interpreted to be deposited in a high to medium energy system.

Lower amplitude values could reflect lower property differences or the lack of fluid within the sediments, potentially water-filled sandstone/mudstone lithologies. A protentional transition zone from the high amplitude parallel reflectors of SF1 into the more sub-parallel reflectors of SF3.

4.1.3 SF3- Sub parallel reflectors (medium-low amplitude)

4.1.3.1 Description

SF3 is characterized by sub-parallel reflectors with presence of internal terminations (Figure 4.1C) usually accompanied by a decrease in amplitude. The observed trend is that presence of internal terminations is usually most prominent on the peaks, displaying a discontinuous reflector. There is an alteration between reflectors that are sub-parallel with little to no internal terminations, and areas with higher internal terminations, leading to less parallel reflectors with buckling/ bending signals. The SF3 is dominant in the southern and central part of the Top Johansen Formation, present in the south, center, and north of Cook, only central and north in Top lower drake (Figure 4.2). The only well that pierces the SF3 in the Lower Drake is 31/3-1, located in the Tusse footwall.

4.1.3.2 Interpretation

Subparallel reflectors are evidence of a rather uniform depositional rate, on a uniformly subsiding or stable surface. The seismic facies displays less uniform deposits than for SF1 and SF2, with a higher degree of interaction with the depositional environment and degree of variable energy system. Internal reflector terminations indicate the presence of a lateral discontinuity.

4.1.4 SF4- Sub parallel to chaotic, internally terminating reflectors

4.1.4.1 Description

Overall higher amplitudes are present on troughs than for peaks, displaying overall lower amplitudes and partly disrupted reflectors terminating towards underlying reflector (Figure 4.1D). Internally terminating sub-parallel to chaotic reflectors dominates SF4, with discontinuous reflections of lower amplitude values appearing as spheres within the over and

underlying reflectors. The SF4 dominates the northern part of the study area but is also present in the southern area of the Johansen and Lower Drake formations (Figure 4.2A, C). Several wells penetrate the SF4 in the Johansen, Cook, and Lower Drake formations; 31/5-2, 31/2-1, 31/3-1, 31/5-7 (Figure 4.2)

4.1.4.2 Interpretation

The seismic facies could represent more heterolithic sediments, with vertical and horizontal frequent property changes, hence the internal terminations. Reflection terminations could also be resultant of seismic resolution, with layer thicknesses below the seismic resolution.

4.1.5 SF5 - Chaotic reflectors

4.1.5.1 Description

The SF5 is characterized by chaotic reflectors and highly disordered arrangement of reflecting surfaces with little to no recognizable stratal pattern (Figure 4.1E). Overall low amplitude values with discontinuous and untraceable reflections are present. The seismic facies are not dominant in extensive areas but are present in the north of Johansen and Cook formations. The presence of SF5 within the Johansen Formation, coincides with thickness increases observed in the seismic section (Figure 4.2C). No wells penetrate SF5, but wells are located nearby (31/5-2, 31/2-1).

4.1.5.2 Interpretation

Small reservoir property differences in the strata can lead to this observed chaotic signal, as seismic reflections are more prominent with presence of large property contrasts. A section with alternating sand and mud deposits would attain stronger seismic reflectors than the ones of SF5. This chaotic seismic expression may indicate more homogenous deposits, most likely sand-rich. SF5 is not penetrated by any wells, but 31/5-2 and 31/2-1 nearby (Figure 4.2) confirm sand-rich deposits with overall low gamma-ray values in the formations (Figure 3.3). Lacking chaotic seismic facies in the mud-rich Lower Drake Formation, indicates that the seismic expression is a result of clean sand deposits.

4.1.6 SF6 -Tilted angular reflectors

4.1.6.1 Description

The SF6 is characterized by tilted angular reflectors, reflectors downlap and terminate downdip toward underlying seismic reflectors of higher amplitudes (Figure 4.1F). The tilted angular reflectors have a westward dip. The expression of the tilted angular reflectors alters between clear continuous to more chaotic discontinuous reflectors. There is a clear trend of SF6 present in the southern footwall of the Tusse Fault, it is also present in the central part of the study area and the northern part of the footwall within the Johansen Formation (Figure 4.2C). 31/6-1 is located exactly in the transition zone from SF6 to SF4 within the Johansen Formation, hence, it may present a more accurate description of SF4 than SF6 (Figure 4.2).

4.1.6.2 Interpretation

From interpreted prograding clinoforms in the central part of the study area, displaying westward progradation implies a N-S trending coastline. Tilted angular reflectors may record the coastline progradation, displaying alternating lithologies of sandstones and silt/mudstone drapes. If the tilted angular reflectors represent beach and barrier island deposits, narrow accumulations of sand parallel to the coast would be expected. From seismic (Figure 4.1F), the tilted angular reflectors dip westward, but protentional striking N-S.

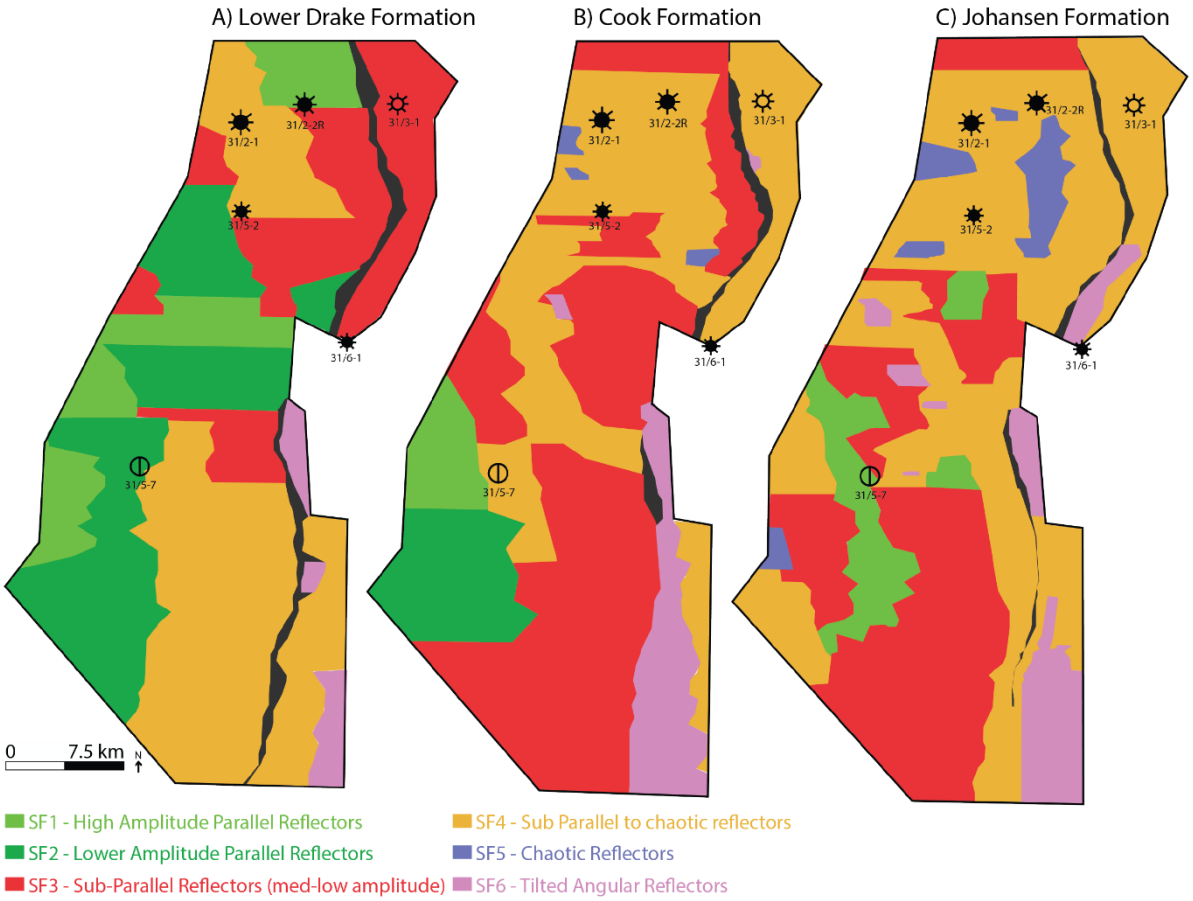

Figur 4.2 Map view of seismic facies distributions. A) Lower Drake Formation, B) Cook Formation (including Top Upper Amundsen Formation), C) Johansen Formation. Note that black infill represents the areas of the Tusse Fault zone that was not defined within the seismic facies map.

4.1.7 Seismic facies change

The seismic facies changes of the different formations are observed both vertically and laterally. In Figure (4.3), all seismic facies are displayed in the seismic composite line, except for SF6. The general trend in seismic facies expressions is an increased presence of high amplitude to lower amplitude parallel reflectors in the southern study area, with a northward increase in sub-parallel to chaotic seismic facies (Figure 4.4). Regionally changing seismic facies patterns are common and seismic facies expressions are locally changing from Johansen to the overlying Cook Formation (Figure 4.3, 4.4). Different seismic facies expressions within the Dunlin Group indicate a high grade of local sedimentary differences within the formations.

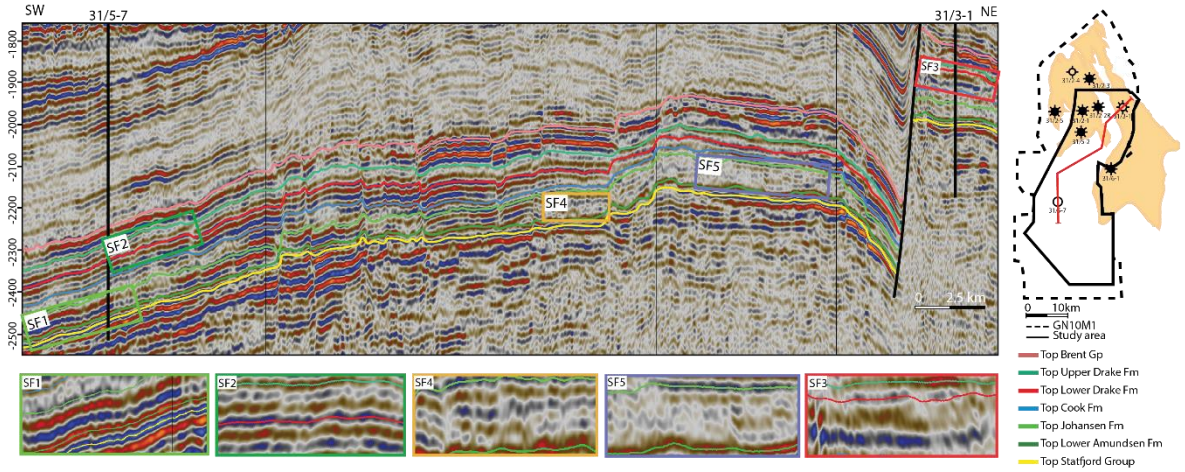

Figur 4.3 Seismic composite line, NE-SW rending. Location of composite line displayed in red on study-are map. The Composite line displays the seismic facies changes observed within the formations when moving across the study area, seismic facies SF1, SF2, SF3, SF4, and SF6. Vertical exaggeration 15.

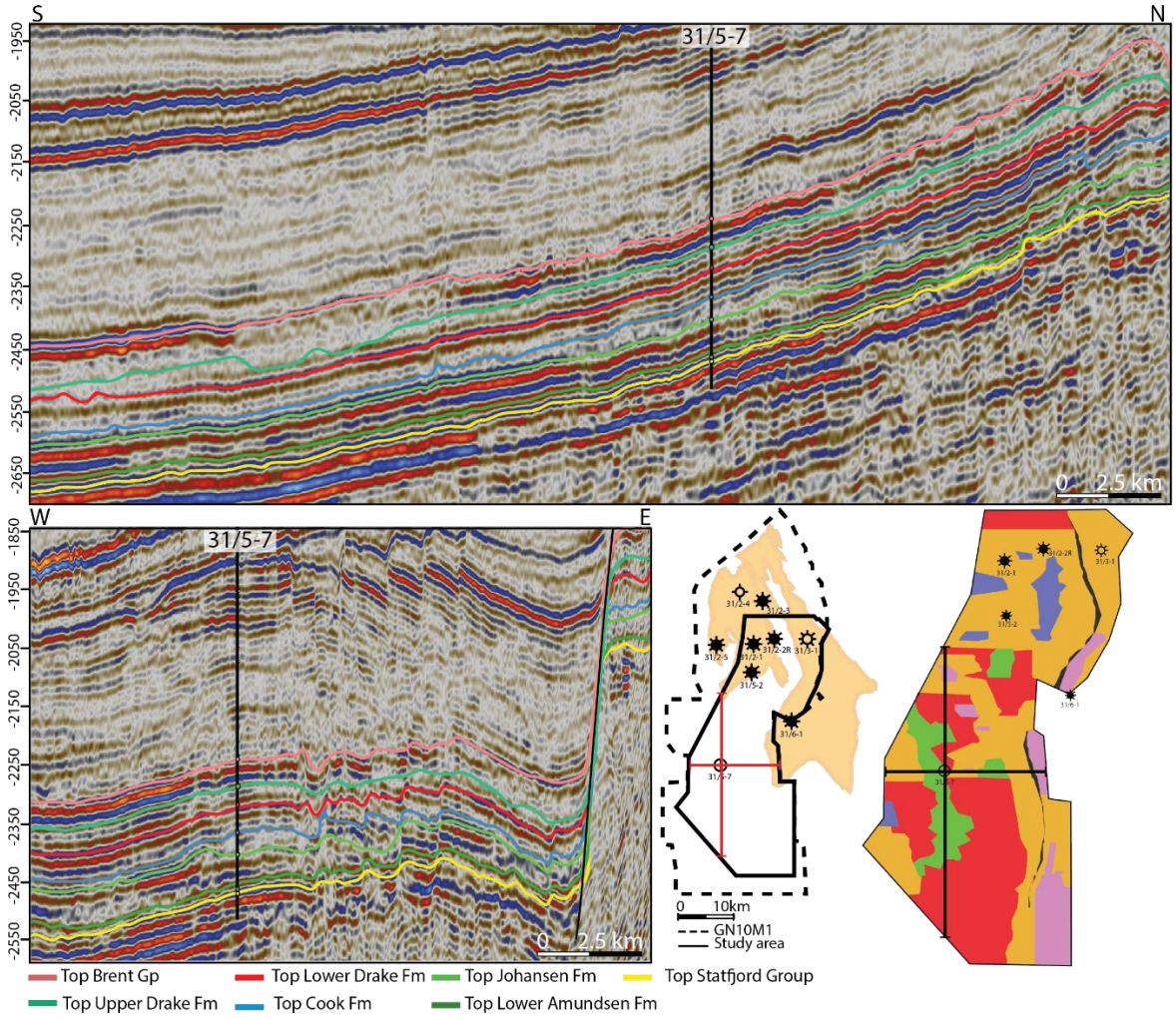

Figur 4.4 Correlation profile for injection well 31/5-7. Inline 1927 (upper seismic section) N-S trending perpendicular to 31/5-7. Crossline 3267 (lower section) E-W trending perpendicular to 31/5-7. Map view displaying the location of inline and crossline in red. Facies distributions in Johansen Formation facies map. Vertical exaggeration 15.

4.2 Stratigraphic characterization

Interpreted surfaces are presented in map view to describe the spatial distributions of the formations within the study area (Figure 4.5). The surfaces include Top Statfjord Group, Lower Amundsen Formation, Top Johansen Formation, Top Cook Formation, Top Lower Drake Formation, Top Upper Drake Formation, and Top Brent Group. The surfaces are interpreted and displayed in TWT (ms).

The time-structure maps display similar geometries. As the surfaces have a southern dip, the shallowest areas are located in the northern part of the study area. The structure maps display a northwest shallowing from the hanging wall creating a structural high (antiform). Along the northern part of the hanging wall, small-order transverse anticlines and synclines are observed, exhibiting a NE-SW striking fold axis.

The deepest successions are in the southern part of the study area and the hanging wall of the Tusse Fault Zone. Along the southern part of the Tusse hanging wall, small-order transverse anticlines and synclines display E-W striking fold axis (Figure 4.5A). In addition, slightly southeast of the injection well (31/5-7), there is a shallowing of the surface creating a high that continues N-W.

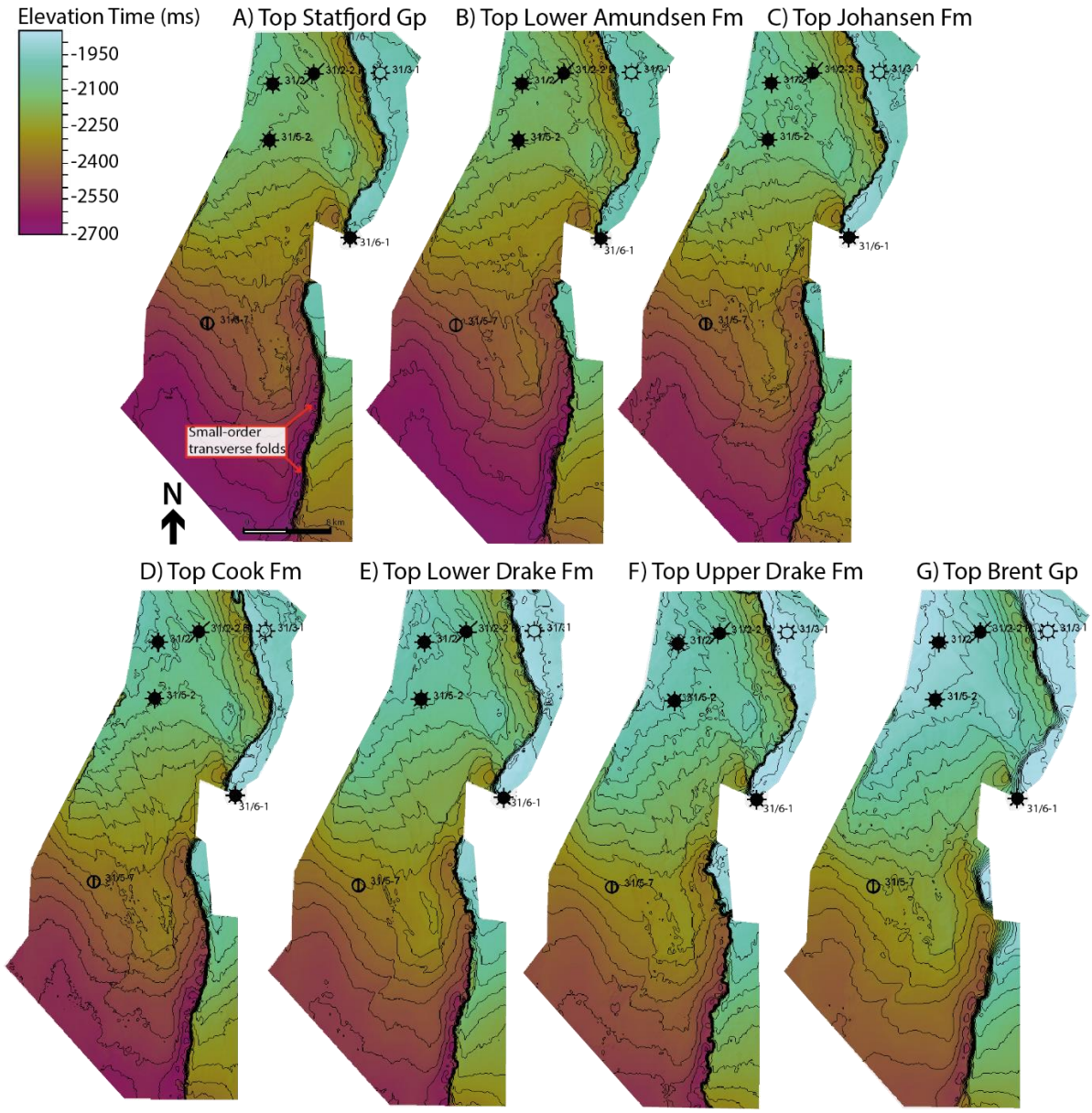

Figur 4.5 Time-structure maps in elevation time (TWT (ms) with contour line spacing of 40 meters. Small order transverse folds are present in Figure 1A).

4.2.1 Lower Amundsen Formation

4.2.1.1 Description

Lower Amundsen Formation displays uniform thickness with no significant thickness variations (Figure 4.6C). Along the Tusse Fault zone, there is an overall thickening towards the south, observed in both the hanging wall and the footwall, and Lower Amundsen measures approximately 20-25 meters in the north and 35-40 meters in the south. The formation reaches its maximum thickness of 40-60 meters in the southern part of the study area, thinning north of

the injection well (31/5-7) towards the footwall of the Svartalv Fault segment and thickens towards the hanging wall of the Tusse Fault Zone. The formation thickens (50-55m) in the southern part of the Tusse hanging wall, thins northward along the fault towards the center of the study area (30-35), and thickens in the northernmost part of the hanging wall (40-45).

The RMS attribute map displays a moderate NW-SE increase in amplitude in the southern area, no other distinct anomalies are present (Figure 4.6A). Conformity with the thickness map is present, and high RMS attribute values coincide with the greatest formation thickness in the southern area. Maximum amplitude attribute values coincide with RMS and the thickness map, displaying the highest amplitude anomalies towards the south (Figure 4.6B). NW-SE trending high maximum attribute values are present in the exact location of RMS.

Relatively high gamma-ray values are present for the Lower Amundsen Formation (Figure 4.7). 31/5-7 displays an upwards coarsening bell-shaped gamma-ray signature into the Johansen Formation, the same signature is present in 31/3-1, while 31/5-2 display an upward fining funnel-shaped gamma-ray signature for the Lower Amundsen Formation.

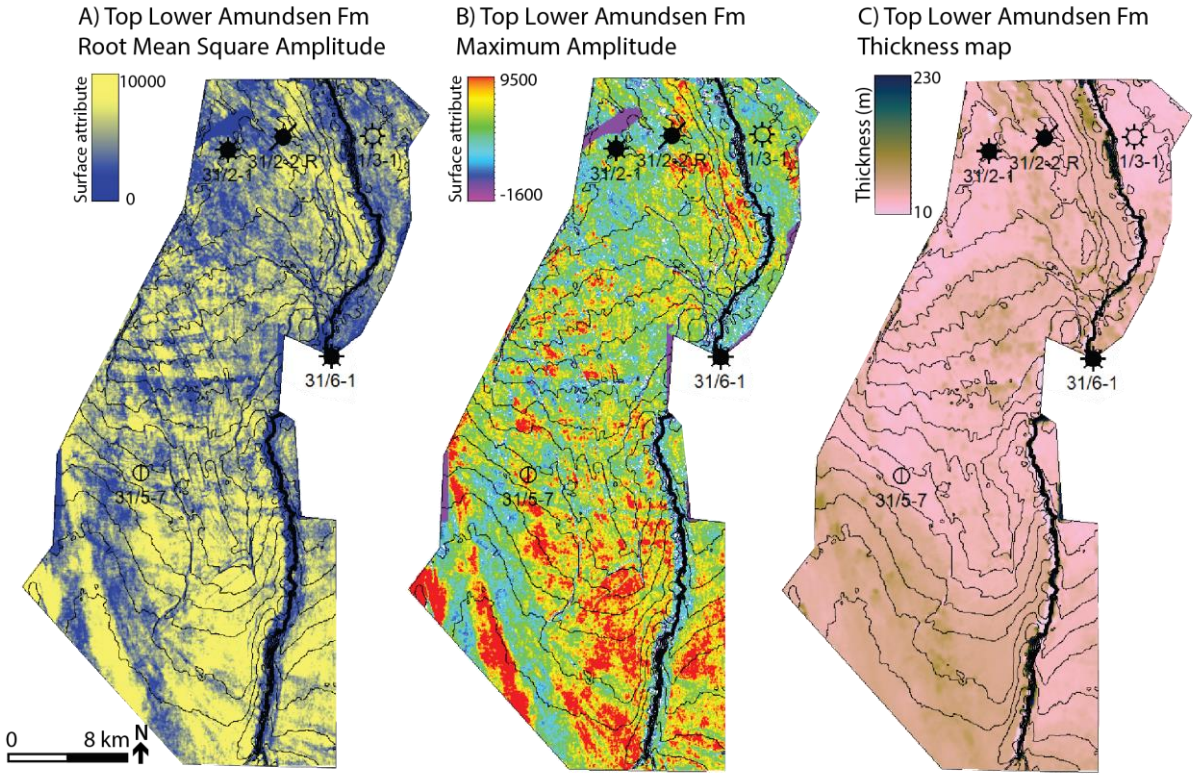

Figur 4.6 Top Lower Amundsen surface attribute and thickness map. A) Root Mean Square amplitude attribute map, B) Maximum Amplitude attribute map, C) Thickness map in meters.

4.2.1.2 Interpretation

The mudstones of the Lower Amundsen formation display generally high gamma-ray values (Vollset & Doré, 1984), the well-log is bell-shaped in 31/5-7, 31/3-1, and 31/2-1, and observed funnel-shaped in 31/5-2, the formation is likely deposited in a low energy depositional environment as fine-grained marine mud deposits. Variations in gamma-ray signature and a southern amplitude increase in RMS attribute map displays possible variations within the depositional environment. This is further highlighted by upwards coarsening gamma-ray logs indicating regression and upwards fining transgression. The Lower Amundsen is likely deposited in a period of transgression, transitioning into the regressive period of the Johansen Formation, as the Amundsen and Johansen formations are part-time equivalents, separated by lithostratigraphic boundaries (Vollset & Doré, 1984). Considering an average thickness of 30-40 meters, the almost tabular Amundsen Formation is likely deposited in a rapid transgressional period as a marine flooding surface (Deegan & Scull, 1977; Røe & Steel, 1985; Ryseth, 2001). The formation is likely deposited in an environment of little to no tectonic influence, confirmed by the relatively uniform thickness with only a slight increase in the south.

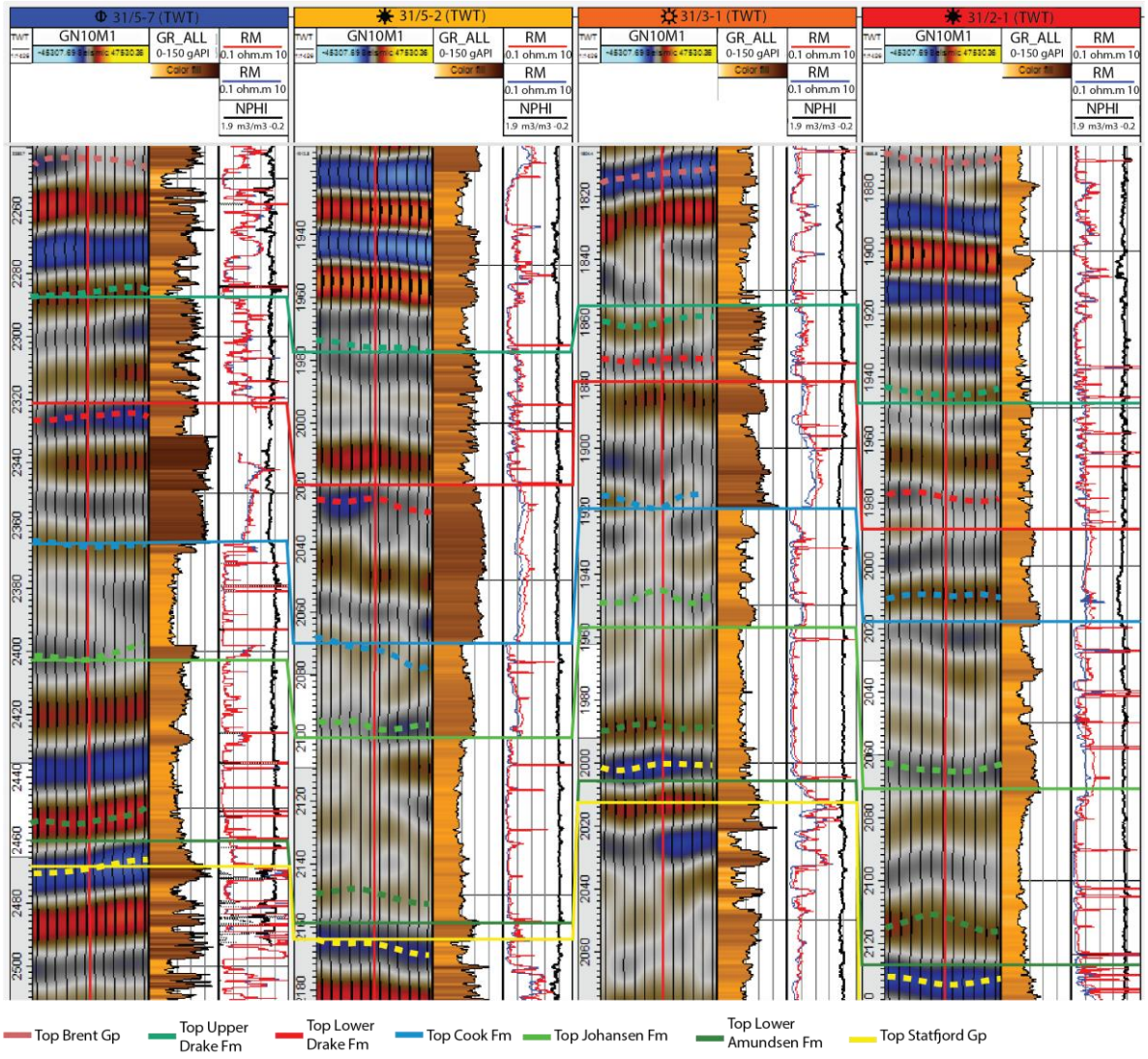

Figur 4.7 Well- logs displayed for well 31/5-7, 31/5-2, 31/3-1 and 31/2-1. Displaying from right: Vertical scale in elevation time (TWT ms), Seismic section of GN10M1 with horizon interpretations (dashed), GR-log, Resistivity log (RM- resistivity medium, RD- resistivity deep) cross plotted with Neutron porosity log (NHPI). Note some derivation from well-tops, 31/5-7 highest grade of reliability.

4.2.2 Johansen Formation

4.2.2.1 Description

The thickness map displays the presence of the Johansen Formation (primary storage) throughout the study area (Figure 4.8 C). It reaches its maximum thickness of 230 meters southwest of the injection well (31/5-7). At the injection well, the formation thickness measures 116 meters. Only 3.5 km northeast of the injection well, the thickness is reduced to 50 meters, then thickens towards the northeast. The thickness increases to 150 meters in the northern part of the Tusse hanging wall and 160-180 meters in the southern hanging wall. Along the Tusse

footwall, the formation displays a relatively tabular thickness ranging from 80-100 meters in the southern part to 60-80 meters in the northern part, except for a thickness increase in the southernmost part of the northern Tusse footwall (150-180 m).

A NW-SE trending elongated amplitude anomaly displays high RMS attribute values west of the injection well, in the southern part of the study area (Figure 4.8A). High reflectivity values are also present in the center of the study area, somewhat lower than for the southern area. The largest negative minimum amplitude attribute values coincide with the areas of high RMS values (Figure 4.8A, B). No other distinct anomalies are observed in the rest of the study area.

The 31/5-7 displays generally low gamma-ray readings for the Johansen Formation (Figure 4.7), with an upwards coarsening serrated bell-shaped signature. At 2430 meters TWT, a prominent individual sharp-based fining upwards unit of five meters is present. The upper part of the Johansen Formation transitions into a faint fining upwards funnel-shaped gamma-ray signature. High amplitude parallel seismic reflectors are present in the formation. 31/5-2 displays a serrated cylindrical gamma-ray signature with overall low values, and the seismic facies display a sub-parallel to chaotic expression with terminations observed on the troughs (Figure 4.1D). The presence of high peaks in the resistivity log within the sand-rich Johansen Formation indicates carbonate stringers, the high peaks are less frequent in 31/5-2 than for 31/5-7. 31/3-1 displays a blocky cylindrical gamma-ray signature for the Johansen Formation, with no observation of high peaks present in the resistivity log contrary to the other well-logs. The lowest gamma-ray values are present in 31/2-1, displayed as a serrated cylindrical to funnel-shaped signature and the seismic facies are sub-parallel (Figure 4.1C).

4.2.2.2 Interpretation

The sandstones of the Johansen Formation, given that the gamma log is serrated bell-shaped to cylindrical shapes (Figure 4.7), suggest a coarsening upwards or continuous grain size, with generally decreasing gamma-ray values from 31/5-7 in the south to the northernmost 31/2-1. It indicates a northwards increase in coarse-grained sand deposits. This is further highlighted by the heterolithic deposits in 31/5-7, indicating closer proximity to fluvial imput and a higher degree of organic material compared to more homogeneous deposits of 31/5-2, 31/3-1, and 31/2-1 (Anell et al., 2021), coinciding with the northward increase in varying energy environments mapped by seismic facies changes (Figur 4.2, 4.3). The depositional environment of the Johansen Formation is laterally changing throughout the study area, reflected by laterally changing seismic facies and lithology variations in well-logs (Figure 4.7) (Sundal et al., 2016;

Vollset & Doré, 1984). The RMS and minimum amplitude map display sand-rich deposits by high amplitude anomalies in an NW-SE trending linear pattern, suggesting a southwestern progradation development of the formation (Gassnova, 2012; Hoyt, 1967; Nielsen & Johannessen, 2008; Sundal et al., 2016; Swift, 1975). As previously mentioned, Johansen and Amundsen are time equivalents, and the Johansen Formation is interpreted as a prograding sand prone delta, proximal to the Amundsen Formation, confirmed by the observation of prograding clinoforms within the Johansen formation (outlined 4.4) (e.g, Charnock et al., 2001; Marjanac & Steel, 1997; Sundal et al., 2016).

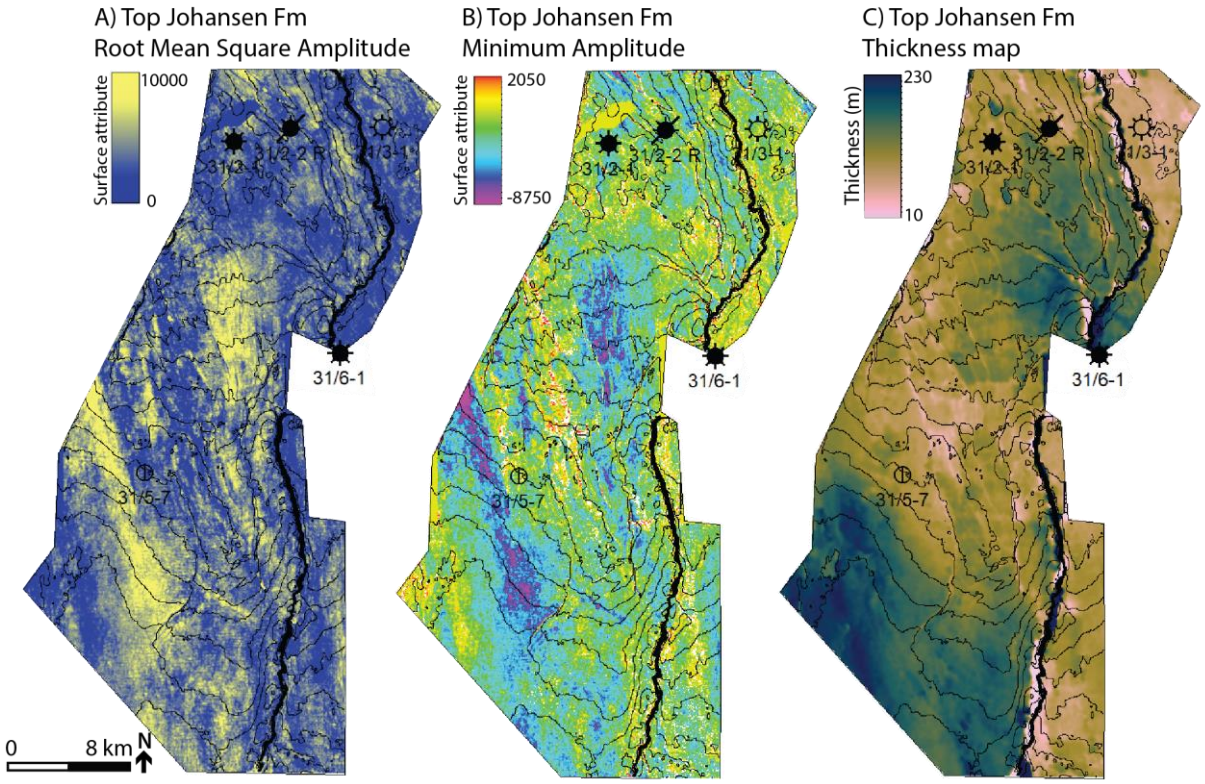

Figur 4.8 Top Johansen Formation surface attribute and thickness maps. A) Root Mean Square amplitude attribute map, B) Maximum Amplitude attribute map, C) Thickness map in meters.

4.2.3 Cook Formation

4.2.3.1 Description

The thickness map displays the Cook Formation (secondary storage unit) throughout the entire study area (Figure 4.9C). The Cook Formation measures 57 meters at the injection well. The underlying Upper Amundsen Formation measures 7 meters at the injection well, and due to its

low thickness has not been interpreted and is therefore included in the thickness map of the Cook Formation. Thus, the thickness is slightly overestimated (~10m).

The Cook storage unit reaches its maximum thickness of 80-100 meters towards the center of the study area northwest of the injection well (31/5-7). The succession displays a trend of southwest and northeast thinning, and the observed thickness trend in the Cook storage unit differs from the underlying Johansen Formation (Figure 4.8C). A slight thickness increase towards the southern part of the Tusse hanging wall is observed (50-80m), while the Tusse footwall displays a uniform thickness of 30-40 meters.

The largest anomalies displayed in the RMS attribute map are observed 4 km north of 31/5-7, towards the center of the study area, W-E trending high reflectivity values are present (Figure 4.9A). High RMS values occur in the north, northeast oriented relative to the Tusse hanging wall. High maximum amplitude attribute values coincide with the areas of high RMS values, this is most prominent in the center and the northern part of the study area (Figure 4.9B)

31/5-7 displays low gamma-ray values for the Cook Formation (Figure 4.7), similar to the overlying Johansen Formation (Figure 4.8). The generally low gamma-ray values form a blocky cylindrical signature with an abrupt resistivity increase at 2380 meters TWT. The seismic reflectors display a sub-parallel to chaotic expression with indications of internal terminations (Figure 4.1D). 31/5-2 displays a serrated cylindrical gamma-ray signature with an overall increase in gamma-ray values of the Cook Formation from 31/5-7, observed seismic reflection patterns are similar to 31/5-7 but with less reflection terminations. Presence of high peaks in the resistivity log within the sand-rich deposits indicates carbonate stringers, the high peaks are less frequent than for 31/5-7. 31/3-1 displays low gamma-ray values with presence of three 5-meter thick units with sharp increasing and rapidly decreasing gamma-ray values (Figure 4.7). These sharp-based gamma-ray alternations from high to low values are also reoccurring in 31/2-1. The seismic reflections display a sub-parallel to internally termination expression (Figure 4.1D).

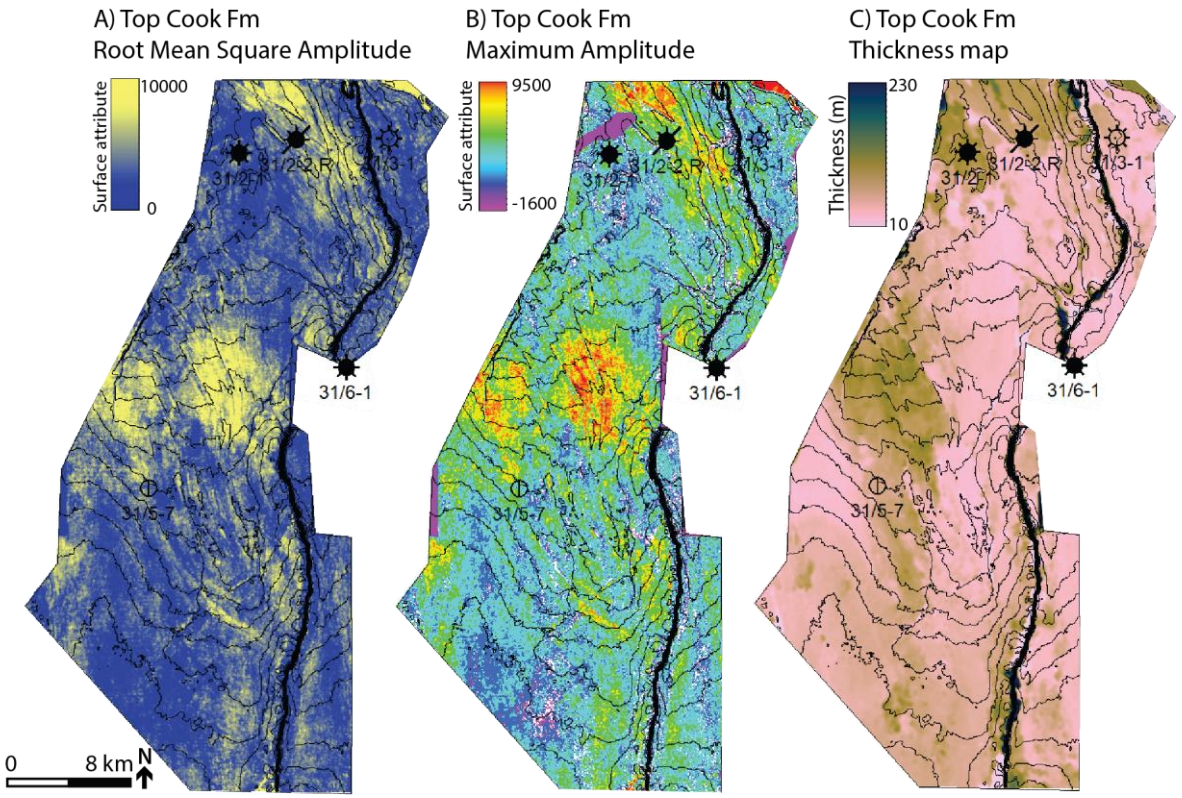

Figure 4.9 Top Cook Formation surface attribute and thickness maps. A) Root Mean Square amplitude attribute map, B) Maximum Amplitude attribute map, C) Thickness map in meters.

4.2.3.2 Interpretation

Local changes in depositional environments and accommodation are implied by the thickness reduction from Johansen to the Cook Formation, regionally changing seismic facies (Figure 4.3, 4.4), and laking observations of Tusse hangingwall growth in the Cook formation. This observed facies change and insufficient hanging wall growth could indicate a change in sediment supply and tectonic quiescence (Deng et al., 2017; Holden, 2021). Given that attribute maps (Figure 4.9A, B) displays high amplitude anomalies in the areas of 31/5-7 with presence of blocky homogeneous coarse-grained sand deposits, these areas likely have presence of wave-dominated sand compared to more heterolithic deposits within the northernmost wells (Marjanac & Steel, 1997). But as the general seismic facies variations indicate a northward increase in varying energy environments (Figure 4.2B), there is potentially a northward coarsening in cook, as observed in Johansen Formation (Figure 4.2C).The depositional environment of Cook is likely dominated by tidal and fluvial influenced deposits, displayed by the repetitive alterations from coarse to fine-grained deposits observed in the well-logs (Figure 4.7), indicating a tidal dominated deltaic setting (Halland et al., 2011; Marjanac & Steel, 1997).

4.2.4 Lower Drake Formation

4.2.4.1 Description

The Lower Drake Formation (primary seal) is present throughout the study area, it is thinnest towards the northeast below the overlying Troll Field (4.10C). There is an overall thinning of the formation from southwest to northeast, a slight thickness increase occurs towards the center, tinning again further northeast. Maximum thickness occurs in the south, ranging from 120-170 meters. At 31/5-7, the formation measures approximately 75 meters, no large thickness variations are observed from the western to the eastern side of the injection well, but a thinning is observed on the horst east of the injection well (60-70 m). Greater thicknesses are present in the southern (90-130 m) Tusse hanging wall than in the northern part (40-60 m). The Tusse footwall displays a generally constant thickness of (40-60 m).

There are no distinct amplitude anomalies observed, overall higher reflectivity divides the southern from the northern part of the study area (Figure 4.10.B). The area east of the injection well displays lower RMS values than the rest of the southern area (Figure 4.10A). The largest negative amplitudes dominate towards the south, except east of the injection well, coinciding with the RMS amplitude anomalies.

In 31/5-7 the Lower Drake Formation displays a serrated cylindrical gamma-ray signature with overall high values (140-150 gAPI), neutron porosity is likely overestimated due to mud containing high amounts of water (Figure 4.7). Parallel seismic reflectors with amplitude values lower than for the Johansen Formation is present (Figure 4.1B). High gamma-ray values with a blocky cylindrical signature are also present in 31/5-2, but observed seismic reflections display sub-parallel to chaotic expression with amplitude differences (Figure 4.1D). In 31/3-1, the gamma-ray signature displays an upwards coarsening signature with a sharp increase in gamma-ray value present at 1877 meters TWT continuing as a blocky and cylindrical with overall higher gamma readings. 31/2-1 displays gamma-ray decrease within all formations, except of the Cook Formation (Figure 4.7). The Lower Drake Formation shows lower gamma readings than for the other wells, with a sharped-based reduction at 2000 meters TWT followed by a sharped-based increase in gamma-ray. Seismic reflections display some internal terminations on the peak, with sub-parallel reflectors. Frequent high resistivity peaks are present throughout the well, but absent in the Lower Drake Formation.

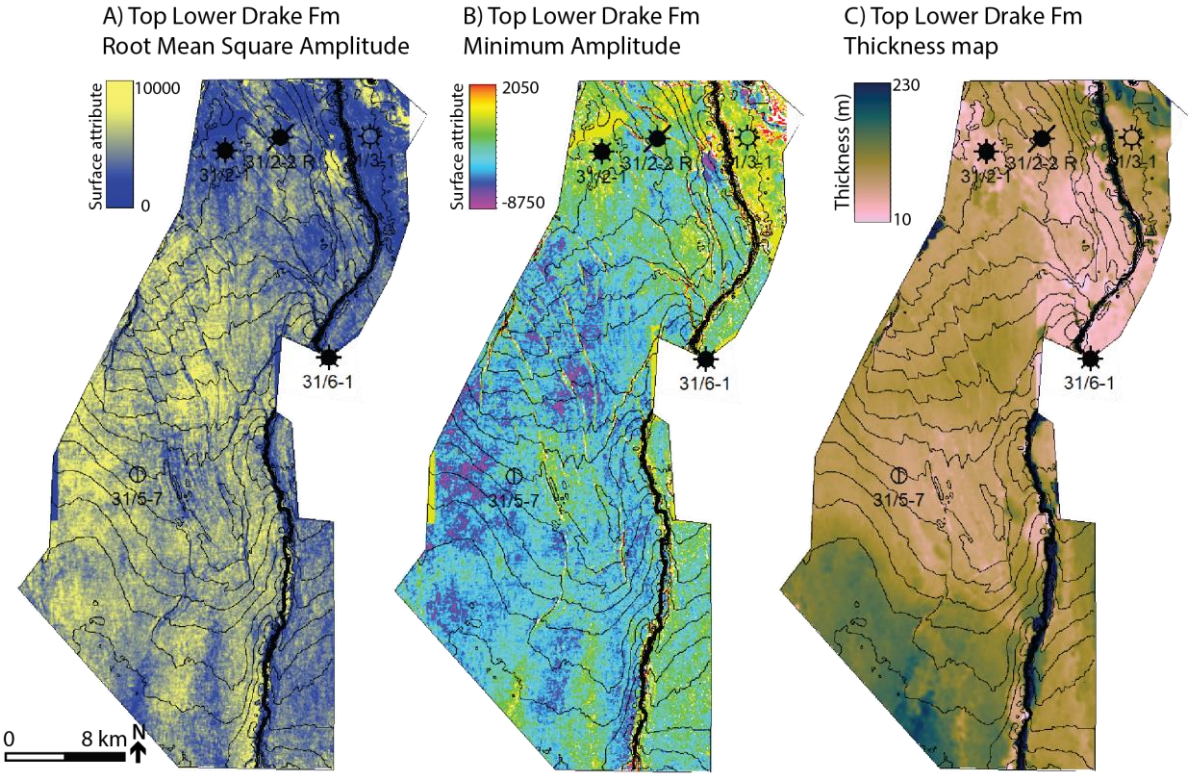

Figur 4.10 Top Lower Drake surface attribute and thickness maps. A) Root Mean Square amplitude attribute map, B) Maximum Amplitude attribute map, C) Thickness map in meters.

4.2.4.2 Interpretation

The deposition of the Lower Drake Formation is related to the global anoxic event associated with marine mudstone deposition (Charnock et al., 2001; Gassnova, 2012). Given that there are no abrupt amplitude anomalies, in addition to relatively consistently high gamma-ray values, the homogeneous layered marine mudstones of Lower Drake Formation are likely deposited in a pro-delta to delta-front environment (Marjanac & Steel, 1997; Thompson et al., 2022). Sharp east-west trending seismic facies boundaries (Figure 4.2 A) indicate distally increasing energy environments.

4.2.5 Upper Drake Formation

4.2.5.1 Description

The Upper Drake Formation thickens from 30-40 meters in the northernmost study area to 100 meters towards the south (Figure 4.11C). The formation measures 53 meters at the location of the injection well, and the thickness decreases to 30-40 east of the well in the Tusse hanging wall. The thickness in the Tusse footwall is relatively tabular and thickness ranges from 40-60, with observed thinning towards the north.

There are no large anomalies present in the RMS attribute map, and the formation is dominated by lower reflectivity values (Figure 4.11A). A moderate reflectivity increase is present west of 31/5-7 and towards the northernmost areas. The largest maximum amplitudes coincide with RMS, located west of 31/5-7 and towards the north (4.11B). The rest of the formation is dominated by no significant attribute anomalies.

In 31/5-7 Upper Drake Formation displays a highly serrated gamma-ray signatures with thinly alternating sedimentary deposits of low and high gamma values. Parallel seismic reflectors with lower amplitude values than for the Johansen Formation are present in the Upper Drake Formation (Figure 4.1B). Sand-rich deposits with low gamma-ray values display large variations in resistivity, with high peaks indicating the presence of carbonate stringers. Low gamma-ray values are present in the lowermost part of Upper Drake Formation. A general gamma-ray decrease is observed in 31/2-1, this also observed in all other formations with the exception of the Cook Formation. Sub-parallel seismic reflections are present within the Upper Drake Formations in 31/2-1 and 31/3-1 (Figure 4.1C).

4.2.5.2 Interpretations

The Upper Drake Formation deposits comprise mixed mudstones, siltstones, and sandstone lenses (Thompson et al., 2022). Given that the gamma log is serrated with alternating fine-grained and coarse, grained deposits, the Upper Drake Formation displays heterogeneous deposits influenced by silt and sand deposits. (Marjanac & Steel, 1997; Thompson et al., 2022). There are likely no large sandstone bodies present within the formation, as no distinct amplitude anomalies are observed, and the presence of fine-grained mud deposits indicates deposition during sea-level rise (Halland et al., 2011; Vollset & Doré, 1984).

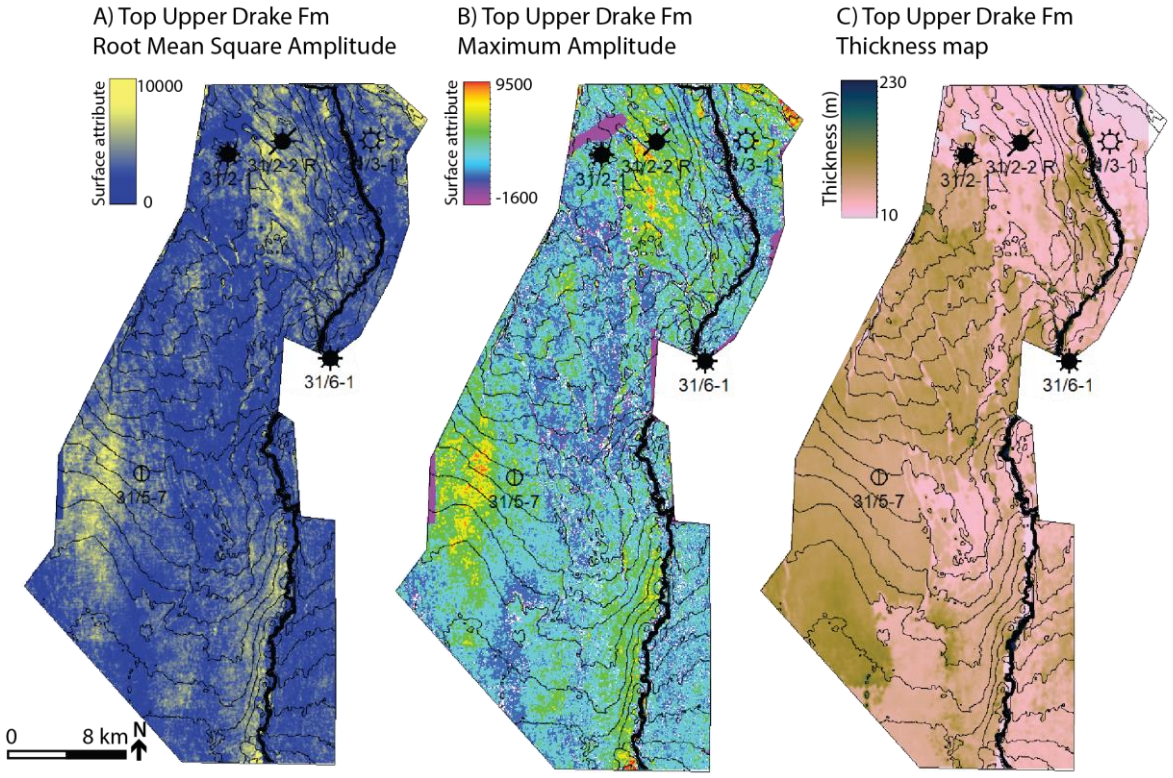

Figur 4.11 Top Upper Drake surface attribute and thicknes maps. A) Root Mean Square amplitude attribute map, B) Maximum Amplitude attribute map, C) Thickness map in meters.

4.2.6 Target units

4.2.6.1 The Primary storage unit

The primary storage unit primarily consists of the Johansen Formation and includes the Lower Amundsen Formation (Fig 4.12). The unit thickens towards the southwestern part of the study area, measuring 300 meters at its thickest. At the location of the injection well (31/5-7) the unit measures 130 meters, Johansen Formation measures 116 meters, and Lower Amundsen Formation 14 meters (Fig 4.7A). Only 3.5 km northeast of the injection well, the unit thins to 80 meters, then thickens towards Tusse hanging wall in the northeast (190-200 m) (Fig 4.12B). The thickness trend in the Tusse footwall is dominated by overall uniform thicknesses in the south and north, with a subtle thickness increase (200-240 m) towards the middle of the footwall. A distinct increase in thickness is present in the southern Tusse hanging wall and east

of 31/5-2 towards the hanging wall, clearly visible on the flattened seismic composite line.

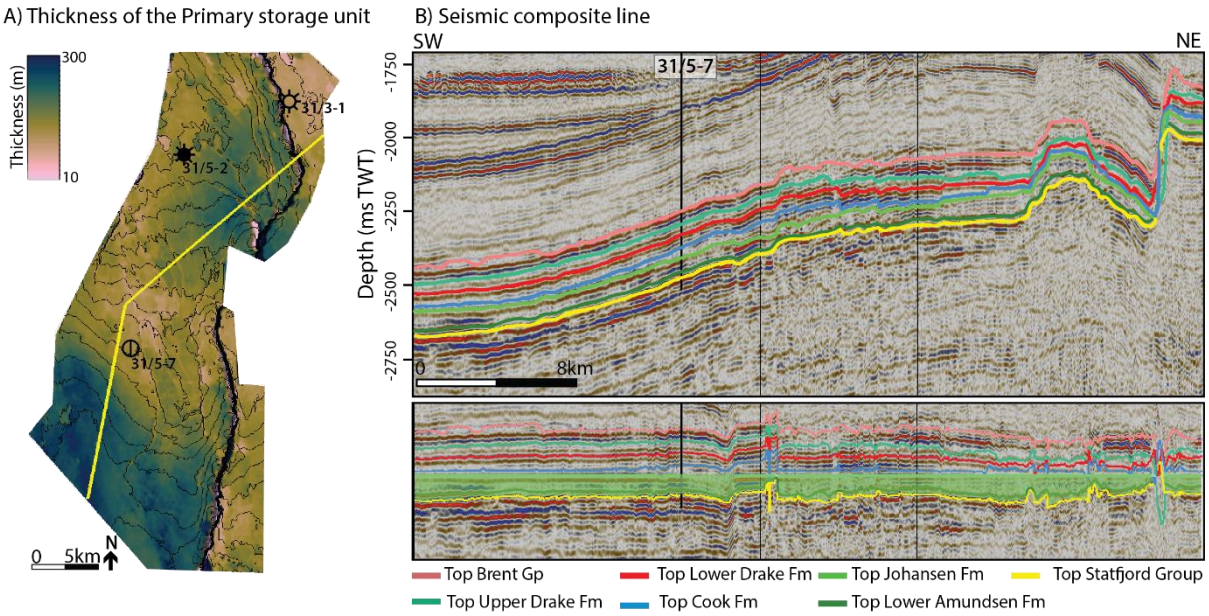

Figur 4.12 A) Thickness map of the primary storage unit with 40-meter contour line spacing. B) Seismic composite line (top) flattened on Top Johansen Formation (bottom) displays thickness variations within the storage unit from southwest to northeast, location of composite line displayed in yellow on the thickness map. Vertical exaggeration 15.

4.2.6.2 The secondary storage unit

The secondary storage unit mainly consists of the Cook Formation and includes the Upper Amundsen Formation (Figure 4.13). The Upper Amundsen does necessarily contribute to increased storage volume but is included in the secondary storage due to seismic resolution. At the location of the injection well the unit is 64 meters thick, comprising 57 meters of Cook Formation and 7 meters of Upper Amundsen Formation (Figure 4.13A). The secondary storage unit is significantly thinner than the primary storage unit. The thickness variations observed in the unit are thinning towards the southwest and northeast, and thickening in the central part of the study area (80-100 m). The trend is clearly present in the flattened seismic composite line (Figure 4.13B). There are no significant thickness variations in the footwall (30-40 m) and a slight increase in thickness towards the southern part of the hanging wall (50-80 m).

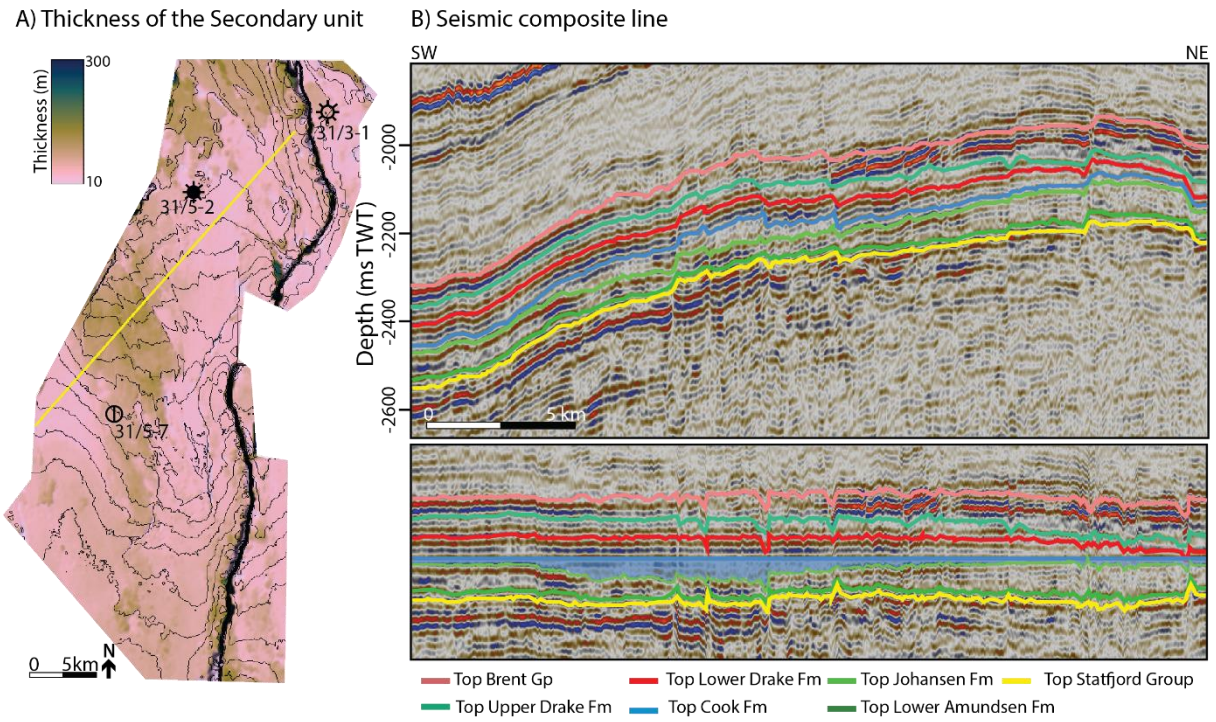

Figur 4.13 A) Thickness map of the secondary storage unit with 40-meter contour line spacing. B) Seismic composite line (top) flattened on Top Cook Formation (bottom) displays thickness variations within the storage unit from southwest to northeast, location of composite line is displayed in time-domain (TWT ms). Vertical exaggeration 15.

4.2.6.3 The primary seal

The primary seal comprises the Lower Drake Formation. The unit is present throughout the study area, with the thinnest part located towards the northeast below the overlying Troll Field (Figure 4.14 A). The thickest part towards the southwest (120-170 m), thinning towards the northeast, except for a thickness increase towards the center. At 31/5-7, it measures approximately 75 meters, with no large thickness variations from the western to the eastern side of the injection well, but an observed thinning on the horst east of the injection well (60-70m).

There is an overall greater formation thickness in the southern part of the Tusse hanging wall (90-130 m) than in the northern part (40-60 m) (Figure 4.14B). The northern part of the footwall displays greater thicknesses (40-100 m) with an overall northward thickening, the southern footwall formation thickness is approximately 80-100 meters.

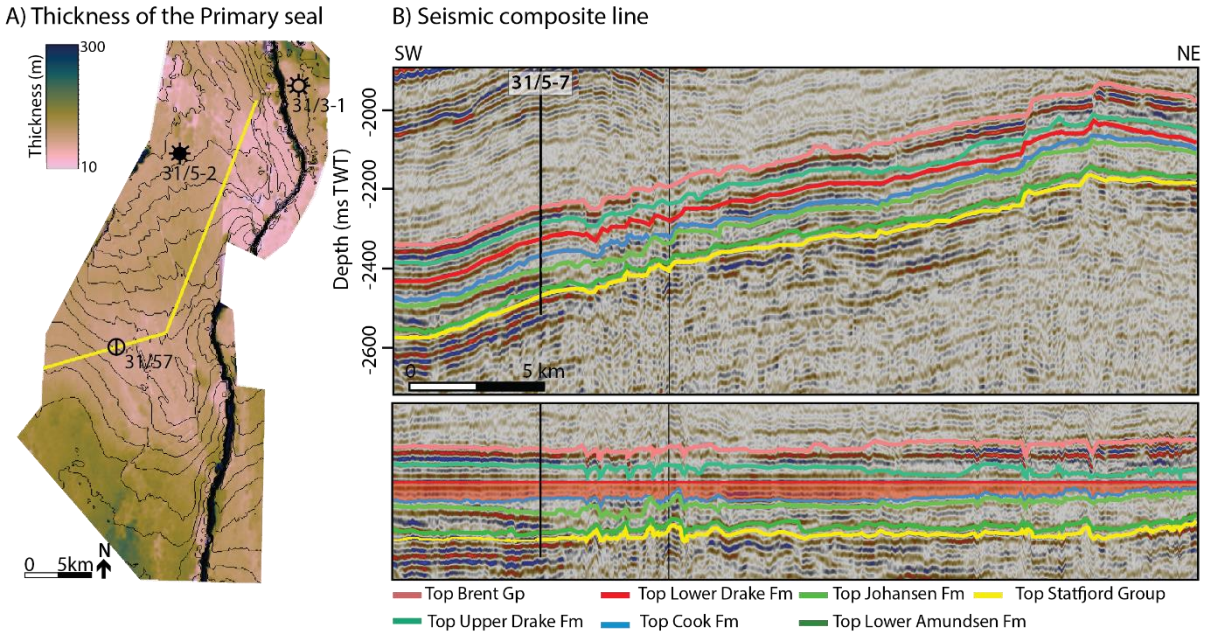

Figur 4.14 A) Thickness map of the primary seal unit with 40-meter contour line spacing. B) Seismic composite line (top) flattened on Top Lower Drake Formation (bottom) displays thickness variations within the storage unit from southwest to northeast, location of composite line displayed in yellow on the thickness map (A)). Note that the thickness map is displayed in depth-domain (m) and the seismic composite line is displayed in time-domain (TWT ms). Vertical exaggeration 15.

4.2.6.4 The Dunlin Group

The Dunlin Group reaches its maximum thickness of approximately 600 meters towards the southwestern part of the study area (Figure 4.15A). A thickness increase in the middle of the unit with a NE-SW orientation is observed, with thicknesses of approximately 360-400m. The maximum thickness of the formation in the Tusse hanging wall is towards the southern part of the fault zone (450-470 m), reaching its thinnest in the mid-part of the fault (270-300 m), then a slight thickening towards the northernmost part of the fault (380-400 m).

A flattened composite line shows the thickness variations in seismic section (Figure 4.15 B). The observed thickness increase towards the Tusse hanging wall is less prominent in the seismic section. In the northern part of the Tusse footwall, the group reaches its thinnest and measures approximately 200 meters, there is a thickening in the footwall towards the south (300-320m). There is a thinning of the group on the horst east of the injection well (31/5-7), with an approximate thickness of 280-300 meters.

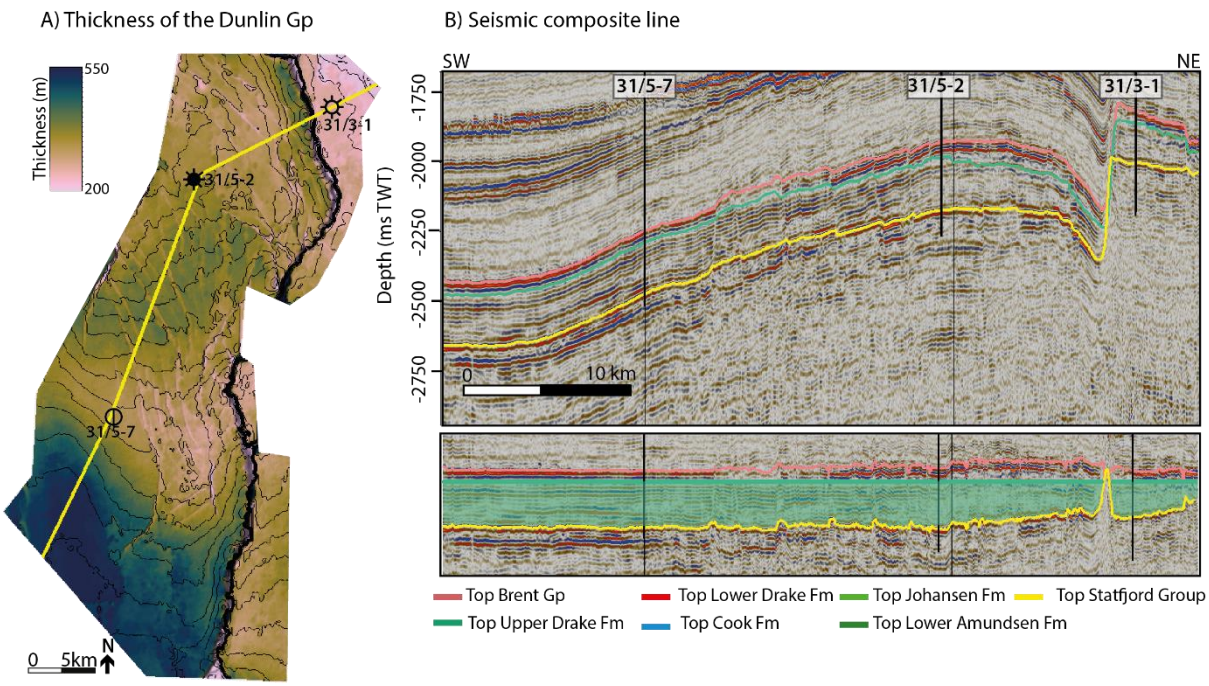

Figur 4.15 Thickness map of the Dunlin Group with 40-meter contour line spacing. B) Seismic composite line (top) flattened on Top Upper Drake Formation (bottom) displays thickness variations within the storage unit from southwest to northeast, location of composite line displayed in yellow on the thickness map (A)). Note that the thickness map is displayed in depth-domain (m) and the seismic composite line is displayed in time-domain (TWT ms). Vertical exaggeration 15.

4.3 Clinoform analysis

In total, 13 small-scale clinoforms were identified and interpreted within the Johansen Formation (Table 4.1). The clinoforms are spread over the study area, analyzed, and characterized in four areas; the southwestern part, the center of the study area, and the north and northwestern part right outside of the defined study area, all within the GN10M1 seismic cube (Figure 4.16). The extent of the clinoforms and length of the traceable coastlines differs in the four different areas. Clinoforms present in the southwest display the longest length with 450 meters, measuring 375 meters in the central part, 334 meters in the north outside the defined study area, and 54 meters in the northwest.

The overlying Cook Formation does not show any evidence of clinoforms overlying the intra Johansen Formation clinoforms. In the southern and central part of the study area seismic reflectors display high amplitude parallel to sub-parallel reflectors, north of the study area angular tilted reflectors to chaotic reflectors with no well-defined geometries overlie the clinoforms.

Seismic sections for clinoform analysis are parallel to depositional dip to be able to obtain and analyze proper geometries. Generally, the clinoform characteristics are best developed in the center of the defined clinoform area. Since the clinoforms are present within the Johansen Formation, differences in burial depth coincide with the variations in the time structure map (Figure 4.5) of the formation, resulting in shallower burial depths in the north (2200-2300 m depth) and a deepening towards the southern part of the study area (2600- 3000 m depth).

CL	Location	Dip	Depth	Shape	Reflector/Amp. description	Front orientation	Shape derscription
1	Center of study area	8,33	-2667	s	Weak countinous, Amp. increases from topset to bottomset	W	Shorter foreset, well developed top and bottomsett, clear reflectors
2	Center of study area	12,25	-2679	s	Weak continous, top and bottomsett highest Amp.	W	Shorter foreset, well developed top and bottomsett, clear reflectors
3	Center of study area	13,02	-2705	s	Weak Continous, Amp. decrease from top to bottomset	W-NW	Well developed foreset, topset and bottomsett less clear
4	Southwest	12,46	-2926	s	Weak dissrupted, similar Amp. Values for entire clinoform	E-NE	Long Foreset, well developed top and bottomset, some reflection dissruptions
5	Soutwest	23,85	-3020	s	Weak continous, similar Amp. values for clinoform	E	Smallest of the clinoforms in the southeastern, shorter foresett, sligthly interrupted reflectors
6	Southwest	12,12	-2970	s	Weak conttinous, small Amp. increase from top to bottomset	E	Slightly interupted reflections, visable top, foreset and bottomsett.
7	North	19,72	-2291	s	Weak dissrupted, similar Amp. values clinoform, well defined topset	N-W	Steep foreset, clearly defined topset, clear reflectors
8	North	19,2	-2281	s	Weak continous, strongest Amp. at top and bottomset	N-W	Steep foreset, clearly defined bottom and toppset, clear reflectors
9	North	18,79	-2281	s	Weak disrupdet, reflection dissrupded on forest. Small Amp. increase on top and bottomset	N-W	The Steepest foreset, clear reflectores, clearly defined bottom and topset
10	North	29,55	-2290	s	Weak dissrupted, small Amp. increasre on top and bottom set	N-W	Steep foreset , clearly defined bottom and topset, clear reflectors
11	North	19,16	-2299	s/ o	Weak continous reflection,	N-NW	Well defined bottomset, poor defined rollover and topset. Indicate low accomodation
12	Northwest	12,73	-2346	s	Weak continous, bottomsett displays small Amp. Increase	N-W	Decrease in foreset steepness, poorly defined bottomset, reflectors slightly interrupted
13	Northwest	17,16	-2322	s	Amp. Weak continous, clearly stronger values present in topset	N-W	Decrease in foreset steepness, poorly defined bottomset, reflectora slightly interrupted

Table 4.1 Description of clinoform observations. Color coded by location clinoform location. Abbreviations: Amp = Amplitude, N = North, W = West, S = South, E = East, S = Sigmoid, O = Oblique.

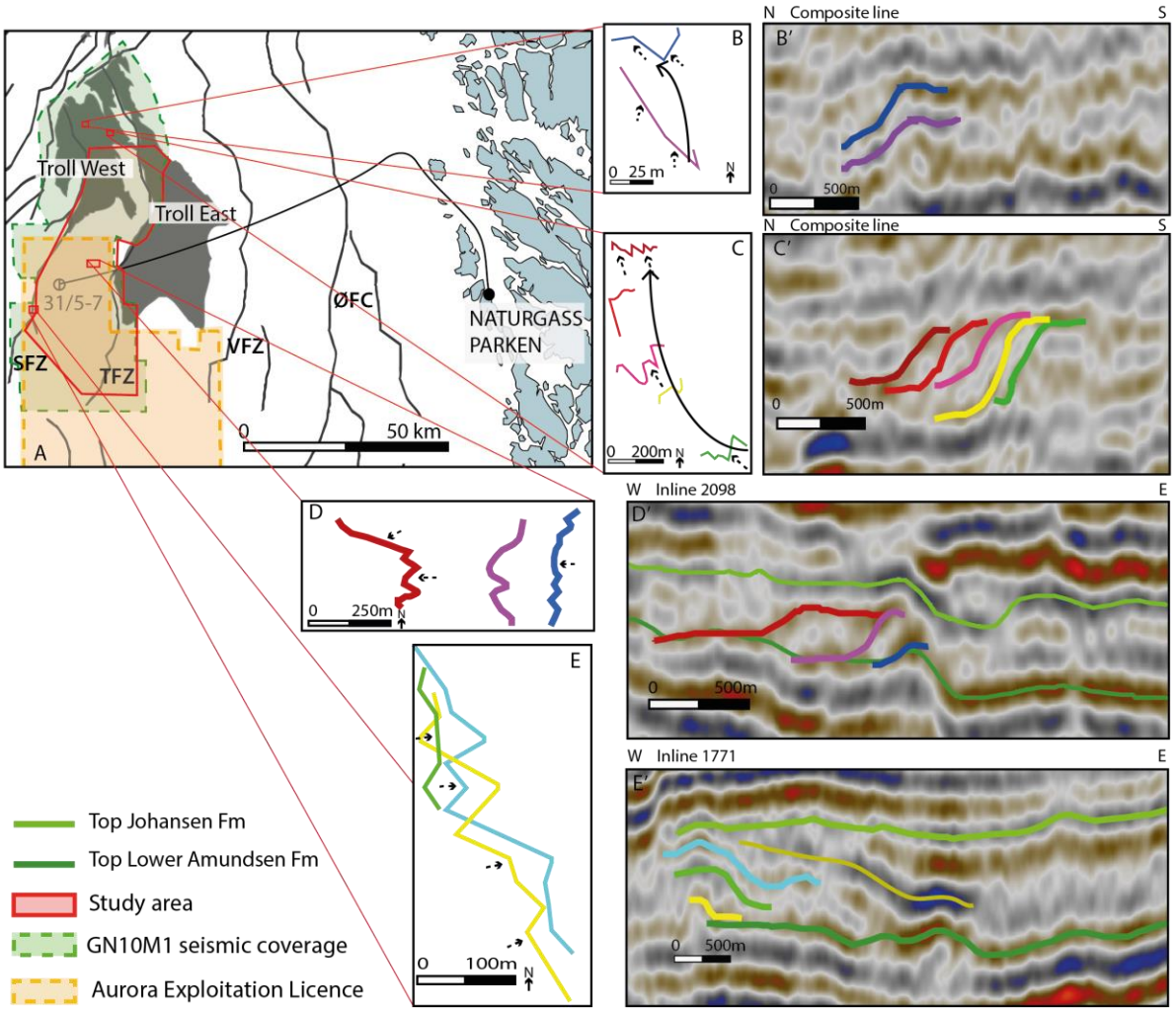

Figur 4.16 A) Location map of the study area, GN10M1 seismic coverage and the Aurora exploration license (EL001). Red boxes indicate the location interpreted and analyzed clinoforms. B) Map view of trajectory lines for CL12-13, B' Seismic composite line with interpreted clinoforms. C) Map view of trajectory lines for CL 7-11, C' Seismic composite line with interpreted clinoforms. D) Map view of trajectory lines for CL 1-3, D' Seismic inline 2098 with interpreted clinoforms. E) Map view of trajectory lines for CL 4-6, E' Seismic inline 1771 with interpreted clinoforms.

4.3.1 Clinoform interpretations

The interpreted clinoforms display sigmoid geometries, with the characteristic s-shape, associated with increasing accommodation rate and high depositional rate (outlined 2.2.2.3) (Adams & Schlager, 2000; Anell & Midtkandal, 2017). A detailed description of the individual clinoforms is presented in table 4.1.

The clinoforms (CL:4, 5, 6 Table 4.1) (Figure 4.16 E,) of the southwestern part of the study area differ from the rest of the interpreted clinoforms, as they build out from west to east, with

an E-NE oriented clinoform front. The three clinoforms create an outbuilding wedge, with reflector terminating on the underlying Lower Amundsen Formation.

The clinoforms of the southwestern and central part of the study area generally display shorter foreset and lower foreset dip than the clinoforms in the north, while the foreset and bottomset are generally well developed (Figure 4.16). This trend is also present with respect to clinoform height, clinoforms with the lowest heights are present in the central part, ranging from 27-28 meters. The clinoform height increases both towards the southwest and the north, with the largest height measured in the north, ranging from 60-114 meters. The greatest lengths of the clinoforms do not coincide with the greatest heights and are present in the southwestern part of the study area.

The foreset dip angles of all interpreted clinoforms range from 8 to 29 degrees (Table 4.1). An observed trend in dip angles is that larges angles are present in the north with the largest clinoform heights, also the southwestern clinoforms display larger foreset dip. The lowest angels are present in the center of the study area.

The clinoform fronts (Figure 4.16) generally displays westward prograding clinoforms, north-west in the northern part, with the exception of the eastward prograding clinoform in the southwestern part of the study area. A lot of variation is present on the trajectory lines displayed in map-view. This may be a result of small-scale clinoforms below seismic resolution, and two different prograding clinoform systems could be interpreted, but due to seismic resolution it is displayed as one, hence the variations. Figure (4.16 C) displays that there is a slight shift in the progradation direction as the clinoforms build out, the youngest clinoform exhibit a clear N-W direction of the clinoform front, and as the clinoform builds out, the progradation direction is shifted northwards. In Figure 4.16 B the opposite trend is present, as the progradation direction shifts from N to NW as the clinoforms build out. The progradation direction of the central and southwestern clinoforms is constant as they build out (Figure 4.16 D, E)

The clinoforms display different trajectory trends (Figure 4.16). The clinoforms in the northwest display ascending to near-vertical trajectory, well-developed foreset and rollover-points, forming fully sigmoidal geometries indicating a relative sea-level rise (Anell & Midtkandal, 2017; Johannessen & Steel, 2005; Patruno, Hampson, & Jackson, 2015) (Figure 4.16 B). In the north (Figure 4.16C) clinoforms displays near flat to slightly descending trajectory. Fully sigmoidal clinoforms formed where topset and rollover points are prominent (CL 7-9). Slightly descending trajectories (Cl0-11) are formed when clinoform topsets are

poorly developed and prominent bottomsets, generating oblique clinoform geometries with a basinward shift in accommodation. The clinoforms in the central part of the study area display ascending regressive trajectories, indicating a relative sea-level rise (Figure 4.16 D´). Moving from east to west, the clinoforms are building out and forset, bottomset, and well-defined rollover-point development increases, implying larger accommodation. In the southwest, the clinoforms are building out from west to east generating an ascending to near vertical trajectory angle, evidence of sea-level rise. Well-developed topsets and rollover points indicates good accommodation, forming fully sigmoidal clinoforms (Adams & Schlager, 2000; Anell & Midtkandal, 2017).

The clinoform reflectors are generally weak with overall low amplitudes. The central clinoforms display solely weak continuous reflectors, with higher amplitudes on the top and bottomsett and decreasing amplitude on the foreset. Weak continuous and disrupted clinoform reflectors are common in the rest of the clinoform locations. Clinoforms in the north generally has higher amplitudes on top and bottomsett, while the southwestern clinoforms show similar amplitude values along the entire clinoform.

4.3.2 Clinoform decompaction analysis

The interpreted clinoforms are located in the Johansen Formation, and are buried at depths ranging from 2280-3020 meters. Decompaction is performed according to Klausen & Helland-Hansen (2018). They differ in present length and height, ranging from 261-676 and 27-114 meters respectively (Table 4.2). The input values used in the decompaction have been set to a 50% sandstone/mudstone ratio, but also performed with 100% sandstone and 100% mudstone.

Clinoform	Location	Length (m)	Height (m) (Present)	Height (m) (restored)	Dip (Present)	Dip (restored)
CL 1	Centre of study area, 6km N-E of 31/5-7	354	33	72 (59-85)*	5,3	11,5
CL 2	Centre of study area, 6km N-E of 31/5-7	293	38	68 (56-81)*	7,4	13,1
CL 3	Centre of study area, 6km N-E of 31/5-7	261	27	49 (40-58)*	5,9	10,6
CL 4	Southwestern part of studyarea	676	72	131 (109-153)*	6,1	10,9
CL 5	Southwestern part of studyarea	177	46	85 (70-101)*	14,5	25,6
CL 6	Southwestern part of studyarea	536	83	150 (125-176)*	8,8	15,7
CL 7	North, outside study area	402	81	98 (82-116)*	11,4	13,7
CL 8	North, outside study area	316	114	192 (162-223)*	19,8	31,3
CL 9	North, outside study area	439	107	180 (152-210)*	13,7	22,4
CL 10	North, outside study area	340	70	120 (100-141)*	11,6	19,4
CL 11	North, outside study area	276	50	86 (72-101)*	10,3	17,3
CL 12	Northwest, outside study area	327	58	100 (83-118)*	10	17
CL 13	Northwest, outside study area	312	45	78 (64-92)*	8,2	14

Table 4.2 Measured and restored stratal thickness and dip angles of interpreted clinoforms (Figure 4.16). Surface porosity (ϕ_0) and depth-porosity compaction coefficient (C) for a 50% Sandstone/mudstone composition were used as an input value for the preformed decomposition. Color coded by clinoform location.* Restored height of the sand endmember and mudstone endmember respectively.

The performed clinoform decompaction led to an overall increase in clinoform height and dip angles, dip angles have in addition to average dip angle been measured for the clinoforms (Table 4.3). Present dip angles range between 8.3°-29.6° and 5.3°-14.5° (average). The large range in present dip angles results in a similar range in restored dip angles. Overall, the restored dip angles, including average angles, display nearly a doubling from present to restored dip angles. Maximum dip angle measured at the foreset is a good indicator to the steepest point of the clinoform, due to the small-scale clinoform, slight measuring errors could lead to large dip differences hence the average slope dip is included in the analysis.

Area	Clinoform	Length (present) (start-mid-end)	Average Length (present)	Height (present) (start-mid-end)	Average Height (present)	Average Angle (present)	Resotred height	Average Angle (restored)	Average angle (Clinoform complex, restored)
Center	CL1	304-242-113	220	31-30-24	28	7,3	51 (42-61)	13,1	
	CL2	309-231-190	243	34-34-40	36	8,4	65 (54-77)	14,9	16,4
	CL3	89-122-88	100	14-25-25	21	12,1	39 (32-46)	21,2	
Southwest	CL4	490-461-324	425	45-53-71	56	7,6	131 (109-153)	17,1	
	CL5	143-103-121	122	30-44-42	39	17,5	72 (59-85)	30,3	22,0
	CL6	287-287-238	271	43-51-55	50	10,4	91 (75-108)	18,6	
North	CL7	384-423-226	344	94-86-80	87	14,1	147 (124-172)	23,1	
	CL8	405-362-356	374	103-108-112	108	16,0	182 (153-211)	25,9	
	CL9	375-320-270	322	110-97-65	91	15,7	154 (129-180)	25,5	22,5
	CL10	380-368-200	316	68-58-57	61	10,9	105 (87-123)	18,3	
	CL11	141-282-275	233	46-50-51	49	11,9	84 (70-100)	19,9	
Northwest	CL12	238-271-249	253	52-53-47	51	11,3	88 (73-104)	19,1	22,5
	CL13	224-200-118	181	55-53-44	51	15,7	87 (98-127)	25,8	

Table 4.3: Average clinoform values of measured and restored stratal thickness and dip angles, reducing the impact of error. Measurements was done on the first, middle and last seismic line displaying the clinoform body, and average calculations was performed utilizing these measurements. Color coded by clinoform location.

CL 1 located 6 km N-E of 31/5-7, measures the gentlest dip angle present, ranging from 5.3°-7.3°(normal/average) dip angles (Table 4.2)(Figure 4.16 D). After preformed clinoform decompaction, the restored dip angles ranges from 11.5-13.1°, displaying nearly a doubling of the dip angle. CL 8 north in the study area, measures 19.8° and restores to 31.3°, representing the steepest restored dip (Fig 4.16 C). The largest slope angle is present in the eastward developing CL5, with a present slope of 14.5° restoring to 25.6° (Figure 4.16E).

A general observed trend in present-day measurements is the clinoforms present in the center of the study display the lowest present-day heights and shortest lengths, coinciding with some of the gentlest dip angles. CL1-CL3 dip angles range between 10.6°-13.1° for restored dip and 13.1° -21.2° and restored average dip. A 50% sandstone/mudstone composition has been set as the main composition, as presence of mud and mud-drapes are required to be able to observe clinoforms in the seismic.

Values for sand and mud end-members is also included in Table (4.2), where the sandstone end-member consistently displays lowest restored heights and mud end-member the highest. This applies for restored clinoform heights and forest heights. Generally,the restored heights increase with a factor of 1.7-1.8, with the exception of CL1 increasing with a factor of 2.1 and CL 7 increasing with a factor of 1.2. The clinoforms north of the study area (CL7-CL11)

restores the greatest heights, ranging from 86-192 meters. The decompacted height of CL 8 is 192 meters for 50% sandstone/mudstone composition, 162 meters for sandstone-endmember and 223 meters for mudstone-endmember. Displaying that the stratal thickness of CL 5 increases by approximately 78 meters when decompacted according to a 50% sandstone/mudstone ratio.

5 Discussion

Previous studies have interpreted the Johansen Formation as a wave dominated delta, prograding north-westward from the mainland (Marjanac & Steel, 1997). Through seismic facies analysis, stratigraphic characterization, clinoform analysis, and decompaction performed in this study, in addition to an observed NW-SE oriented elongated land-detached sand body (Sundal et al., 2016), delta progradation development towards NW, W, and SW of the primary storage unit is confirmed (e.g., Johansen Formation). Seismic facies variation, well-logs, and clinform development display a northwards increase in coarse-grained homogeneous sand deposits from a southern, more heterogeneous succession. The observed lateral variations in depositional environments within the primary and secondary storage units will have implications for CO_2 migration, as reservoir heterogeneities greatly influence the subsurface behavior of CO_2. Seismic facies maps will benefit reservoir characterization, as increased control regarding reservoir properties is desirable for estimating CO_2 migration.

5.1 Seismic facies analysis

Seismic facies analysis was performed for the primary (e.g., Johansen Formation) and secondary storage reservoir (e.g., Cook Formation), in addition to the primary seal (e.g. Lower Drake Formation). From well-logs (Figure 4.7) and previous studies (e.g.,Gassnova, 2012; Halland et al., 2011; Marjanac & Steel, 1997; Thompson et al., 2022; Vollset & Doré, 1984) it is established that the Lower Drake Formation is a marine shale rich unit, with a mean thickness of 72 meters in the study area with sealing capacity. All seismic facies present within the sand-rich Johansen and Cook formations, with the exception of the chaotic seismic facies of SF5, is present for the mud-rich Lower Drake formation (Figure 4.1, 4.2). As observations of different environments and lithologies displays similar seismic facies signatures, it is arguable how much detailed information this analysis can provide regarding the reservoir qualities. Seismic facies may correspond to geological facies, but in situations of poor seismic resolution or influences such as the overlying gas accumulations of the Troll Field, this can result in a change in seismic facies expression that cannot be related to geological facies (Roksandic, 1978; White, 1975). In addition, thickness, and overlying lithologies may influence the seismic facies character, and as

the GN10M1 is a merge of three different datasets (Gassnova, 2012), it will likely influence seismic resolution and the seismic facies expressions as the southern GN1001 provides excellent quality while the two other surveys are of good quality (Tabel 3.1). Hence, factors as overlying gas accumulations, thickness and differences within the seismic survey need to be taken into consideration with regard to seismic facies interpretations.

Illustrated by Figure (5.1) is the sharp transition between SF1 to SF3 shown by the abrupt change in seismic signature, interpreted as the sharp transition from a NW-SE elongated sand body to a more proximal back basinal environment. This facies change fits the interpreted depositional model of the Johansen Formation within the study area (Figure 5.1) (Gassnova, 2012; Sundal et al., 2016), but caution has to be shown as there is limited well control in the southern area (Figure 3.2, 3.3), and when calculating impedance in thin and thick sand, there is much information that may have been lost due to relative thin deposits (Brown, 2011). Precautions when interpreting the tilted angular reflectors of SF6 dominant on the southern Tusse footwall is necessary (Figure 4.2). As it is present in the eastern proximal areas, it may be the result of alternating lithologies from coast progradation. But as this area is located on the outer edge of the seismic coverage (Figure 3.1), in proximity to the large Tusse fault zone, the seismic expression and resolution are likely influenced by these aspects.

On the contrary, if such seismic facies analysis were neglected, information regarding the larger prominent observations of an N-S trend in seismic facies distribution would have been overlooked (Figure 5.1). High amplitude parallel to sub-parallel continuous seismic reflectors (SF1, SF2, SF3) (Figure 4.1, 4.2, 5.1), are dominant in the southern study area, and increasingly chaotic seismic facies are present in the northern study area (SF3, SF4, SF5)(Figure 4.1, 4.2, 5.1). In the Johansen Formation, presence of high amplitudes is resultant from property differences in a heterogeneous succession with presence of organic material and fluctuating energy environment in a tidal environment, and expected redistribution and washover processes in relation to spit development (Gassnova, 2012; Nielsen & Johannessen, 2008; Sundal et al., 2016). While the northern increase in chaotic seismic facies is likely influenced by the observed coarsening and cleaning of the proven homogeneous sand deposits from better northern well-coverage (Figure 4.7), deposited in a coastal environment dominated by constant high energy. Leading to decreased property differences resulting in poor seismic imaging (White, 1975). The observed northern coarsening within the Johansen Formation is in alignment with observations by Gassnova (2012) and Sundal et al. (2016). Observations by Sundal et al. (2016) defined chaotic seismic facies east of the spit deposits, in a lagoonal environment dominated by sand

deposits from tidal washoverprocesses. No observations of southern chaotic seismic facies have been done in this study, but sub-parallel to chaotic seismic facies is interpreted in these southern areas. This implies that similar seismic facies could represent different lithologies, as this study did not define any chaotic southern facies, the reservoir properties east of the spit bar are likely not as coarse and homogeneous as the northern study area and the chaotic expression may result from highly disorted reflecting surfaces.

The observed N-S trend in seismic facies, is not only a result of lithological and depositional changes, but is likely influenced by the Sognefjord gas accumulations of the Troll Field present in the northern area (Figure 4.15, 4.16, 5.1). According to White (1975)(1975), gas accumulations will have a greater effect on travel time and reflection amplitude than seismic imaging can compensate for. As seismic facies are defined based on the change in seismic character, reflection, and amplitude there is reason to believe that the observed facies change to a higher degree of chaotic and disrupted reflectors is partly a result of this gas effect (Berg, 1982; Boggs, 2014; Roksandic, 1978). The northern dominance of sub-parallel to chaotic seismic facies (SF3, SF4, SF5) (Figure 4.2) could partly be a consequence of the overlying gas accumulations, in addition to the northern area being heavily faulted as the Troll West gas province experienced faulting prior to the deposition if the Quarternary package, likely affecting the seismic signal (Thompson et al., 2022; Whipp et al., 2014; Wu et al., 2021). Another aspect to consider is that due to the presence of the large Troll Field, well coverage is considerably better in the north than in the south. This leads to a higher degree of certainty when correlating seismic facies expressions to facies interpretations from well-logs and cores in the north, compared to the southern area.

The location of chaotic seismic facies (SF5) coincides with the observed thickening of the Johansen Formation in the northeast (Figure 4.3C), where seismic reflection patterns changes both laterally and vertically (Figure 4.3, 5.1). There is no well penetrating SF5 (Figure 4.2C) hence detailed lithological information is absent, but low gamma-ray values are present in 31/2-1 and 31/2-2R (Figure 4.7) in proximity of SF5 within the Johansen Formation. According to 31/2-1, 31/5-2, 31/2-2R, and 31/31 (Figure 3.2), there is a northward increase in coarse-grained, clean sandstone deposits. Absence of SF5 in the shale-rich Lower Drake Formation (Figure 4.2A) in addition to the established northern increase in coarse-grained sand-rich deposits (Sundal et al., 2016), indicates that chaotic seismic facies expression is an effect of high sand-content and lack of large property contrasts. On the other hand, it could be an expression of a highly distorted arrangement of reflecting surfaces keeping in mind that seismic facies

expression can display similar signatures for different lithological successions. Steel (1993) suggested brackish water conditions for Johansen east of this study area (31/6-6), which coincides with Sundal et al.'s (2016) interpretation of lagoonal deposits in that area defined by chaotic seismic facies east of the observed spit bar. Lagoonal deposits are ofthen characterized by silt and mud deposits from predominantly low water-energy systems (Boggs, 2014), influence of tidal currents and high-energy tidal washower processes could lead to a sandrich environment as interpreted by Sundal et al. (2016). According to well observations (Figure 4.7) there is an northwards increase in homogeneous sand-rich deposits opposing an interpretation of SF5 representing a lagoonal environment. In light of these observations, it is likely that the observed SF5 is an expression of a depositional system with a higher ratio of clean sandstones and the chaotic reflections are a result of insufficient property contrasts, as it is absent in the heterolithic southern study area and the mud rick Lower Drake Formation (Figure 4.2A).

Relative formation thickness will affect the seismic facies analysis. Information regarding important parameters such as reflection abundance and geometries is lost due to vertical seismic resolution, as a result, the seismic signal is reduced to one seismic reflector in the thinnest parts of the Cook Formation (Figure 4.9C, 5.1)(Roksandic, 1978; Sheriff, 1977). In the Sognefjord Formation (e.g, Dreyer et al., 2005; Patruno, Hampson, Jackson, & Dreyer, 2015; Patruno, Hampson, Jackson, & Whipp, 2015; Vollset & Doré, 1984), the greater relative formation thickness provides geometrical information, and clinoform geometries provide information regarding the depositional environments. This is also applicable to the Johansen Formation, although the relative formation thickness is small compared to Sognefjord Formation, providing less information regarding depositional environment and geometries displayed in smaller-scaled clinoforms compared to Sognefjord Formation (outlined 5.3.3). As the Cook Formation thickens towards the center of the study area (Figure 5.1) the seismic signatures changes, this observation could be an effect of the change in relative thickness (Figure 4.9C) or a change in seismic facies.

It is likely that formation thickness forms a cut-off to regional seismic facies analysis, as it is reoccurring that the seismic signal of Cook is reduced to one reflector when formation thins, limiting the seismic facies analysis to reflector amplitude and continuity while formation regarding geomorphology is lost. In light of these observations, relative formation thickness below 30 meters is displayed by one single reflector for the Cook Formation (Figure 5.1), resulting in a cut-off-value for when seismic facies analysis won't be as reliable, informative or achievable as for formation thicknesses above this value. Observations from this study

indicate that formation thickness has to be sufficient if a seismic facies analysis shall contribute to additional significant information regarding differences in reservoir characteristics and qualities. Indicating that the seismic facies analysis of the Johansen Formation can reflect the geological facies of the formation, and provide important information regarding reservoir differences and potential different reactions to injected CO_2.

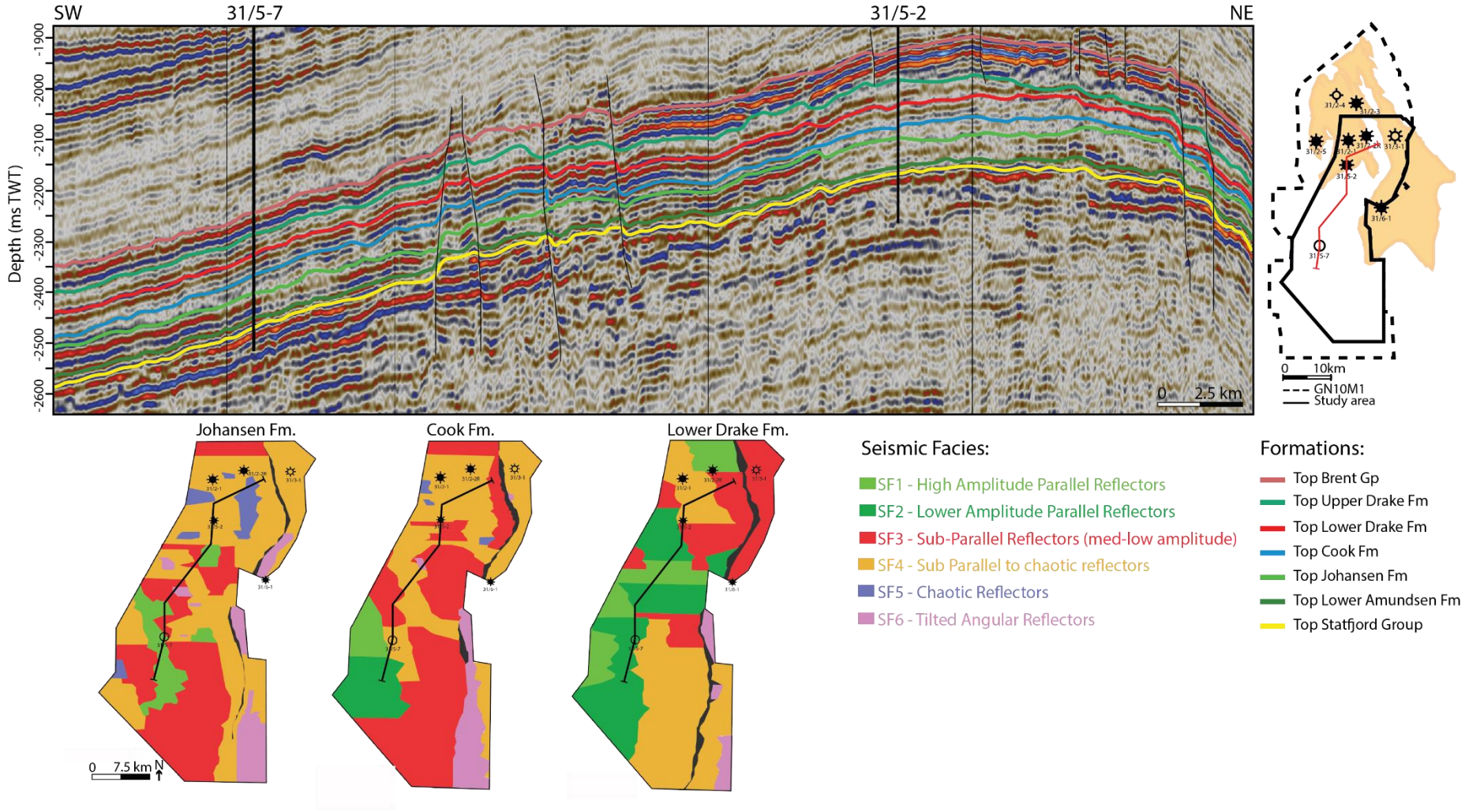

Figur 5.1 Seismic composite line SW-NE trending. Location of composite line displayed in red on the study-area outline. Notice that the Troll West Field overlies the northern study area. Composite line displays lateral and regional variations within the study area. Vertical exaggeration 15.

5.2 Evolution of depositional environment

The Dunlin Group was deposited during Late Sinemurian to Early Pliensbachian in a thermally subsiding post-rift basin following Permo-Triassic rifting (Gabrielsen et al., 2010; Partington et al., 1993). The structural evolution of the northern North Sea and the Horda Platform have been described by numerous studies (e.g., Bartholomew et al., 1993; Bell et al., 2014; Duffy et al., 2015; Færseth, 1996; Gabrielsen et al., 2010; Gee et al., 2008; Wu et al., 2021; Ziegler, 1975), and will significantly influence the sedimentary basin infill, stratigraphy and depositional environment (Deegan & Scull, 1977; Gassnova, 2012; Halland et al., 2012; Marjanac & Steel, 1997; R. J. Steel, 1993; Sundal et al., 2016; Vollset & Doré, 1984). The relatively uniform thickness of the Lower Jurassic Dunlin group (Figure 4.15B) reflects generation of accommodation mainly through thermal subsidence (Gabrielsen et al., 2010). However, the observed thickness increase in the south of the study area and hanging-wall growth across the southern Tusse fault zone (Figure 4.15), indicate minor local to regional tectonic activity during deposition that may have influenced facies and thickness distributions within the Dunlin Group. Observation of Early to Middle Jurassic NW-SE striking faults in the Oseberg Field by Deng et al. (2017) confirmed significant tectonic stretching during the late-inter-rift stage. Similar observations by Holden (2021) established fault growth across the Tusse and Svartalv falt zones in the Lower Jurassic Dunlin Group and the Middle Jurassic Brent Group within the Aurora storage site. As syn-depositional fault growth is absent in the Lower Amundsen Formation (Figure 4.6), most prominent in the Johansen Formation (Figure 4.8), and not significant for the overlying Cook or Drake formations. The observed fault growth is most prominent for the thickness map (Figure 4.12), but is also visible in seismic. It indicates that there may be some tectonic influence of the inter-rift phase on the Horda Platform, and the Johansen Formation displays a loose correlation between the observed fault growth and the mapped SF4, demonstrating that the thickness increase may influence the seismic facies expression.

5.2.1 Primary reservoir

The shallow-marine deltaic sandstones of the Johansen Formation (e.g., primary seal) and the marine Amundsen Formation (e.g., secondary seal) are partially time equivalent, separated by lithostratigraphic boundaries and facies changes (Vollset & Doré, 1984). The Amundsen

Formation reflects a mud-rich distal pro-delta to open shelf environment, deposited in a basin dominated by relative tectonic quiescence and thermal subsidence. A low energy depositional environment prevailed in the early phase of the Amundsen deposition, as fine-grained mud deposits are present in well-logs (Figure 4.7) and high amplitude reflectors are dominant. Overlying the heterolithic deposits of the Statfjord Group, the Lower Amundsen marks a regionally extensive period of transgression (Deegan & Scull, 1977; Røe & Steel, 1985; Ryseth, 2001). In alignment with Ryseth`s (2001) interpretation of the Lower Amundsen Formation as a marine flooding surface and a regional transgressive surface, the average formation thickness of 30-40 meters indicates a relatively rapid transgression (Figure 4.6). Little to no influence of local tectonics, as the formation is observed displaying generally uniform thickness throughout the study area with faint thickening to the south (Figure 4.6) also visible in seismic (Figure 5.1, 4.4).

The Johansen Formation deposits marks the next depositional phase during Sinemurian to Pliensbachian. As the Johansen and Amundsen formations are time equivalent, the Johansen Formation is interpreted as a north-westward prograding sandstone-rich delta, proximal to the pro-delta Amundsen Formation, in agreement with Marjanac and Steel (1997). Dominantly west to northwest prograding subaqueous delta-scale clinoforms are observed within the Johansen Formation in alignment with Marjanac and Steel (1997). The observed eastward prograding clinoforms in the southwestern study area are opposite to the main delta progradation direction, potentially caused by a higher degree of sediment redistribution in the southern study area. However, Marjanac and Steel (1997) suggest that the formation was dominantly deposited in restricted incised valleys, of which there is no evidence below the Johansen Formation (Sundal et al., 2016). Presence of the NW-SE trending elongated sandstone body is consistent with the observations of Sundal et al. (2016) (Figure 4.2C, 4.8C), indicating that the Johansen Formation was deposited as a prograding delta system with spit development by alongshore currents causing sediment bypass and delta front reworking during the middle aggradational phase. Charnock et al. (2001) defined the Johansen Formation northwest of the Horda Platform as tidally influenced, estuarine sandstone deposits. In light of previous literature (e.g, Charnock et al., 2001; Marjanac & Steel, 1997; Sundal et al., 2016) and indications from this study, it is inferred that deltaic deposition of a dominantly westward prograding delta developed in a shallow marine environment dominated by longshore currents, redistributing sediments, and was in fact not restricted by incised valleys (Marjanac & Steel, 1997).

The Johansen Formation can be subdivided into three units dominated by different depositional settings; progradational, aggradational, and retrogradational phases (Sundal et al., 2016; Vollset & Doré, 1984), likely resulting in different depositional stacking patterns and geometries. The depositional environment of the Johansen Formation is laterally changing throughout the study area, lateral changing seismic facies and lithology are displayed in well-logs within the formation (Figure 4.7). The observed trend of a northward increase in chaotic seismic facies (SF3, SF4, SF5)(Figure 4.1, 4.2, 5.2), from high amplitude parallel to sub-parallel facies in the south (SF1, SF2, SF3) (Figure 4.1, 4.2, 5.2), is likely influenced by the overlying gas accumulations in the Sognefjord Formation as it influences the seismic signal and potentially changes the seismic signature. In addition, there is a northward change in depositional processes from the southern energy fluctuating tidal environment with redistribution and washover processes related to potential spit development (Nielsen & Johannessen, 2008), causing a heterogeneous sediment composition (Figure 4.7), to coastal processes of a high energy dominated shallow marine shelf environment (Vollset & Doré, 1984), leading to deposition of the observed homogeneous coarse-grained sand deposits in the north (Figure 4.7).

The NW-SE oriented elongated sand body is observed southwest in the study area, and displays high amplitude anomalies in RMS and minimum amplitude attribute maps (Figure 4.8) marked by high amplitude parallel reflectors of SF1 (Figure 4.1A, 4.2C). The observations imply a significant contrast in acoustic impedance to the over-and underlying lithologies. It is likely that coarse-grained brine-filled sand deposits cause this high impedance contrast captured by SF1 (Gassnova, 2012; Sundal et al., 2016), potentially formed as a spit bar during an aggradational phase of the E-W prograding Johansen delta (Hoyt, 1967; Nielsen & Johannessen, 2008b; Swift, 1975). SF1 defines the spit bar with the presence of sharp boundaries to SF3 in seismic lines through the spit, supporting this interpretation (Figure 4.1A, 4.2C, 5.1). The geometry is consistent with a coast parallel spit bar, as it measures over 20 km in length and is 2-3 km wide, overlying marine mud of the Amundsen Formation (Nielsen & Johannessen, 2008). Another feature implying spit deposits is the low SW depositional dip, contradicting the steeply westerly dipping clinoforms in the northern parts, as the seismic facies expression is consistent with high amplitude parallel-reflectors lacking any clear angular dipping reflectors. The assumption of large-scale coastward spit progradation by mainland-beach detachment, can only occur as regression passes into transgression (Hoyt, 1967; Swift, 1975). Such a development would be associated with beach ridges underlying transgressive mud deposits. However, this does not apply to observations in the seismic, indicating southward

spit progradation through alongshore currents supplying the spit from the source further up-dip, instead of through mainland-beach detachment (Nielsen & Johannessen, 2008). Alongshore sediment supply would demand relatively strong N-S currents, indicating an increase in delta plain sediment supply with sediment bypass to the spit system. Spit bar development in the prograding Johansen Formation is likely developed from a rather stationary anchor point at a river mouth (Sundal et al., 2016).

Well 31/5-7 confirms the presence of coarse-grained sand deposits within the Johansen interval, a relatively high amount of organic material compared to the northern wells (Figure 4.7), and trough cross-stratification. The deposits thus formed through deposition of large-scale 3D dunes and the high degree of organic material suggests close proximity to a fluvial outlet (Anell et al., 2021). As 31/5-7 does not intersect the interpreted spit bar (Figure 4.2C), but the more proximal areas, suggest the well is located in what is interpreted as a back basin lagoonal environment formed landward of the spit (Nielsen & Johannessen, 2008). This observation aligns with facies map and depositional model illustrated by Sundal et al. (2016), displaying a lagoonal environment developing landward of the spit bar. Facies distribution map of the northern North Sea for Pliensbachian (190-183 Ma) interpreted by Husmo et al. (2003), displays similar observations but detailed information such as spit deposits and the delta development is not present due to little details in the map. Varying energy environment, degree of organic material, and presence of large scale through cross-stratification are likely caused by storm deposits in shallow marine water depths (Duke, 1985). The high grade of organic material indicates proximity to fluvial input, likely from fluvial channels on the distal delta plain. The SF3 dominates the southwestern part of the Johansen Formation, representing a fluctuating energy environment as it is dominated by sub-parallel reflectors, internal terminations, and fluctuating degree of discontinuity. It is likely that the presence of a fluvial influenced delta plain east of the more distal delta front would effect the seismic facies expression.

5.2.2 Secondary reservoir

The primary (e.g, Johansen Formation) and secondary (e.g, Cook Formation) storage reservoir is partly separated by the Upper Amundsen Formation in the north of the study area, and interpreted to be directly in contact in the southern study area (Gassnova, 2012). Justified by the thin deposits of Upper Amundsen, it is integrated in the interpretation of the overlying Cook Formation, measuring 7 meters at the injection well but thickening towards the north. Inferred by the well-preserved spit bar deposits preservation within the Johansen Formation, the marine

mudstones of Upper Amundsen were likely deposited by rapid transgression partly dividing the Johansen and Cook formations (subunit 2.3.1) (Charnock et al., 2001; Deegan & Scull, 1977; Marjanac & Steel, 1997; Vollset & Doré, 1984). This interpretation is challenged by the recent studies of Meneguolo et al. (in prep) that include the biostratigraphy. The Cook Formation displays an average value of approximately 60 meters but generally thinning towards the East (Figure 4.9C), generally displayed by one seismic reflector resultant of the seismic resolution. The prograding sandstone of the Cook Formation can be subdivided into three units (Deegan & Scull, 1977; Vollset & Doré, 1984). Lower tidally influenced to lower marine heterolithic facies, wave-influenced sand bed deposits, and an upper coarse-grained massive cross-stratified sandstone (Halland et al., 2011; Marjanac & Steel, 1997) As the Cook Formation is displayed generally as one reflector in this study area, it is not possible to observe different seismic expressions for the different units in this data set.

Observed changes in seismic facies expression and well-log data from Johansen to the overlying Cook Formation implies differences in the depositional environments of the primary and secondary storage reservoirs (Figure 5.1, 4.7, 4.2B,C, 4.4). The Cook Formation displays a thinner average thickness than the Johansen Formation, this may influence the seismic facies expression, as similar facies expressions are present in the area of 31/5-2 where the formation thickness increases and are displayed by several seismic reflectors (Figure 5.1). A northwards increase in chaotic seismic facies (SF3, SF4, SF5)(Figure 4.1, 4.2, 5.1) is observed, similar to the Johansen Formation, and is likely resultant of the overlying gas accumulation in Sognefjord. Observed from well-log`s (Figure 4.7), the Cook Formation displays a northward increase in heterogeneous deposits. The presence of homogeneous sand deposits in Cook is likely dominated by coastal processes of higher energy environment overlying the heterogeneous Johansen in the southern 31/5-7 (Figure 4.7), displaying a change in depositional processes from the primary to the secondary storage reservoir. While there is an observed northward change in depositional processes, to an energy fluctuating fluvial environment, as the northern wells display alternating sand and silt deposits within the Cook Formation (Halland et al., 2011; Marjanac & Steel, 1997). This alternating presence of different lithologies is likely the result of both tidal and fluvial influenced depositional processes dominating the northern study area of the Cook Formation (Gassnova, 2012).

Since 31/5-7 is the only well present in the southern study area, and seismic facies analysis does not provide sufficient information regarding the depositional environment and lateral changes of the secondary storage unit, comprehensive core studies would provide essential information

regarding the Cook Formation. However, this is beyond the scope of this study. Regionally changing seismic facies from the Johansen Formation to the Cook Formation (Figure 5.1, 4.3, 4.4), indicates changing depositional environments from the primary to the secondary storage unit. There is little to no observed growth or deformation of the Cook Formation towards the Tusse hangingwall in proximity to. The thin deposits of the Cook formation compared to the Johansen Formation implies a possible change in accommodation and sediment supply in the inter-rift tectonic stretching present for the Lower to Middle Jurassic (Deng et al., 2017; Holden, 2021).

5.2.3 Primary seal

The deposits of the overlying Drake Formation is related global sea-level increase, the maxiumum transgressive surface (J18) defined by Parkinson and Hines (1995), supported by Jenkyns (1988), linking the formation to the global anoxic event associated with marine mudstone deposition (Charnock et al., 2001; Gassnova, 2012). As well-logs (31/5-7, 31/5-2, 31/3-1) (Figure 4.7) display a well-defined lithology change from shale rich deposits of high gamma-value to alternating sand and shale deposits in the upper part of the Drake Formation, the formation is sub-divided into an Upper heterogeneous shale-rich unit with silt deposits and possible sand lenses, and a Lower shallow-marine homogeneous layered shale deposited in a pro-delta to delta front environment (Marjanac & Steel, 1997; Thompson et al., 2022) . These previous interpretations fit the observations of the Lower Drake Formation.

The reoccurring trend of a northwards increase in chaotic seismic facies (SF3, SF4, SF5)(Figure 4.1, 4.2, 5.2) is present for the Lower Drake Formation, as the shale rich formation provides the primary seal of the Aurora storage complex (Gassnova, 2012), this reoccurring northern increase in chaotic seismic facies is the result of the overlying gas accumulation in the Sognefjord Formation (Gassnova, 2012) rather than a lithology effect (outlined 5.2). The formation thickness reaches its thinnest in the northeast, loosely in agreement with presence of SF3 and likely an effect of thickness change (Figure 4.7C, 4.2A). Sharp east-west trending seismic facies boundaries inferring distally increasing lower energy environments, furthest west of the study area is dominated by high amplitude parallel reflectors followed by somewhat lower amplitude parallel reflectors indicating property changes within Lower Drake (Figure 4.2A). This represents a westward prograding system, as the more distal depositional environments are present to the west indicating a pro delta environment, with a higher degree

of mixed energy systems to the more proximal areas of the east, potentially reflecting a delta front depositional environment.

5.3 Clinoform decompaction analysis

Clinoforms are frequently used to provide information regarding depositional environments and relative sea level, as they demonstrate extensive timelines capturing the transition from shallow to deep waters (e.g., Rich, 1951; Mitchum et al., 1977; Helland-Hansen & Hampson, R.2009; R. Steel & Olsen, 2002; Patruno, Hampson, & Jackson, 2015; Klausen & Helland-Hansen, 2018). Decompaction allows for describing and analyzing the original clinoform geometry prior to burial, and contributes to understanding and predicting facies distributions, architecture, sand bodies, and the depositional environment in the areas of clinoform development (Anell & Midtkandal, 2017; Klausen & Helland-Hansen, 2018; R. Steel & Olsen, 2002). In addition, clinoforms are indicators of paleobathymetry, and through clinoform analysis estimations of basin configuration at the time of deposition can be performed. Reconstructing ancient clinoform geometries within the Johansen Formation brings additional information regarding depositional environments and predictions of expected reservoir qualities, properties, and geometries. Combined with the seismic interpretation performed on formations within the storage complex, this brings a higher level of certainty to the evolution of the depositional environment and implications for CO_2 storage.

The small scale of the clinoforms (tens of meters) (Figure 4.16 Table 4.2, 4.3) suggests delta-scale clinoforms (Patruno & Helland-Hansen, 2018). As increasingly larger clinoforms are deposited in increasingly deeper waters, the depositional environment of the Johansen is likely to have been shallow-marine (Patruno, Hampson, & Jackson, 2015). Increasing accommodation and high rates of deposition are implied for the Johansen Formation as the characteristic sigmoidal cross-sectional clinoform geometry is dominant, defined by the Gaussian curvature with well-defined topset (Adams & Schlager, 2000; Anell & Midtkandal, 2017) . According to Patruno et al. (2015), sigmoidal cross-sectional clinoform geometries are a common characteristic of delta-scale subaqueous clinoforms, contrasting to the oblique cross-sectional geometries that characterize subaerial deltas. As the average restored clinoform height ranges from 51-182 meters (50% sandstone/mudstone composition), it fits the characteristic

measurements of delta-scale subaqueous clinoforms. In addition, evidence of subaqueous clinoform deposition and well-developed topsets and topset-to-foreset rollovers, confirms that there is little to no presence of subaerial exposure (e.g, Burgess & Hovius, 1998; Hampson & Storms, 2003).

The delta development in the north indicated progradation towards the northwest (Figure 4.16) (Marjanac & Steel, 1997; Sundal et al., 2016; Vollset & Doré, 1984) , as the shoreline trajectories from the accreting clinoforms in the north display an overall northwestward shift, changing to a predominantly westward prograding delta in the center of the study area (Helland-Hansen & Gjelberg, 1994; Helland-Hansen & Martinsen, 1996). As outlined in (5.3.1), observations of rapid trajectory line fluctuations may be a consequence of sub-seismic clinoforms. Accommodation was likely present during clinoform development, reflected by ascending to near-vertical trajectory lines within the sigmoidal clinoform geometries which indicates a stable to increasing relative sea level, with sufficient sediment rates also reflected by the sigmoidal geometry (Bullimore et al., 2005; Helland-Hansen & Hampson, 2009; Kertznus & Kneller, 2009; Mellere et al., 2002; R. Steel & Olsen, 2002). The observed ascending clinoform trajectories are located northwest and southwest within the study area (Figure 4.16 C,E). Holden (2021) defined a Lower Jurassic reactivation of the Svartalv fault zone (Figure 1.1), implying fault activity during the deposition of the Johansen and Cook formations. Reactivation of the Svartalv fault zone was prior to the middle Jurassic reactivation of the Tusse fault zone. Hence, generation of accommodation was likely greater in the west during deposition of the Dunlin Group, reflected by the observed ascending clinoform trajectories northwest and southwest in the study area (Figure 4.16 C, E). The observation of stable to increasing sea levels within the Johansen Formation agrees with the depositional model by Sundal et al. (2016), implying that the middle to upper Johansen is dominated by an aggradational to retrogradational phase. As the most distal northern clinoforms (CL10-11) with similarities to oblique clinoform geometries display slightly descending trajectory lines, it indicates higher sediment-bypass dominating in the distal areas of the northern delta development (Johannessen & Steel, 2005).

5.3.1 Limitations to clinoform decompaction analysis

Many potential sources of error accompany clinoform decompaction (Klausen & Helland-Hansen, 2018). Nevertheless, there might be a significant difference between the restored and original clinoforms providing important information regarding the depositional environment.

Observation of great variations within the clinoform measurements, before and after preformed decompaction, could be a result of the small scale of the clinoforms, wherein minor errors in measurement generate sizeable variation in the results (Table 4.2). As a consequence of scale, a potential risk when calculating the dip angles are the ability to be precise in the placement of clinoform rollover points that define the clinoform slope (Patruno, Hampson, & Jackson, 2015). At such small scales, a small displacement when measuring on the seismic reflectors could potentially lead to over-or-underestimated dip angles affecting the clinoform geometry. Hence, the degree of error for foreset dip angles (i.e. the maximum angle) was considered too large, and slope dip angle measured between inflection points was utilized for the clinoform analysis. In addition average clinoform measurements were performed to even out potential measurement errors (Table 4.3). The steepest dipping clinoform (CL 8) displayed the highest restored clinoform height (Figure 4.16C, Table 4.2), the analysis is in agreement with the literature (Patruno, Hampson, & Jackson, 2015).

Another important factor is the vertical seismic resolution, ranging from 8.5 to 16.5 meters (outlined 3.2.3), forming a limitation as the analyzed clinoforms are on the verge of the seismic resolution. The trajectory lines (Figure 4.16) display frequent shifts in progradation direction within single clinoforms and is likely the result of sub-seismic clinoforms interfering with clinoform interpretations and measurements. This leads to different prograding clinoform systems being displayed as one, leading to frequent trajectory variations. Meanwhile, the overall progradational direction becomes well-established when applying such an analysis, providing clear evidence of sediment influx directions and variations. In addition, the GN10M1 seismic survey is a merge of three 3D seismic surveys, and quality is considered good to very good for the Lower Jurassic storage complex (Gassnova, 2012), but variations in the different surveys may interfere with the interpretations. Orientation of seismic inline and crossline may influence the clinoform interpretation, as seismic lines should ideally be oriented parallel to the clinoform depositional dip to correctly display the clinoform geometry (Patruno & Helland-Hansen, 2018).

As mentioned in 5.2, low contrast in property differences and acoustic impedance leads to poor seismic imaging (outlined 2.2.1) (Brown, 2011; Sheriff, 1977). Therefore, a clinoform system of high sand/mud ratio lacking heterogeneities and significant mud drapings would be poorly imaged by seismic. Clinoform geometries are common characteristics of a prograding delta system, and as they are prominent in the overlying Sognefjord Formation (Patruno, Hampson, Jackson, & Dreyer, 2015; Patruno, Hampson, Jackson, & Whipp, 2015), therefore it could be

reasonable to expect clinoform development within Johansen as the formation display similarities to the Sognefjord Formation in regards of depositional processes and delta development. A northward increase in coarse-grained clean sandstone deposits for the Johansen Formation is established (Figure 4.7) (Eigestad et al., 2009; Gassnova, 2012; Halland et al., 2011), and as the chaotic SF5 interpreted as a result of high sand/mud ratio present in the north, this high ratio could lead to poorly imaged clinoforms. Hence, there is a potential explanation to poor clinoform resolution in a prograding sand-rich delta system where clinoforms are a common characteristic.

5.3.2 North-South changing clinoform characteristics

Reconstruction of clinoform geometries resulted in unexpectedly steep clinoform angles, as present clinoform geometries also display surprisingly steep dip angles, there is little reason to believe that this is an effect of the preformed decompaction analysis. As previously mentioned, high-porosity clean sand-rich deposits within the Johansen primary storage unit are expected (outlined 5.3.1). The gradient of siliciclastic clinoforms of similar heights is proportional to the average sediment grain size (Orton & Reading, 1993; Patruno, Hampson, Jackson, & Dreyer, 2015) and sediment composition will influence the slope gradient of the clinoform, as steeper slopes are expected for coarse-grained less cohesive sediments (Anell & Midtkandal, 2017; Gilbert, 1885; Kenter, 1990; Orton & Reading, 1993). The Johansen Formation is likely coarsening to the north, in agreement with the revised depositional model of the Johansen Formation by Sundal et al. (2016), and coarser-grained sand-rich, distinctly wave-dominated spit or shoreface deposits of the northern part of Johansen are observed to retain steeper slope angles (Table 4.2, 4.3).

Clinoform observations in the north correspond to the interpretation of coarse sand-rich deposits, as they measure the highest and steepest restored average foreset dip angle of 22.5 ° (Table 4.3). The observed clinoform height (Table 4.2, 4.3) and steep slopes imply deposition of the northern clinoforms in deeper water, as shallow waters cause gentler slopes (Anell et al., 2021; Anell & Midtkandal, 2017; Pirmez et al., 1998). These steeply dipping clinoforms are in alignment with the interpretation of subaqueous delta-scale clinoforms. According to Patruno et al. (2015), delta-scale sand-prone subaqueous clinoforms have diagnostically steep foreset (0,7-23 °), gentler foreset dip values are expected for subaerial delta-scale clinoforms (0.1-2.7 °) and mud-prone subaqueous delta-scale clinoforms (0.03-1.50°). The quantitative

characteristics fit with the measurements of the Johansen Formation, verifying the interpretation of delta-scale sand-prone subaqueous clinoform systems.

Observations of gentlest clinoforms slopes (16.4 °average angle) (Table 4.3) are present in the center of the study area, potentially indicative of a southward increase in fine-grained cohesive sediments. This assumption is not opposed by the 31/5-7 well, approximately 6 km south of these clinoforms, confirming higher amounts of fine-grained sediments and organic material within the Johansen (Figure 4.7). As the southern study area has poor well coverage, the injection well (31/5-7) forms a representative of the depositional environment in the south, however, the Johansen Formation is deposited as a prograding delta and it is unlikely to assume that the depositional environment of the injection well is applicable for the southern area. The southwestern clinoforms show increased average slope angle (Table 4.3), with potentially sandier deposits than the central clinoforms. On the contrary, these west to east prograding clinoforms may be fed by a western source, potentially affecting the clinoform geometries (Figure 4.16 E'). The prograding system is likely more sand-prone in the north considering the presence of the highest and steepest dipping clinoforms, while the south is likely less sandy influencing the clinoform development in the area.

Change in clinoform slope angles is not only a consequence of sediment content, but the result of many overlapping processes, resulting in a complex composition of plausible factors affecting the clinoform geometry (Anell & Midtkandal, 2017; Patruno & Helland-Hansen, 2018). High sedimentation rates result in gentler slope angles than starved conditions (Anell et al., 2021 and references therein), while limited accommodation often results in gentler slope angles than rapid generation of accommodation by sea-level rise. In addition, tidal delta reworking tends to result in longer, gentler clinoforms as sediment is transported basin wards (Plink-Björklund, 2012). Bypass erosion will result in steeper angles, due to clinoform erosion by turbidities or mass flows. The sediment dispersion associated with the transition from high-energy environments into deeper less disturbed waters can cause clinoform nucleation, which is usually applicable for delta-scale subaqueous clinoforms and most likely one of the causes for clinoform development within the Johansen Formation (Patruno & Helland-Hansen, 2018).

Step clinoform dip angles (> 40°) can occur as a result of carbonate early slope cementation or carbonate secreting organisms generating rigid frameworks (Hubbard et al., 1986; Kenter, 1990). Calcite precipitation and cementation are commonly present within shallow marine sandstones and frequently found as laterally extensive carbonate layers within the Jurassic formations of the northern North Sea (Kantorowicz et al., 1987; Walderhaug & Bjorkum, 1992).

Relatively thin lateral extensive carbonate layers are present within the Johansen Formation (Bjørkum & Walderhaug, 1990; Gassnova, 2012; Sundal et al., 2016), displayed in 31/5-7 by high peaks in the resistivity log as frequently reoccurring carbonate layers in the southern area (Figure 4.7). Also presence of carbonate layers in the northern wells but as rarer occurring layers. Keeping this in mind, there are no observations of clinoforms exceeding >40° (Table 4.2). As the clinoform dip angle does not attain expected values for carbonate cemented clinoforms, the unexpectedly steep dip is likely a result of composition and depositional rate coarse-grained sand deposits and accommodation that acts as the dominant control on clinothem geometry (Anell & Midtkandal, 2017; Orton & Reading, 1993; Patruno, Hampson, & Jackson, 2015; Patruno, Hampson, Jackson, & Dreyer, 2015).

5.3.3 Similarities to Sognefjord Formation clinoform development

Seismic and well-coverage of the Sognefjord Formation is superior to the Johansen Formation, as it is the main reservoir of the Troll Field and is therefore well documented. The earliest interpretations of the Sognefjord Formation by Whitaker (1984) and Hellem et al. (1986) defined the thick coarse-grained reservoir sandstone bodies as offshore bars formed during transgressive reworking of older sediments. Reinterpretations by Stewart et al. (1995) and Dreyer et al. (2005) defined the Sognefjord Formation as coastal spit system deposits, prograding westward through deposition of westerly dipping clinothems bounded in the east by tidal back basin (Patruno, Hampson, Jackson, & Dreyer, 2015). The Upper Jurassic Sognefjord and Lower Jurassic Johansen are fed by the same major fluvial feeder north-east of the Troll Field and distributed southwards by longshore currents, thickness variations and accommodation indicate different tectonic environments in the two westward prograding delta systems (Dreyer et al., 2005; Sundal et al., 2016). Patruno et al. (2015) defined the clinoforms of the Sognefjord Formation as sand-prone delta-scale subaqueous clinoforms, as the clinoforms met the four critical factors defined by Field & Roy (1984); *"1) steep shoreface profile, 2) high-wave energy, 3) coarse-grained sediment supply and 4) a long period of relatively stable sea-level"*.

As the Johansen and Sognefjord formations are fed by the same major fluvial feeder north-east of Troll, developed through westward delta progradation with clinoform development, comparison to the Sognefjord delta-scale subaqueous clinoforms can provide additional information regarding the depositional environment of the clinoforms present in the defined study area (Dreyer et al., 2005; Patruno, Hampson, Jackson, & Dreyer, 2015; Patruno,

Hampson, Jackson, & Whipp, 2015). Patruno et al. (2015) performed an extensive quantitative clinoform characterization of ancient and modern clinoform systems to better characterize diagnostic features, cross plotting morphological, architectural, and chronostratigraphic parameters separately to distinguish different clinoform types. It is important to note that for clinoforms this small, even small difference in measuring points will have a large impact on the results, and that there are uncertainties to Patruno's et al. (2015) measurements as they are interpreted on the verge of seismic resolution. In the clinoform cross-plots (Figure 5.2) Patruno et al. (2015) measured slope length from rollover points, while in this thesis it is measured from the inflection points, leading to slightly longer slope measurements. Although greater clinoform length will decrease slope angle, the clinoforms of Johansen contain steeper slope angles.

The cross-plots of the Johansen clinoforms display great similarities in terms of height and length with the trends of the Sognefjord clinoforms (Figure 5.2A, B) and the other plotted delta-scale sand-prone subaqueous clinoforms (Figure 5.2C), increasing the reliability of delta-scale subaqueous clinoforms within the Johansen. The decompaction of the Johansen clinoforms displays an average increase of 185% in height and 168% in length. As the clinoforms of Patruno et al. (2015) are not decompacted, the best-fit correlation with Johansen is the present values (Figure 5.2 A, B), with only slightly higher values present for the restored clinoforms. In light of these observations, clinoform compaction does not affect the clinoform geometries to the degree of disturbing the quantitative characterization of the delta type, as the restored and present values are plotted in proximity to the average values of delta-scale sand-rich subaqueous clinoforms (Figure 5.2C). Sand-prone delta-scale clinoforms are usually associated with active tectonic settings, while mud-rich are associated with tectonic quiescence, being evidential of local tectonic activity, previously indicated by the observed thickness differences (Figure 4.8C) within the Johansen Formation (Patruno, Hampson, & Jackson, 2015). This is in alignment with the observations of Lower-Middle Jurassic tectonic stretching during the late inter-rift stage on the Horda Platform (Deng et al., 2017; Holden, 2021).

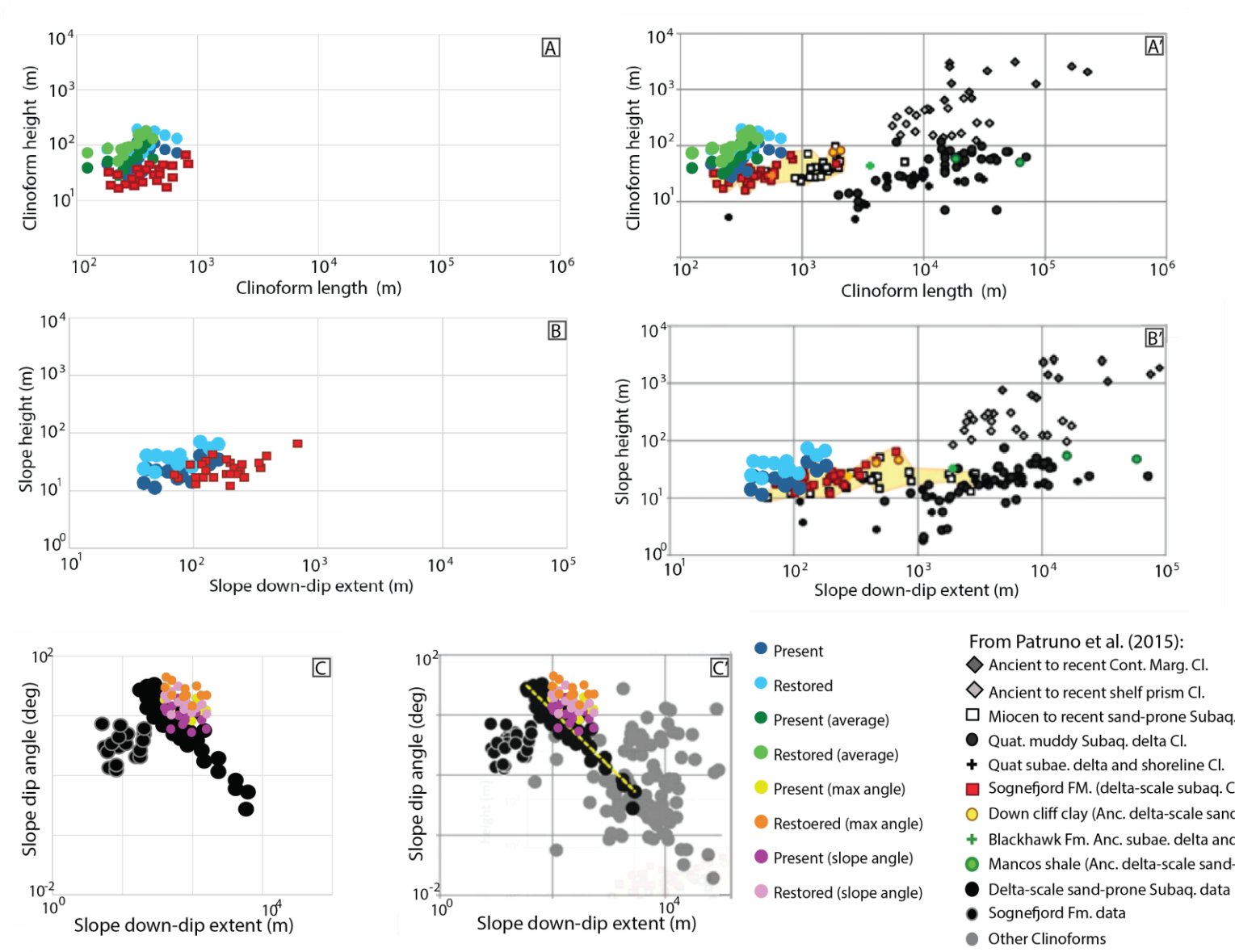
A
Clinoform height (m)
Clinoform length (m)
A'
Clinoform height (m)
Clinoform length (m)
B
Slope height (m)
Slope down-dip extent (m)
B'
Slope height (m)
Slope down-dip extent (m)
C
Slope dip angle (deg)
Slope down-dip extent (m)
C'
Slope dip angle (deg)
Slope down-dip extent (m)
Present
Restored
Present (average)
Restored (average)
Present (max angle)
Restoered (max angle)
Present (slope angle)
Restored (slope angle)
From Patruno et al. (2015):
Ancient to recent Cont. Marg. Cl.
Ancient to recent shelf prism Cl.
Miocen to recent sand-prone Subaq. delta Cl.
Quat. muddy Subaq. delta Cl.
Quat subae. delta and shoreline Cl.
Sognefjord FM. (delta-scale subaq. Cl.)
Down cliff clay (Anc. delta-scale sand-prone Subaq. Cl.
Blackhawk Fm. Anc. subae. delta and shoreline Cl.
Mancos shale (Anc. delta-scale sand-prone Subaq. Cl.
Delta-scale sand-prone Subaq. data
Sognefjord Fm. data
Other Clinoforms

Figur 5.2 Clinoform morphological parameters of Johansen Formation cross-plotted with the quantitative characterizations of deltaic and subaqueous clinoforms by Patruno et al. (2015). Slope down dip correspond to Patruno et al. (2015) Foreset down-dip extent, Slope height corresponds to foreset height, Clinoform length corresponds to Total relief down-dip extent, Clinoform heigt corresponds to Total relief height, and Slope dip angle corresponds to foreset slope gradient. Different types of clinoforms tend to plot in different, but overlapping fields. Clinoforms of Johansen greatly correlates with clinoforms of the Sognefjord Formation. Note that Patruno et al. (2015) measures slope down-dip extent from rollover points, as for this thesis it is measured from inflection points. Abbreviations: Cl = Clinoform, Cont = Continental, Marg = Margin, Subaq= Subaqueous, Quat = Quaternary, Subae = Subaerial, FM = Formation, Anc = Ancient.

5.4 Controls

The sandy units of the Dunlin Group are represented by two prograding sand formations draped by mud-rich deposits formed during transgression and representing flooding surfaces (Deegan & Scull, 1977; Vollset & Doré, 1984). Reoccurrence of the same depositional environment and sequence stratigraphic surfaces through geological times is evidence of cycles effecting accommodation or sediment supply, the observed recurrence within the Dunlin Group may be due to allocyclic factors (Catuneanu et al., 2011). Allocyclic processes such as rise and fall in sea level will influence the nature of depositional structures and hence seismic facies and clinoform development. Observed cycles in depositional environment indicate that the processes are recurring but not necessarily periodic, resulting in the reoccurring prograding sand units of Johansen and Cook formations, but also striking similarities in the overlying Sognefjord Formation. The rapid lateral and vertical changes in seismic facies expressions (Figure 4.2), unpredictable seismic facies stacking patterns (Figure 5.1, 4.15, 4.16), and the presence of chaotic facies imply an interplay between allocyclic external and autogenic internal processes (Ghandour & Fürsich, 2022).

As established by literature (e.g., Færseth, 1996; Gabrielsen et al., 2010; Whipp et al., 2014; Wu et al., 2021), the Dunlin Group was deposited after the Permian-Jurassic rift period in a thermally subsiding basin, with observed thickness variations and growth towards the Tusse hangingwall within the Johansen Formation (Figure 4.8, 4.12). These local variations could be a result of external allogenic influence (Yang et al., 1998), as the interpreted sand-rich delta-scale clinoforms often are associated with tectonic setting (Patruno, Hampson, & Jackson, 2015), and accommodation is likely a result of regional thermal subsidence and local extensional tectonics in the inter-rift stage on the Horda Platform (Deng et al., 2017; Holden, 2021). Although the Johansen Formation and the overlying Sognefjord Formation are fed by

the same northeastern source re-distributed by longshore currents, there are significant differences in clinoform dip (Dreyer et al., 2005; Sundal et al., 2016). Calculated clinoform dip angles in this study range from 10.6°-31.3°, compared to the gentler dipping clinoforms of the Sognefjord Formation displaying dip angles of 1°-16° (Patruno, Hampson, Jackson, & Dreyer, 2015). The clinoforms in Johansen according to analysis, appear to be steeper more akin to the other delta-scale sand-prone subaqueous clinoforms systems (Figure 5.2 C), and steeper than the clinoforms of the Sognefjord Formation. Defining the exact control factors of the complex clinoform development is difficult, but the development of steeper clinoforms could be the result of potentially lower sedimentation rates in Johansen compared to Sognefjord (Anell et al., 2021 and references therein). Accommodation is likely not the main controlling factor as the clinoforms are similar in size, possibly indicating that the difference in slope angles is related to grain size and composition as the southeastern Sognefjord clinoform comprises fine-grained sand and silt deposits in addition to coarse-grained deposits, coarsening northwestwards towards Troll West (Patruno, Hampson, Jackson, & Whipp, 2015). Potentially, the geometries in Johansen is the product of depositional features, for instance coarse grained deposits and lower sediment supply, resulting in the steeply dipping slope angles observed (Anell et al., 2021 and references therein). While the Sognefjord Formation has been exposed to a higher degree of tidal reworking transporting sediment basinward, resulting in gentler dipping clinoforms (Plink-Björklund, 2012). As the Upper Jurassic Sognefjord Formation was deposited in the early phase of the secondary major rift event (Late Jurassic to Early Cretaceous) (Whipp et al., 2014; Wu et al., 2021), deposited along active faults leading to rapid accommodation generation and increased sediment supply from eroded fault creasts of the tilted fault bloks (Færseth, 1996; Whipp et al., 2014). Enhanced sediment supply potentially lead to the observed gentler dipping clinoforms with the Sognefjord Formation, and the development of a much thicker succession than the Johansen Formation.

5.5 Implications for CO_2 storage

The structural dip of the Dunlin Group established in this thesis (Figure 4.5), and previous studies (e.g., Eigestad et al., 2009; Gassnova, 2012; Holden, 2021; Sundal et al., 2015, 2016), establishes a northward migration path of the injected CO_2 plume and the laterally varying seismic facies will have implications for CO_2 migration through the reservoir (Figure 4.2). The best fit seismic facies concerning reservoir properties for CO_2 are dependent on several factors such as porosity, permeability, and heterogeneities. Contradicting to hydrocarbon exploration, heterogeneities within the CO_2 storage reservoir could enhance residual tapping and increase storage potential as CO_2 readily enters small pore spaces (Hovorka, Doughty, Benson, et al., 2004). Simulation of heterogeneous saline formations by Flett et al. (2007) favored heterogeneous reservoirs that provide sufficient injectivity and meet the reservoir qualities and containment criteria, as small increase in reservoir heterogeneities (80:20 sand/shale values) increased migration tortuosity of the injected CO_2 plume, attaining better reservoir contact and enhances CO_2 dissolution. Resulting in enhanced secondary trapping mechanisms, increased migration control, reduced early reliance on the primary sealing unit as the only trapping mechanism, and is desirable to fully exploit the storage capacity of the Johansen reservoir (Baklid et al., 1996; Doughty & Pruess, 2004; Flett et al., 2007; Hovorka, Doughty, & Holtz, 2004). A homogeneous reservoir contributes to faster migration rates, poorer reservoir contact and earlier reliance on the formation seal as the only trapping mechanism, this could be an expected scenario for injection into the interpreted NW-SE trending spit bar deposit (Figure 4.1A, 4.2C). The Lower Drake primary seal can solely act as the main caprock for the storage site in an in-situ stress state, but the effect of injection-increased pressure changes on the caprock needs future evaluations, and secondary trapping mechanisms can reduce the impact on the primary seal (Rahman et al., 2022).

As established, the southern study area is more heterogeneous, and presence of baffling carbonate layers and organic material is likely (Figure 4.7). It potentially implies that seismic facies in the south would be preferred for CO_2 migration (SF1, SF2, SF3 (Figure 4.1A, B, C, 4.2), under the assumption of the additional critical reservoir properties being attained, as it could increase the storage capacity of the reservoir by enhances residual trapping (Flett et al., 2007; Hovorka, Doughty, Benson, et al., 2004) As experienced in the Snøhvit CO_2 injection project, reservoir properties of Tubåen Formation in combination with injection well placement

in fault segment, significantly impacted the injectivity (Shi et al., 2013). Insufficient flow capacity and rapid pressure buildup led to unfeasible injections, resulting in injection into a new overlying reservoir unit in the Stø Formation. Hence, a thorough understanding of the depositional environment is of great significance for the Johansen Formation to better predict injection and flow rates. Heterogeneities are expected in coastal prograding depositional environments, potentially increasing storativity or negatively impact to injection and migration. Reservoir qualities and heterogeneities need to be considered in the selection processes for suitable sequestration reservoirs, as even small-scale heterogeneities have a significant impact on the subsurface behavior of CO_2 (Flett et al., 2007; Frykman et al., 2009).

Clinoforms within the reservoir will contribute to prograding sand reservoirs, with varying degrees of baffles to fluid flow and heterogeneities (R. Steel & Olsen, 2002). According to simulations by Graham et al. (2015a, 2015b) presence of clinoforms within a reservoir will affect fluid flow and needs to be assessed when predicting plume migration. As clinoform mud drapes are effective barriers to fluids, parallel orientation to the depositional strike would be favored as better communication is retained (Flett et al., 2007). Hence, poorer communication would be expected in the central and southwestern clinoform systems within Johansen (Figure 4.16D, E), as they are oriented perpendicular to depositional strike. The NW-SE oriented clinoforms in the northen study area (Figure 4.16B, C) display favorable orientation in regards to the northward CO_2 migration. Laterally connecting clinform topsets of the central and north clinoform system (Figure 4.16C, D) would generate local extensive mud-rich baffles possibly restraining vertical fluid migration into the overlying secondary storage unit (Cook Formation). Clinoforms outcrop analogs of the Chimney Rock Tounge, from the Cretaceous Western interior seaway, United States, form a regressive to transgressive tongue (Plink-Björklund, 2008), similarly to the development of the Johansen Formation. Facies changes from wave-dominated delta systems to mixed-energy and tidal-dominated estuary deposits are captured in the clinoform system. The sand-rich wave-dominated delta clinoforms display an overall upwards coarsening. However, mud deposits are present in the clinoform toe, and 20-40 cm thick layers of bioturbated mudstone, sandstone, and siltstone are present in the lower part of the clinothem body. Compared to the sand-prone delta scale subaqueous clinofoms of the Johansen Formation, it is likely that the homogeneous coarse-grained sand deposits in the north contain interbedded layers of mud and siltstone in the lower part of the clinform systems. Differential distribution is present in the clinoforms of the mixed energy dominated estuary deposits, with proximal and distal coarsening of the clinothem body with finer-grained deposits

in the center of the clinoform, supporting the previous interpretation of higher degree of heterogeneous deposits in the southern study area influenced by fluctuating energy environments. According to forward seismic modeling from these analogs by (Holgate et al., 2014), clinoforms with permeable drapings thinner than 50 cm will not be properly imaged by seismic. Inferring that the observed clinoforms of the Johansen Formation likely contain clinoform drapings >50 cm acting as baffles for fluid flow. In addition, it is likely that there is presence of non-imaged clinoforms in the study area, as the northern area is highly sand-rich.

As decompacted clinoforms displays steeply dipping slope angles (> 10º), a potential migration risk could be vertical placement of the injection well into such steeply dipping clinforms . Mud drapes would act as baffles for lateral plume migration (Graham et al., 2015b, 2015a), leading to CO_2 migrating straight up into the clinoform, potentially resulting in rapidly unsustainable pressure increase within the storage unit. There are no mapped clinoform systems in close proximity to 31/5-7, but as previously mentioned, high sand ratio may lead to poorly imaged clinoforms and the potential presence of non-imaged geometries in the sand-rich prograding delta system (Brown, 2011; Sheriff, 1977). According to the plan of increasing storage potential within the Aurora storage site (Equinor, 2019; Furre et al., 2020; Lothe et al., 2019), additional injection wells will be drilled, and clinoform systems within the Johansen Formation should be considered in this planning phase, as they could potentially hinder migration and lead to unacceptable pressure increase. Based on performed analysis the Johansen Formation contains good reservoir qualities, the observed variations from south to north are likely caused by variations in depositional processes. The progradational system can contribute to heterogeneities and higher degree of trapping mechanisms, but precautions should be taken in terms of rapid pressure buildup caused by potential extensive baffles.

Interpretations of high confidence are desirable as they provide better control of the depositional environment and reservoir properties influencing CO_2 migration and trapping mechanisms. As seismic facies can correspond to geological facies when seismic resolution is sufficient, providing essential information and not influence by secondary processes unrelated to geomogical facies (Roksandic, 1978). According to geomechanical testing at near reservoir conditions in relation to CO_2 storage by Rinehart et al. (2016), different facies responds differently to injected CO_2, and confidence in interpretations is essential. The southern study area generally displays reflectors of higher amplitude, providing a higher level of confidence in the interpretations, than the lower amplitude disrupted reflectors underlying the gas field in the

north as they are most subject to noise (Brown, 2011). On the other hand, the northern study area has better well coverage and hence better well-to-seismic correlation, but potential leakage from wells is one of the critical risks in geological CO_2 sequestration (Li et al., 2018). As the northern study area underlies the Troll West field, an area of densely spaced older abandoned wells where records may be limited, risks related to poor cement job, chemical reactions between CO_2 and cement, and downhole tubulars are existent (Halland et al., 2011).

The CO_2 storage atlas of the northern North Sea (Halland et al., 2011) implies a large potential (70 Gt) for safe long-term storage of CO_2 in saline aquifers and abandoned production fields, that attain the temperature and pressure requirements of supercritical CO_2 (Bachu, 2003; Shukla et al., 2010). This thesis emphasizes the importance of sedimentological assessment in addition to structural assessment, as reservoir heterogeneities in addition to porosity and permeability, seismic facies variations, and internal reservoir geometries will have implications on plume migration, storativity, and injectivity rates (Doughty & Pruess, 2004; Flett et al., 2007; Frykman et al., 2009; Hovorka, Doughty, Benson, et al., 2004; Sundal et al., 2015). In the Aurora storage site, the up-dip CO_2 migration towards the Troll West field to facilitates residual trapping along, increasing storability and reducing the impact on the final sealing unit and leakage potential from abandoned wells of the Troll West field. In the assessment of new potential storage sites, seismic facies analysis will be beneficial when reservoir thickness is higher than the established cut-off value of 30 meters. As little presence of penetrating wells is preferred related to leakage, seismic facies analysis captures changes in depositional environments that relates to reservoir properties, combined with clinoform analysis provides characteristic information related to depositional environment and enhances reservoir predictions.

5.6 Recommendations for further work

This study provides an enhanced understanding of the stratigraphic characterization and evolution of the depositional environment of the Aurora storage site and its implications for CO_2 storage. However, additional research is necessary, especially in regards to monitoring while injecting, to enhance the understanding of reservoir properties such as porosity, permeability, heterogeneity, and baffles implications will be beneficial for the Aurora storage site. This includes:

- The seismic facies analysis and clinoform decompaction method in this thesis has proven to have limitations. The utilized seismic survey GN10M1 is affected by the overlying gas accumulations of the Troll West field towards the north, as seismic processing only marginally compensates for this gas effect, the seismic resolution and character are influenced (Roksandic, 1978; White, 1975)(Roksandic, 1978; White, 1975). In addition, the overburden of the study area is heavily faulted (Thompson et al., 2022; Whipp et al., 2014; Wu et al., 2021). These components will influence the seismic facies analysis and decrease the seismic reliability towards the northern area. Formation thickness and vertical seismic resolution lead to a cut-off value for seismic facies interpretation of 30 meters, values below this cut-off value won't benefit from such analysis. Performed clinoform decompaction following the principles of Klausen and Helland-Hansen (2018), the porosity and compaction coefficient estimates are inferred from Sclater and Christie (1980). Utilizing precise coefficients specifically for the Aurora study area would enhance the confidence of the decompaction.
- Monitoring while injection can address site-specific risks that may affect the project performance, containment, and observations of plume migration according to predictions, or if simulations need alterations based on the observations (Furre et al., 2020; IEAGHG, 2020). Monitoring could provide enhanced information regarding the interpreted effects of secondary trapping mechanisms and the influence of heterogeneities. This would contribute to an improved understanding of plume migration from a more heterolitich reservoir (south) to more homogeneous reservoir properties (north). In addition, it could increase knowledge regarding the Aurora storage site and the northern North Sea, resulting in better premises for future plume simulations

and CO_2 storage assessments for potential storage sites and future plans of increasing storage in Aurora (Halland et al., 2011; Lothe et al., 2019)

- Future work within the Aurora storage site to determine the optimal placing of injection wells, according to the plan of increasing injectivity rates from 1.5 to over 5 million tonnes annually by ramping up numbers of injection wells (Lothe et al., 2019; Northern Lights, 2020). It would be desirable to investigate further the NW-SE-oriented spit bar as a possible location for a new injection well, as reservoir properties are expected to be suitable in terms of porosity and permeability. Future sites of injection wells should be assessed in the southern more heterolithic study area, as extending the migration path can increase secondary trapping mechanisms and hence increase the storage capacity (Zhang & Song, 2014). However, there is a stratigraphical pinch out of the Johansen Formation towards the south and west that needs to be considered when planning for injection wells in the south (Sundal et al., 2016).

- Further assess the influence of the Upper Amundsen, as it is too thin to provide a primary seal (Sundal et al., 2015), but might have a baffling effect on buoyant CO_2 migration into the secondary storage reservoir (e.g., Cook Formation). The formation thickens to the north and will likely have an increased influence on migration and vertical communication within the reservoir. Therefore it could be beneficial to map the lateral continuity, presence, and potential influence of the Upper Amundsen Formation.

6 Conclusions

This study emphasizes the importance of reservoir characterization and sedimentological interpretation. Given that reservoir heterogeneities, together with porosity and permeability, will have implications for CO_2 plume migration, storativity, and injectivity rate. Seismic facies analysis, clinoform description, and decompaction were applied to locate and characterize reservoir variations within the Aurora storage complex as a means of de-risking the storage site. In light of this, the main objectives of this study were to: i) assess the presence and distribution of seismic facies and clinoform geometries, ii) establish sedimentary environments and sediment partitioning within the succession, and iii) discuss the plausible influence of reservoir heterogeneities for CO_2 injection, migration, and storage. The main findings and concluding remarks of this thesis are given below:

- This study has proven seismic facies analysis to be beneficial in assessing depositional environment in reservoir and seal units with thicknesses greater than the established cut-off value of 30 meters: e.g., Johansen Formation and Drake Formation. As the seismic facies are defined by changes in seismic reflection patterns and impedance, the analysis will be influenced by seismic data quality. However, critical information regarding reflection abundance and geometries is lost for successions thinner than the cut-off value (e.g., Cook Formation). In this case, performed seismic facies analysis might entail uncertainties, and the formation will not benefit from such analysis.

- This study supports the previous findings regarding lateral changing depositional environments of The Johansen Formation (e.g., primary storage unit), supported by the seismic facies analysis. In the southern study area, heterogeneous sediments were deposited in a fluctuating tidal energy environment influenced by redistribution and washower processes related to the observed NW-SE prograding spit. Meanwhile, the northern study area comprises homogeneous coarse-grained sand deposited in a high-energy shallow marine shelf environment.

- Clinoform decompaction allows restoration of original clinoform geometries. Through the restoration of small-scale clinoforms within the Johansen Formation, this study revealed dominantly westward prograding delta-scale sand-prone subaqueous clinoforms. The clinoforms displayed unexpectedly steeply dipping angles of 10.6°-

31.3° (min/max), which increased northwards and is inferred to be a result of the increasing grain size. Although of similar height and length to the clinoforms of the Sognefjord Formation, the studied clinoforms are steeper, suggesting grain size and/or sediment rate contributed to the observed variation.

- The sand-rich prograding Johansen Formation, supported by trajectory analysis and confirmed by northwest to westward prograding sand-prone delta-scale subaqueous clinoforms, supports the previous findings of the Johansen Formation deposited as a westerly prograding delta system. Clinoforms nucleated from sediment dispersion associated with the transition from a high-energy environment to less disturbed waters. Implying delta development in a shallow marine environment, as the clinoform scale, associated with water depth, measures 21-108 meters in height.

- The southern study area of the Lower Jurassic storage complex is preferred for CO_2 injection as it is located downdip of the final closure located below the Troll field, in an area of sparsely spaced wells reducing leakage potential. In addition to comprising heterogeneous deposits that contribute to plume dispersion, enhances CO_2 dissolution and reaction with formation water. This increases secondary trapping mechanisms along the northward migration path, and storativity within the storage complex is enhanced. No clinoforms are observed at the injection site, and as seismically imaged clinoforms are inferred to contain clinoform mud drapes exceeding 50 cm, there is potential presence of non-imaged clinoform systems as a result of thin mud drapes, clinoform composition, and seismic resolution. As steeply dipping clinoforms may lead to rapid pressure increase, parallel orientation to the depositional dip would retain better communication and should be assessed when planning for new injection wells.

7 References

Adams, E. W., & Schlager, W. (2000). Basic types of submarine slope curvature. *Journal of Sedimentary Research*, *70*(4), 814–828. https://doi.org/10.1306/2DC4093A-0E47-11D7-8643000102C1865D

Allen, P. H., & Allen, J. R. (2005). Chapter 9–Subsidence and thermal history. Basin Analysis, Principles and Applications. *Blackwell Publishing*, *349*, 395.

Anell, I., & Midtkandal, I. (2017). The quantifiable clinothem – types, shapes and geometric relationships in the Plio-Pleistocene Giant Foresets Formation, Taranaki Basin, New Zealand. *Basin Research*, *29*, 277–297. https://doi.org/10.1111/bre.12149

Anell, I., Zuchuat, V., Röhnert, A. D., Smyrak-Sikora, A., Buckley, S., Lord, G., Maher, H., Midtkandal, I., Ogata, K., Olaussen, S., Osmundsen, P. T., & Braathen, A. (2021). Tidal amplification and along-strike process variability in a mixed-energy paralic system prograding onto a low accommodation shelf, Edgeøya, Svalbard. *Basin Research*, *33*(1), 478–512. https://doi.org/10.1111/bre.12482

Arts, R., Eiken, O., Chadwick, A., Zweigel, P., van der Meer, B., & Kirby, G. (2004). Seismic monitoring at the Sleipner underground CO 2 storage site (North Sea). *Geological Society Special Publication*, *233*, 181–191. https://doi.org/10.1144/GSL.SP.2004.233.01.12

Bachu, S. (2003). Screening and ranking of sedimentary basins for sequestration of CO2 in geological media in response to climate change. *Environmental Geology*, *44*(3), 277–289. https://doi.org/10.1007/s00254-003-0762-9

Bachu, S., & Adams, J. J. (2003). Sequestration of CO2 in geological media in response to climate change: Capacity of deep saline aquifers to sequester CO2 in solution. *Energy Conversion and Management*, *44*(20), 3151–3175. https://doi.org/10.1016/S0196-8904(03)00101-8

Baklid, A., Korbøl, R., & Owren, G. (1996). Sleipner Vest CO2 Disposal, Co2 Injection Into A Shallow Underground Aquifer. *Society of Petroleum Engineers*, 269–277.

Bartholomew, I. D., Peters, J. M., & Powell, C. M. (1993). Regional structural evolution of the North Sea: Oblique slip and the reactivation of basement lineaments. *Petroleum Geology Conference Proceedings*, *4*(0), 1109–1122. https://doi.org/10.1144/0041109

Bell, R. E., Jackson, C. A. L., Whipp, P. S., & Clements, B. (2014). Strain migration during multiphase extension: Observations from the northern North Sea. *Tectonics*, *33*(10), 1936–1963. https://doi.org/10.1002/2014TC003551

Berg, O. R. (1982). Seismic Detection and Evaluation of Delta and Turbidite Sequences: Their Application to Exploration for the Subtle Trap. *AAPG*, *66*(9), 1271–1288.

Bjørkum, P. A., & Walderhaug, O. (1990). Geometrical arrangement of calcite cementation within shallow marine sandstones. *Earth Science Reviews*, *29*(1–4), 145–161. https://doi.org/10.1016/0012-8252(0)90033-R

Bjørlykke, K., & Høeg, K. (1997). Effects of burial diagenesis on stresses, compaction and fluid flow in sedimentary basins. *Marine and Petroleum Geology*, *14*(3), 267–276. https://doi.org/10.1016/S0264-8172(96)00051-7

Bjørlykke, K., & Jahren, J. (2015). Sandstones and Sandstone Reservoirs. In *Petroleum Geociense* (pp. 119–147).

Boggs, S. Jr. (2014). *Principles of Sedimentology and Stratigraphy* (fifth). Pearson Education Limited.

Brown, A. R. (2011). *Interpretation of three-dimensional seismic data* (Issue 7). AAPG and the Society of Exploration Geophysicists.

Bullimore, S., Henriksen, S., Liestøl, Frode. M., & Helland-Hansen, W. (2005). Clinoform stacking patterns, shelf-edge trajectories and facies associations in Tertiary coastal deltas, offshore Norway: Implications for the prediction of lithology in prograding systems. *Norwegian Journal of Geology , 85*, 169–187.

Burgess, P. M., & Hovius, N. (1998). Rates of delta progradation during highstands: consequences for timing of deposition in deep-marine systems. In *Journal of the Geological Society* (Vol. 155). http://jgs.lyellcollection.org/

Carvajal, C., Steel, R., & Petter, A. (2009). Sediment supply: The main driver of shelf-margin growth. *Earth-Science Reviews*, *96*(4), 221–248. https://doi.org/10.1016/j.earscirev.2009.06.008

Catuneanu, O., Galloway, W. E., Kendall, C. G. S. C., Miall, A. D., Posamentier, H. W., Strasser, A., & Tucker, M. E. (2011). Sequence Stratigraphy: Methodology and nomenclature. *Newsletters on Stratigraphy*, *44*(3), 173–245. https://doi.org/10.1127/0078-0421/2011/0011

Charnock, M. A., Kristiansen, I. L., Ryseth, A., & Fenton, J. P. G. (2001). Sequence stratigraphy of the Lower Jurassic Dunlin Group, northern North Sea. *Norwegian Petroleum Society , 10*, 145–174.

Crameri, F., Shephard, G. E., & Heron, P. J. (2020). The misuse of colour in science communication. *Nature Communications*, *11*(1). https://doi.org/10.1038/s41467-020-19160-7

Davies, R. J., Turner, J. D., & Underhill, J. R. (2001). Sequential dip-slip fault movement during rifting: A new model for the evolution of the Jurassic trilete North sea rift system. *Petroleum Geoscience*, *7*(4), 371–388. https://doi.org/10.1144/petgeo.7.4.371

Deegan, C. E., & Scull, B. J. (1977). A standard lithostratigraphic nomenclature for the Central and Northern North Sea. In *Norwegian Petroleum Directorate Bulletin* (Vol. 1, p. 36).

Deibert, J. E., Benda, T., Løseth, T., Schellpeper, M., & Steel, R. J. (2003). Eocene clinoform growth in front of a storm-wave-dominated shelf, Central Basin, Spitsbergen: No significant sand delivery to deepwater areas. *Journal of Sedimentary Research*, *73*(4), 546–558. https://doi.org/10.1306/011703730546

Deng, C., Fossen, H., Gawthorpe, R. L., Rotevatn, A., Jackson, C. A. L., & FazliKhani, H. (2017). Influence of fault reactivation during multiphase rifting: The Oseberg area, northern North Sea rift. *Marine and Petroleum Geology*, *86*, 1252–1272. https://doi.org/10.1016/j.marpetgeo.2017.07.025

Denham, L. R., & Sheriff, R. E. (1981). What is horizontal resolution? *Indonesian Petroleum Association, 10th Annual Convetion, May 1981*, 119–134.

de Silva, G. P. D., Ranjith, P. G., & Perera, M. S. A. (2015). Geochemical aspects of CO2 sequestration in deep saline aquifers: A review. *Fuel*, *155*, 128–143. https://doi.org/10.1016/j.fuel.2015.03.045

Doughty, C., & Pruess, K. (2004). Modeling supercritical carbon dioxide injection in heterogeneous porous media.

Dreyer, T., Whitaker, M., Dexter, J., Flesche, H., & Larsen, E. (2005). From spit system to tide-dominated delta: Integrated reservoir model of the upper Jurassic Sognefjord formation on the Troll West Field. *Petroleum Geology Conference Proceedings*, *6*(0), 423–448. https://doi.org/10.1144/0060423

Duffy, O. B., Bell, R. E., Jackson, C. A. L., Gawthorpe, R. L., & Whipp, P. S. (2015a). Fault growth and interactions in a multiphase rift fault network: Horda Platform, Norwegian North Sea. *Journal of Structural Geology*, *80*, 99–119. https://doi.org/10.1016/j.jsg.2015.08.015

Duke, W. L. (1985). Hummocky cross-stratification, tropical hurricanes, and intense winter storms. *Sedimentology*, *32*, 167–194.

Eigestad, G. T., Dahle, H. K., Hellevang, B., Riis, F., Johansen, W. T., & Øian, E. (2009). Geological modeling and simulation of CO2 injection in the Johansen formation. *Computational Geosciences*, *13*(4), 435–450. https://doi.org/10.1007/s10596-009-9153-y

Equinor. (2019). *Northern Lights Project Concept report. RE-PM673-00001*. 139. Available: Northern Lights Concept report (northernlightsccs.com) [Accessed 07/05/2022].

Færseth, R. B. (1996). Interaction of permo-triassic and jurassic extensional fault-blocks during the development of the northern North Sea. *Journal of the Geological Society*, *153*(6), 931–944. https://doi.org/10.1144/gsjgs.153.6.0931

Faleide, J. I., Bjørlykke, K., & Gabrielsen, R. H. (2015). Geology of the Norwegian Continental Shelf. In *Petroleum Geoscience: From Sedimentary Environments to Rock Physics, Second Edition* (pp. 603–635). https://doi.org/10.1007/978-3-642-34132-8

Fawad, M., & Mondol, N. H. (2018). *Fifth CO 2 Geological Storage Workshop 21-23*.

Fawad, M., Mondol, N. H., Jahren, J., & Bjørlykke, K. (2011). Mechanical compaction and ultrasonic velocity of sands with different texture and mineralogical composition. *Geophysical Prospecting*, *59*(4), 697–720. https://doi.org/10.1111/j.1365-2478.2011.00951.x

Field, M. E., & Roy, P. S. (1984). Offshore transport and sand-body formation: Evidence from a steep, high-energy shoreface, Southeastern Australia. http://pubs.geoscienceworld.org/sepm/jsedres/article-pdf/54/4/1292/2809386/1292.pdf

Flett, M., Gurton, R., & Weir, G. (2007). Heterogeneous saline formations for carbon dioxide disposal: Impact of varying heterogeneity on containment and trapping. *Journal of Petroleum Science and Engineering*, *57*(1–2), 106–118. https://doi.org/10.1016/j.petrol.2006.08.016

Frykman, P., Bech, N., Sørensen, A. T., Nielsen, L. H., Nielsen, C. M., Kristensen, L., & Bidstrup, T. (2009). Geological modeling and dynamic flow analysis as initial site investigation for large-scale CO2 injection at the Vedsted structure, NW Denmark. *Energy Procedia*, *1*(1), 2975–2982. https://doi.org/10.1016/j.egypro.2009.02.074

Furre, A. K., Meneguolo, R., Pinturier, L., & Bakke, K. (2020a). Planning deep subsurface CO2 storage monitoring for the Norwegian full-scale CCS project. *First Break*, *38*(10), 55–60. https://doi.org/10.3997/1365-2397.fb2020074

Gabrielsen, R. H., Faleide, J. I., Pascal, C., Braathen, A., Nystuen, J. P., Etzelmuller, B., & O'Donnell, S. (2010). Latest Caledonian to Present tectonomorphological development of

southern Norway. *Marine and Petroleum Geology*, *27*(3), 709–723. https://doi.org/10.1016/j.marpetgeo.2009.06.004

Gassnova. (2012). *Geological storage of CO2 from Mongstad. Interim report Johansen Formation*. *TL02-GTL-Z-RA-000*, 1–308.

Gee, D. G., Fossen, H., Henriksen, N., & Higgins, A. K. (2008). From the early Paleozoic platforms of Baltica and Laurentia to the Caledonide Orogen of Scandinavia and Greenland. *Episodes*, *31*(1), 44–51. https://doi.org/10.18814/epiiugs/2008/v31i1/007

Ghandour, I. M., & Fürsich, F. T. (2022). Allogenic and autogenic controls on facies and stratigraphic architecture of the Lower Jurassic Mashabba Formation, Gebel Al-Maghara, North Sinai, Egypt. *Proceedings of the Geologists' Association*, *133*(1), 67–86. https://doi.org/10.1016/j.pgeola.2021.12.001

Gilbert, G. K. (1885). The Topographic feature of lake shores. *US Government Printing Office*.

Graham, G. H., Jackson, M. D., & Hampson, G. J. (2015a). Three-dimensional modeling of clinoforms in shallow-marine reservoirs: Part 1. Concepts and application. *AAPG Bulletin*, *99*(6), 1013–1047. https://doi.org/10.1306/01191513190

Graham, G. H., Jackson, M. D., & Hampson, G. J. (2015b). Three-dimensional modeling of clinoforms in shallow-marine reservoirs: Part 2. Impact on fluid flow and hydrocarbon recovery in fluvial-dominated deltaic reservoirs. *AAPG Bulletin*, *99*(6), 1049–1080. https://doi.org/10.1306/01191513191

Gunter, W. D., Bachu, S., & Benson, S. (2004). The role of hydrogeological and geochemical trapping in sedimentary basins for secure geological storage of carbon dioxide. *Geological Society Special Publication*, *233*, 129–145. https://doi.org/10.1144/GSL.SP.2004.233.01.09

Halland, E. K., Leader, P., Gjeldvik, I. T., Johansen, W. T., Magnus, C., Meling, I. M., Pedersen, S., Riis, F., Solbakk, T., & Tappel, I. (2014). The Norwegian North Sea. *Norwegian Petroleum Directorate*, 1–45.

Halland, Eva. K., Gjeldvik, Ine. T., Johansen, Wenche. T., Magnus, C., Meling, I. M., Pedersen, S., Riis, F., Solbakk, T., & Tappel, I. (2011). CO2 storage Atlas - Norwegian North Sea. Norwegian Petroleum Directorate, Stavanger, Norway.

Hampson, G. J., & Storms, J. E. A. (2003). Geomorphological and sequence stratigraphic variability in wave-dominated, shoreface-shelf parasequences. *Sedimentology*, *50*(4), 667–701. https://doi.org/10.1046/J.1365-3091.2003.00570.X

Helland-Hansen, W., Ashton, M., Lømo, L., & Steel, R. (1992). Advance and retreat of the Brent delta: Recent contributions to the depositional model. *Geological Society Special Publication*, *61*(61), 109–127. https://doi.org/10.1144/GSL.SP.1992.061.01.07

Helland-Hansen, W., & Gjelberg, J. G. (1994). Conceptual basis and variability in sequence stratigraphy: a different perspective. In *Sedimentary Geology* (Vol. 92).

Helland-Hansen, W., & Hampson, G. J. (2009). Trajectory analysis: Concepts and applications. *Basin Research*, *21*(5), 454–483. https://doi.org/10.1111/j.1365-2117.2009.00425.x

Helland-Hansen, W., & Martinsen, Ole. J. (1996). Shoreline Trajectories and Sequences: Description of Variable Depositional-Dip Scenarios. *Jornal of Sedimentary Reaserch* , *66*(4), 670–688.

Hellem, T., Kjemperud, A., & Ovrebo, O. K. (1986). The Troll Field: a geological/geophysical model established by the PL085 Group. *Habitat of Hydrocarbons on the Norvegian Continental Shelf. International Conference*, 217–238.

Holden, N. (2021). *Structural characterization and across-fault seal assessment of the Aurora CO 2 storage site, northern North Sea* [University of Oslo]. http://www.duo.uio.no/

Holgate, N. E., Hampson, G. J., Jackson, C. A.-L., & Petersen, S. A. (2014). Constraining uncertainty in interpretation of seismically imaged clinoforms in deltaic reservoirs, Troll field, Norwegian North Sea: Insights from forward seismic models of outcrop analogsCharacterization of Seismically Imaged Clinoforms Using Forward Seismic Models of Outcrop Analogs. *AAPG Bulletin*, *98*(12), 2629–2663.

Hovorka, S. D., Doughty, C., Benson, S. M., Pruess, K., & Knox, P. R. (2004). The impact of geological heterogeneity on CO 2 storage in brine formations: a case study from the Texas Gulf Coast Problem and approach. *Geologcial Society of London, Special Publications 233*, 147–163. http://sp.lyellcollection.org/Downloadedfrom

Hovorka, S. D., Doughty, C., & Holtz, M. H. (2004). Testing Efficiency of Storage in the Subsurface: Frio Brine Pilot Experiment. In *7th International Conference on Greenhouse Gas Control Technologies, Vancouver, Canada,September 5-9 unpaginated [5p.] GCCC Digital Publication Series #04-01*.

Hoyt, Johan. H. (1967). Barrier Island Formation. *Geological Society of America Bulletin , 78*, 1125–1136.

Hubbard, D. K., Burke, R. B., & Gill, I. P. (1986). Styles of Reef Accretion Along a Steep, Shelfe-Edge Reef, ST.Croix, U.S Virgin Islands. *Journal of Sedimentary Petrology*, *56*(6), 848–861. http://pubs.geoscienceworld.org/sepm/jsedres/article-pdf/56/6/848/2809755/848.pdf

Husmo, T., Hamar, G. P., Høiland, O., Johannessen, E. P., Rømuld, A., Spencer, A. M., & Titterton, R. (2003). Lower and Middle Jurassic. In D. Evans, C. Graham, A. Armour, & P. Bathurst (Eds.), *The Millennium Atlas: Petroleum Geology of the Central and Northern North Sea*. The GEological Society. https://www.researchgate.net/publication/285129506

IEA. (2021). *Net Zero by 2050 - A Roadmap for the Global Energy Sector*. www.iea.org/t&c/

IEAGHG. (2020). *Monitoring and Modelling of CO_2 Storage: The Potential for Improving the Cost-Benefit Ratio of Reducing Risk*. www.ieaghg.org

IPCC. (2021). *AR6 Climate Change 2021: The Physical Science basis*.

Jenkyns, H. C. (1988). The early Toarcian (Jurassic) anoxic event: stratigraphic, sedimentary, and geochemical evidence. *American Journal of Science*, *288*(2), 101–151. https://doi.org/10.2475/ajs.288.2.101

Johannessen, E. P., & Steel, R. J. (2005). Shelf-margin clinoforms and prediction of deepwater sands. *Basin Research*, *17*(4), 521–550. https://doi.org/10.1111/j.1365-2117.2005.00278.x

Kantorowicz, J. D., Bryant, I. D., & Dawans, J. M. (1987). Controls on the geometry and distribution of carbonate cements in Jurassic sandstones: Bridport Sands, southern England and Viking Group, Troll Field, Norway. *Diagenesis of Sedimentary Sequences (Ed. J. D Marshall), Spec. Publ. Geol. Soc. London , 36*, 103–118. http://sp.lyellcollection.org/

Kenter, Jeroen. A. M. (1990). Carbonate platform flanks: slope angle and sediment fabric. In *Sedimentology* (Vol. 37).

Kertznus, V., & Kneller, B. (2009). Clinoform quantification for assessing the effects of external forcing on continental margin development. *Basin Research*, *21*(5), 738–758. https://doi.org/10.1111/j.1365-2117.2009.00411.x

Klausen, T. G., & Helland-Hansen, W. (2018). Methods for restoring and describing ancient Clinoform surfaces. *Journal of Sedimentary Research*, *88*(2), 241–259. https://doi.org/10.2110/jsr.2018.8

Lervik, K. S. (2006). Triassic lithostratigraphy of the Northern North Sea Basin. *Norsk Geologisk Tidsskrift*, *86*(2), 93–115.

Li, B., Zhou, F., Li, H., Duguid, A., Que, L., Xue, Y., & Tan, Y. (2018). Prediction of CO2 leakage risk for wells in carbon sequestration fields with an optimal artificial neural network. *International Journal of Greenhouse Gas Control*, *68*, 276–286. https://doi.org/10.1016/j.ijggc.2017.11.004

Lindsey, J. P. (1989). The Fresnel zone and its interpetive significance. *The Leading Edge*, *8*(10), 33–39. https://doi.org/10.1190/1.1439575

Lothe, A. E., Bergmo, P. E. S., & A.-A.Grimstad. (2019).Storage resources for future European CCS deployment; A roadmap for a Horda CO_2 storage hub, Offshore Norway. *SINTEF Proceedings No 4, June 2019*, 39–48.

Marjanac, T., & Steel, R. J. (1997). Dunlin group sequence stratigraphy in the northern North Sea: A model for cook sandstone deposition. *AAPG Bulletin*, *81*(2), 276–292. https://doi.org/10.1306/522b4307-1727-11d7-8645000102c1865d

Mellere, D., Plink-Björklund, P., & Steel, R. (2002). Anatomy of shelf deltas at the edge of a prograding Eocene shelf margin, Spitsbergen. In *Sedimentology* (Vol. 49).

Meneguolo, R., Sundal, A., Martinius, A. W., Veselovsky, Z., Cullum, A., & Milovanova, E. (2022). Impact of the Lower Jurassic Dunlin Group depositional elements on the Aurora CO_2 storage, EL001, Northen North Sea, Norway. International Journal of Greenhouse Gas Control, accepted manuscript.

Midtkandal, I., Faleide, T. S., Faleide, J. I., Planke, S., Anell, I., & Nystuen, J. P. (2020). Nested intrashelf platform clinoforms—Evidence of shelf platform growth exemplified by Lower Cretaceous strata in the Barents Sea. *Basin Research*, *32*(2), 216–223. https://doi.org/10.1111/bre.12377

Mitchum, R. M., Vail, P. R., & Sangree, J. B. (1977). *Stratigraphic Interpretation of Seismic Reflection Patterns in Depositional Sequences:Seismic Stratigraphy and Global Changes of Sea Level: Part 6.*

NCCS. (2019). *Norwegian CCS Research Centre (NCCS) Annual Report 2019*. https://www.sintef.no/globalassets/project/nccs/annual-2019/nccs_annual_report_2019_rev_lr.pdf

Nielsen, L. H., & Johannessen, P. N. (2008). Are some isolated shelf sandstone ridges in the Cretaceous western interior seaway transgressed, detached spit systems? In *Recent advances in models of siliciclastic shallow-marine stratigraphy* (Vol. 90, pp. 333–354). SEPM (Society for Sedimentary Geology).

Northern Lights. (2020). *Annual report Northern Lights | 2021*.

Northern Lights. (2022, May 3). *About the Longship Project* . https://norlights.com/about-the-longship-project/. [Accessed 03/05/2022].

Norwegian Minestry of Petroleum and Energy. (2020). *Longship – Carbon capture and storage* (Vol. 33).

NPD. (2014). *Norwegian Petroleum Directorate - Geology of the North Sea*. https://www.npd.no/en/facts/publications/co2-atlases/co2-atlas-for-the-norwegian-continental-shelf/4-the-norwegian-north-sea/4.1-geology-of-the-north-sea/. [Accessed 03/05/2022].

NPD. (2020). *Exploration Resource report 2020*. 1–77.

NPD Factpages. (2022). *31/5-7 Wellbore/ Exploration*. https://factpages.npd.no/en/wellbore/pageview/exploration/by/bycompletiondate/8951. [Accessed 14/05/2022].

Nystuen, J. P., Kjemperud, A. v, Müller, R., Adestål, V., & Schomacker, E. R. (2014). Late Triassic to Early Jurassic climatic change, northern North Sea region: impact on alluvial architecture, palaeosols and clay mineralogy. In T. Stewens, A. W. Martinium, R. Ravnås, J. A. Howell, R. J. Steel, & J. P. Wonham (Eds.), *Int. Assoc. Sedimentol. Spec. Publ* (Vol. 46, pp. 59–100).

Orton, G. J., & Reading, H. G. (1993). *Variability of deltaic processes in terms of sediment supply, with particular emphasis on grain size* (Vol. 40).

Parkinson, D. N., & Hines, F. M. (1995). The Lower Jurassic of the North Viking Graben in the context of Western European Lower Jurassic stratigraphy. *Norwegian Petroleum Society , 5*, 97–107.

Partington, M. A., Copestake, P., Mitchener, B. C., & Underhill, J. R. (1993). Biostratigraphic calibration of genetic stratigraphic sequences in the Jurassic-lowermost Cretaceous (Hettangian to Ryazanian) of the North Sea and adjacent areas. *Petroleum Geology Conference Proceedings*, *4*(0), 371–386. https://doi.org/10.1144/0040371

Patruno, S., Hampson, G. J., & Jackson, C. A. L. (2015). Quantitative characterisation of deltaic and subaqueous clinoforms. In *Earth-Science Reviews* (Vol. 142, pp. 79–119). Elsevier B.V. https://doi.org/10.1016/j.earscirev.2015.01.004

Patruno, S., Hampson, G. J., Jackson, C. A. L., & Dreyer, T. (2015). Clinoform geometry, geomorphology, facies character and stratigraphic architecture of a sand-rich subaqueous delta: Jurassic Sognefjord Formation, offshore Norway. *Sedimentology*, *62*(1), 350–388. https://doi.org/10.1111/sed.12153

Patruno, S., Hampson, G. J., Jackson, C. A. L., & Whipp, P. S. (2015). Quantitative progradation dynamics and stratigraphic architecture of ancient shallow-marine clinoform sets: A new method and its application to the Upper Jurassic Sognefjord Formation, Troll Field, offshore Norway. *Basin Research*, *27*(4), 412–452. https://doi.org/10.1111/bre.12081

Patruno, S., & Helland-Hansen, W. (2018). Clinoforms and clinoform systems: Review and dynamic classification scheme for shorelines, subaqueous deltas, shelf edges and continental margins. *Earth-Science Reviews*, *185*(June), 202–233. https://doi.org/10.1016/j.earscirev.2018.05.016

Pirmez, C., Pratson, L. F., & Steckler, M. S. (1998). Clinoform development by advection-diffusion of suspended sediment: Modeling and comparison to natural systems. *Journal of*

Geophysical Research: Solid Earth, *103*(10), 24141–24157. https://doi.org/10.1029/98jb01516

Plink-Björklund, P. (2008). Wave-to-tide facies change in a Campanian shoreline complex, Chimney Rock Tongue, Wyoming-Utah, USA. *Society of Sedimentary Geology* , *90*, 265–291.

Plink-Björklund, P. (2012). Effects of tides on deltaic deposition: Causes and responses. *Sedimentary Geology*, *279*, 107–133. https://doi.org/10.1016/j.sedgeo.2011.07.006

Quiquerez, A., & Dromart, G. (2006). Environmental control on granular clinoforms of ancient carbonate shelves. *Geological Magazine*, *143*(3), 343–365. https://doi.org/10.1017/S0016756806001749

Rahman, M. J., Fawad, M., Jahren, J., & Mondol, N. H. (2022). Influence of Depositional and Diagenetic Processes on Caprock Properties of CO2 Storage Sites in the Northern North Sea, Offshore Norway. *Geosciences*, *12*(5), 181. https://doi.org/10.3390/geosciences12050181

Regjeringen. (2020). *Regjeringa lanserer "Langskip" for fangst og lagring av CO2 i Noreg*. https://www.regjeringen.no/no/aktuelt/regjeringa-lanserer-langskip-for-fangst-og-lagring-av-co2-i-noreg/id2765288/. [Accessed 15/05/2022].

Rinehart, A. J., Dewers, T. A., Broome, S. T., & Eichhubl, P. (2016). Effects of CO2 on mechanical variability and constitutive behavior of the Lower Tuscaloosa Formation, Cranfield Injection Site, USA. *International Journal of Greenhouse Gas Control*, *53*, 305–318. https://doi.org/10.1016/j.ijggc.2016.08.013

Røe, S. -L, & Steel, R. (1985). Sedimentation, Sea-Level Rise and Tectonics At the Triassic-Jurassic Boundary (Statfjord Formation), Tampen Spur, Northern North Sea. *Journal of Petroleum Geology*, *8*(2), 163–186. https://doi.org/10.1111/j.1747-5457.1985.tb01009.x

Roksandic, M. M. (1978). Seismic facies analysis. *Geophysical Prospecting*, *26*(2), 383–398. https://doi.org/10.1111/j.1365-2478.1978.tb01600.x

Ryseth, A. (2001). Sedimentology and palaeogeography of the statfjord formation (Rhaetian-Sinemurian), North Sea. *Norwegian Petroleum Society Special Publications*, *10*(C), 67–85. https://doi.org/10.1016/S0928-8937(01)80009-6

Sclater, J. G., & Christie, P. A. F. (1980). Continental stretching: An explanation of the Post-Mid-Cretaceous subsidence of the central North Sea Basin. *Journal of Geophysical Research: Solid Earth*, *85*(B7), 3711–3739. https://doi.org/10.1029/jb085ib07p03711

Sheriff, R. (1977). Limitations on resolution of seismic reflections and geologic detail derivable from them: Section 1. Fundamentals of Stratigraphic Interpretation of Seismic Data. *AAPG Memoir: Seismic Stratigraphy--Applications to Hydrocarbon Exploration*, *26*, 3–14. http://scholar.google.com/scholar?hl=en&btnG=Search&q=intitle:limitations+on+resolution+of+seismic+reflections+and+geologic+detail+derivable+from+them#0

Shi, J. Q., Imrie, C., Sinayuc, C., Durucan, S., Korre, A., & Eiken, O. (2013). Snøhvit CO2 storage project: Assessment of CO2 injection performance through history matching of the injection well pressure over a 32-months period. *Energy Procedia*, *37*(April 2011), 3267–3274. https://doi.org/10.1016/j.egypro.2013.06.214

Shukla, R., Ranjith, P., Haque, A., & Choi, X. (2010). A review of studies on CO2 sequestration and caprock integrity. *Fuel*, *89*(10), 2651–2664. https://doi.org/10.1016/j.fuel.2010.05.012

Steel, R. J. (1993). *Triassic-Jurassic megasequence stratigraphy in the Northern North Sea: rift to post-rift evolution*. http://pgc.lyellcollection.org/

Steel, R., & Olsen, T. (2002). Clinoforms, Clinoform Trajectories and Deepwater Sands. *Sequence Stratigraphic Models for Exploration and Production: Evolving Methodology, Emerging Models, and Application Histories: 22nd Annual, January*, 367–380. https://doi.org/10.5724/gcs.02.22.0367

Stewart, D. J., Schwander, M., & Bolle, L. (1995). Jurassic depositional systems of the Horda Platform, Norwegian North Sea: practical consequences of applying sequence stratigraphic models. *Norwegian Petroleum Society , 5*, 291–323.

Sundal, A., Miri, R., Ravn, T., & Aagaard, P. (2015). Modelling CO2 migration in aquifers; considering 3D seismic property data and the effect of site-typical depositional heterogeneities. *International Journal of Greenhouse Gas Control*, *39*, 349–365. https://doi.org/10.1016/j.ijggc.2015.05.021

Sundal, A., Nystuen, J. P., Rørvik, K. L., Dypvik, H., & Aagaard, P. (2016). The Lower Jurassic Johansen Formation, northern North Sea – Depositional model and reservoir characterization for CO2 storage. *Marine and Petroleum Geology*, *77*, 1376–1401. https://doi.org/10.1016/j.marpetgeo.2016.01.021

Swift, D. J. P. (1975). Barrier-island genesis: evidence from the central atlantic shelf, eastern U.S.A. *Sedimentary Geology*, *14*(1), 1–43. https://doi.org/10.1016/0037-0738(75)90015-9

Thompson, N., Andrews, J. S., Wu, L., & Meneguolo, R. (2022). Characterization of the in-situ stress on the Horda platform – A study from the Northern Lights Eos well. *International Journal of Greenhouse Gas Control*, *114*(December 2021). https://doi.org/10.1016/j.ijggc.2022.103580

Underhill, J. R., & Partington, M. A. (1993). Jurassic thermal doming and deflation in the North Sea: Implications of the sequence stratigraphic evidence. *Petroleum Geology Conference Proceedings*, *4*(0), 337–345. https://doi.org/10.1144/0040337

United Nations. (2015). *Adoption of the Paris Agreement, 21st Conference of the Parties, Paris: United Nations.*

Veeken, P. C. H. (2007). The Seismic Reflection Method and Some of Its Constraints . In K. Helbig & S. Treitel (Eds.), *Seismic Stratigraphy, Basin Analysis and Reservoir Characterisation : Vol. Volume 37* (First edition, pp. 7–74). Elsevier.

Vollset, J., & Doré, A. G. (1984). *A revised Triassic and Jurassic lithostrategraphic nomenclature for the Norwegian North Sea: Norwegian Petroleum Directorate* (p. 53).

Walderhaug, O., & Bjorkum, P. A. (1992). Effect of meteoric water flow on calcite cementation in the Middle Jurassic Oseberg Formation, well 30/3-2, Veslefrikk Field, Norwegian North Sea. *Marine and Petroleum Geology , 9*, 308–318.

Whipp, P. S., Jackson, C. A. L., Gawthorpe, R. L., Dreyer, T., & Quinn, D. (2014). Normal fault array evolution above a reactivated rift fabric; a subsurface example from the northern Horda Platform, Norwegian North Sea. *Basin Research*, *26*(4), 523–549. https://doi.org/10.1111/bre.12050

Whitaker, M. F. (1984). *Usage of palynostratigraphy and palynofacies in definition of Troll field geology*.

White, J. E. (1975). Computed Seismic Speeds and Attenuation in Rocks with Partial Gas Saturation. *Geophysics*, *40*(2), 224–232. https://doi.org/10.1190/1.1440520

Wu, L., Thorsen, R., Ottesen, S., Meneguolo, R., Hartvedt, K., Ringrose, P., & Nazarian, B. (2021). Significance of fault seal in assessing CO2 storage capacity and containment risks—an example from the Horda Platform, northern North Sea. *Petroleum Geociense*.

Yang, W., Kominz, Michelle. A., & Major, R. P. (1998). Distinguishing the roles of autogenic versus allogenic processes in cyclic sedimentation, Cisco Group (Virgilian and Wolfcampian), north-central Texas. *GSA Bulletin* , *110*(10), 1333–1353.

Zhang, D., & Song, J. (2014). Mechanisms for geological carbon sequestration. *Procedia IUTAM*, *10*, 319–327. https://doi.org/10.1016/j.piutam.2014.01.027

Ziegler, P. A. (1975). The Geological Evolution of the North Sea Area in the Tectonic Framework of North Western Europe. *Norges Geologiske Undersøkelse*, *316*, 1–27.